



UNIVERSITA' DEGLI STUDI DI VERONA

DEPARTMENT OF

DIAGNOSTICS AND PUBLIC HEALTH

GRADUATE SCHOOL OF

NATURAL AND ENGINEERING SCIENCES

DOCTORAL PROGRAM IN

NANOSCIENCE AND ADVANCED TECHNOLOGIES

Cycle / year (1° year of attendance) 35th cycle

TITLE OF THE DOCTORAL THESIS

BIOMEDICAL APPROACHES IN REGENERATIVE MEDICINE: A NEW
ALGORITHM FOR TISSUE ENGINEERING AND REGENERATIVE MEDICINE

S.S.D.: MED/46 – BIO/17

Coordinator: Prof. ADOLFO SPEGHINI

Signature _____

Tutor: Prof. ANDREA SBARBATI

Signature _____




Co-tutorship: Dr. Giamaica Conti and Dr. Alice Busato

Doctoral Student: Dott.ssa LINDSEY ALEJANDRA QUINTERO SIERRA

Signature

This work is licensed under a Creative Commons Attribution-NonCommercial-NoDerivs 4.0 International Unported License, Italy. To read a copy of the license, visit the web page:

<http://creativecommons.org/licenses/by-nc-nd/4.0/>

-  **Attribution** — You must give appropriate credit, provide a link to the license, and indicate if changes were made. You may do so in any reasonable manner but not in any way that suggests the licensor endorses you or your use.
-  **NonCommercial** — You may not use the material for commercial purposes.
-  **NoDerivatives** — If you remix, transform, or build upon the material, you may not distribute the modified material.

*BIOMEDICAL APPROACHES IN REGENERATIVE MEDICINE:
A NEW ALGORITHM FOR TISSUE ENGINEERING AND REGENERATIVE MEDICINE*
Lindsey Alejandra Quintero Sierra

Ph.D. thesis
Verona, 7 March 2023
ISBN

*To my husband Erwin and my beloved family;
who, despite the distance, knew how to cheer me up
even though I didn't even know I needed it.*

*“Do the best you can until you know better.
Then when you know better, do better.”*

Maya Angelou.

ACKNOWLEDGMENTS

Initially, I would like to express my gratitude to my supervisor, Andrea Sbarbati, who allows us to improve our knowledge with his unique guidance. I would also like to thank two amazing co-tutors, Giamaica Conti and Alice Busato, who supported me throughout this project at a professional and personal level.

Additionally, I wish to acknowledge the help provided by my lab co-workers at the Anatomy and Histology Department, especially Anita Conti, Alessandro Negri, Riccardo Ossanna, Francesca Mengoni, Valentina Salari and Giulia Spagnoli, who patiently taught me the hidden secrets of the mouse anatomy and Italian culture.

I would also like to extend my gratitude to the technical and support staff of the Anatomy and Histology Department and the Centro Piattaforme Tenologiche (CPT) of the University of Verona.

Furthermore, I would like to thank Fidia Farmaceutici S.P.A. and the medical team involved in the different projects for providing us with the necessary materials to develop this work. Specifically, Dr. Michele Riccio, Dr. Francesco De Francesco, Dr. Nicola Zingaretti and Dr. Carlo Soranzo.

Last but not least, I want to thank Erwin Ciro for his constant teaching, counsel and patience that gave me the courage to conclude this part of the journey. Likewise, I want to thank my family and friends who always supported me and cheered me up to take this adventure.

ABSTRACT

Organ Regeneration as a field of study was introduced in the late 1980s; however, as a notion, was part of humankind since ancient times. The inability to self-repair/self-regenerate has been a growing medical issue, as accidents provoke significant injuries. To overcome this inconvenience, Tissue Engineering and Regenerative Medicine (TERM) has emerged as a multidisciplinary field that combines engineering futures with biological elements such as cells and growth factors.

The usual approach of TERM has been using specific platforms (scaffolds) made of biocompatible materials with the ability to mimic the microenvironment surrounding the cell. Notwithstanding, this system focused on finding the perfect result to “fill in” the area of damaged tissue with poor consideration of the biological pathways for self-healing.

This thesis proposes a novel methodological algorithm, henceforth named Regenerative Algorithm. In this regard, it is proposed a three-step process that considers the main stages of the self-healing mechanisms of the human body. This thesis is divided into four main chapters; each one shows a case study related to each of the steps proposed in the Regenerative Algorithm.

Chapter 1 presents a validation study of a novel collagenase extracted from the anaerobic bacterial culture of *Vibrio alginolyticus*. In clinical practice, collagenases are used in the treatment of damaged tissue as a debriding instrument, which is related to the first part of the algorithm, which is the destructuring of the tissue. This study evaluated the *V. alginolyticus*-based collagenase *in vitro* compared with the effects provoked by commercial collagenases obtained from the *Clostridium histolyticum* strain. Initially, the *V. alginolyticus*-based collagenase was optimized in terms of concentration and reaction time for extracting Stem Cells from Adipose Tissue. Once the best concentration and incubation time were detected, the novel collagenase was compared with two *C. histolyticum*-based collagenases, one the standard used in laboratory practice and the other a commercial collagenase, evaluating cellular yield, clonogenic and proliferation capacity of the extracted cells. In addition, the three evaluated collagenases were placed in contact with expanded cells to evaluate the cytotoxic effect. The results showed that the novel collagenase at a concentration of 3.6 mg/mL and 20 min of incubation time allows for obtaining a comparable number of cells with the other two evaluated collagenases; moreover, the cytotoxicity test showed that the *V. alginolyticus*-based collagenase does not affect the vitality of the cells while the commercial one presents an essential reduction of vitality. The results indicate that there is high potential for using the *V. alginolyticus*-based collagenase in clinical practice, given its efficacy on stem cell extraction without affecting cellular integrity.

Chapter 2 displays an *in vitro* and *in vivo* evaluation of decellularized collagen membranes as one approach for the second step of the algorithm, which involves the recreation of the tissue structure with external materials to support the regeneration process. There are diverse methods to accomplish the second stage according to the degree of damage, in this chapter it is presented an invasive method using a 3D scaffold for the specific treatment of capsular contracture formation during breast reconstruction. Three decellularized collagen membranes were placed in contact with stem cells to evaluate the migration and proliferation and the

possible stimulation guided by the membranes. Consequently, the membranes were implanted on the left flank of balb/c mice to evaluate dermal integration, absorption degree and biostimulation *in vivo*. The results showed that the physicochemical characteristics of the membranes influence the differentiation capacities of cells and tissue stimulation, affecting the development of well-organized adipose tissue.

Chapter 3, on the other hand, presents a non-invasive method for the second step of the algorithm by studying an injectable Low Molecular Weight Hyaluronic Acid (LMW-HA) in a case study of aberrant scar treatment. Initially, the LMW-HA was tested *in vitro* at different concentrations to analyze its influence on the differentiative stimulation of stem cells and their interaction through CD44 cell surface receptor, and later it was used in a double-blinded clinical study for the scar treatment. The results indicated that HA influences the differentiation mechanisms of cells, where the process depends on the concentration, being faster with concentrations ranging from 2 to 5 mg/mL. It seems that lower concentrations of HA slowly stimulate cellular processes while higher concentrations saturate the cells reducing their activation. Moreover, in the clinical study, the patients treated with HA presented a more structured and smoother tissue, which means that the use of HA may increase the total recovery of the tissue and therefore improve the quality of life of patients.

Chapter 4 exposes a study of the validation of a device that introduces the last stage of the algorithm, which is the use of cellular elements that enhance the regeneration process of the tissue. This chapter presents the characterization of the product obtained after processing fat tissue with a novel Nanofat system in terms of cellular yield, morphology, proliferation and clonogenic capacity, immunophenotyping and differentiation potential. The results demonstrated that the product could differentiate into the three mesodermal lineages, and more importantly, the immunophenotyping analysis revealed the presence of pluripotent stem cells. Moreover, the main secretome of the product presents proliferative, pro-angiogenic, pro-differentiative and pro-antiapoptotic factors, which are vital in the regenerative process.

According to the results obtained with each approach, following the proposed Regenerative Algorithm, the regenerative process of damaged tissue can be significantly improved.

RESUME

La rigenerazione degli organi come campo di studio è stata introdotta alla fine degli anni '80; tuttavia, come nozione, faceva parte dell'umanità fin dai tempi antichi. L'incapacità di auto-ripararsi/auto-rigenerarsi è stato un problema medico crescente, poiché gli incidenti provocano lesioni significative. Per superare questo inconveniente, l'ingegneria dei tessuti e la medicina rigenerativa (TERM) è emersa come un campo multidisciplinare che combina il futuro dell'ingegneria con elementi biologici come cellule e fattori di crescita.

L'approccio abituale di TERM ha utilizzato piattaforme specifiche (scaffold) realizzate con materiali biocompatibili con la capacità di imitare il microambiente che circonda la cellula. Nonostante ciò, questo sistema si è concentrato sulla ricerca del risultato perfetto per "riempire" l'area del tessuto danneggiato con scarsa considerazione dei percorsi biologici per l'autoguarigione.

Questa tesi propone un nuovo algoritmo metodologico, d'ora in poi chiamato Algoritmo Rigenerativo. A tal proposito si propone un percorso in tre fasi che considera le fasi principali dei meccanismi di autoguarigione del corpo umano. Questa tesi è suddivisa in quattro capitoli principali; ognuno mostra un caso di studio relativo a ciascuno dei passaggi proposti nell'algoritmo rigenerativo.

Il capitolo 1 presenta uno studio di validazione di una nuova collagenasi estratta dalla coltura batterica anaerobica di *Vibrio alginolyticus*. Nella pratica clinica, le collagenasi sono utilizzate nel trattamento del tessuto danneggiato come strumento di sbrigliamento, che è correlato alla prima parte dell'algoritmo, che è la destrutturazione del tessuto. Questo studio ha valutato la collagenasi basata su *V. alginolyticus in vitro* rispetto agli effetti provocati dalle collagenasi commerciali ottenute dal ceppo *Clostridium histolyticum*. Inizialmente, la collagenasi a base di *V. alginolyticus* è stata ottimizzata in termini di concentrazione e tempo di reazione per l'estrazione di cellule staminali dal tessuto adiposo. Una volta individuate la migliore concentrazione e il tempo di incubazione, la nuova collagenasi è stata confrontata con due collagenasi a base di *C. histolyticum*, una standard utilizzata nella pratica di laboratorio e l'altra una collagenasi commerciale, valutando la resa cellulare, la capacità clonogenica e proliferativa delle cellule estratte. Inoltre, le tre collagenasi valutate sono state poste a contatto con cellule espanse per valutare l'effetto citotossico. I risultati hanno mostrato che la nuova collagenasi ad una concentrazione di 3,6 mg/mL e 20 min di tempo di incubazione consente di ottenere un numero comparabile di cellule con le altre due collagenasi valutate; inoltre il test di citotossicità ha dimostrato che la collagenasi a base di *V. alginolyticus* non intacca la vitalità delle cellule mentre quella commerciale presenta una sostanziale riduzione della vitalità. I risultati indicano che esiste un alto potenziale per l'utilizzo della collagenasi basata su *V. alginolyticus* nella pratica clinica, data la sua efficacia nell'estrazione di cellule staminali senza compromettere l'integrità cellulare.

Il capitolo 2 mostra una valutazione *in vitro* e *in vivo* delle membrane di collagene decellularizzate come un approccio per la seconda fase dell'algoritmo, che prevede la ricreazione della struttura del tessuto con materiali esterni per supportare il processo di rigenerazione. Esistono diversi metodi per realizzare la seconda fase in base al grado di danno, in questo capitolo viene presentato un metodo invasivo che utilizza uno scaffold 3D per il trattamento specifico della formazione di contratture capsulari durante la ricostruzione del seno. Tre membrane di collagene

decellularizzato sono state poste a contatto con cellule staminali per valutarne la migrazione e la proliferazione e l'eventuale stimolazione guidata dalle membrane. Di conseguenza, le membrane sono state impiantate sul fianco sinistro dei topi balb/c per valutare l'integrazione dermica, il grado di assorbimento e la biostimolazione *in vivo*. I risultati hanno mostrato che le caratteristiche fisico-chimiche delle membrane influenzano le capacità di differenziazione delle cellule e la stimolazione dei tessuti, influenzando lo sviluppo di tessuto adiposo ben organizzato.

Il capitolo 3, invece, presenta un metodo non invasivo per la seconda fase dell'algoritmo studiando un acido ialuronico a basso peso molecolare iniettabile (LMW-HA) in un caso studio di trattamento di cicatrici aberranti. Inizialmente, l'LMW-HA è stato testato *in vitro* a diverse concentrazioni per analizzare la sua influenza sulla stimolazione differenziativa delle cellule staminali e la loro interazione attraverso il recettore di superficie cellulare CD44, e successivamente è stato utilizzato in uno studio clinico in doppio cieco per il trattamento della cicatrice. I risultati hanno indicato che l'HA influenza i meccanismi di differenziazione delle cellule, dove il processo dipende dalla concentrazione, essendo più veloce con concentrazioni comprese tra 2 e 5 mg/mL. Sembra che concentrazioni più basse di HA stimolino lentamente i processi cellulari mentre concentrazioni più alte saturino le cellule riducendone l'attivazione. Inoltre, nello studio clinico, i pazienti trattati con HA presentavano un tessuto più strutturato e più liscio, il che significa che l'uso di HA può aumentare il recupero totale del tessuto e quindi migliorare la qualità della vita dei pazienti.

Il capitolo 4 espone uno studio sulla validazione di un dispositivo che introduce l'ultima fase dell'algoritmo, ovvero l'utilizzo di elementi cellulari che potenziano il processo di rigenerazione del tessuto. Questo capitolo presenta la caratterizzazione del prodotto ottenuto dopo la lavorazione del tessuto adiposo con un nuovo sistema Nanofat in termini di resa cellulare, morfologia, proliferazione e capacità clonogenica, immunofenotipizzazione e potenziale di differenziazione. I risultati hanno dimostrato che il prodotto poteva differenziarsi nelle tre linee mesodermiche e, cosa più importante, l'analisi di immunofenotipizzazione ha rivelato la presenza di cellule staminali pluripotenti. Inoltre, il secretoma principale del prodotto presenta fattori proliferativi, pro-angiogenici, pro-differenziati e pro-antiapoptotici, vitali nel processo rigenerativo.

Secondo i risultati ottenuti con ciascun approccio, seguendo l'algoritmo rigenerativo proposto, il processo rigenerativo del tessuto danneggiato può essere notevolmente migliorato.

TABLE OF CONTENTS

INTRODUCTION.....	17
TISSUE ENGINEERING AND REGENERATIVE MEDICINE SHORT HISTORY AND FUTURE PERSPECTIVES	18
CHAPTER I:	24
ISOLATION OF ADIPOSE-DERIVED STEM CELLS USING <i>Vibrio alginolyticus</i>-based COLLAGENASE: CASE STUDY	24
1. BACKGROUND	25
2. MATERIALS AND METHODS	26
3. RESULTS	31
4. DISCUSSION.....	39
5. CONCLUSION	40
CHAPTER II:.....	48
COLLAGEN MEMBRANES FOR RECONSTRUCTIVE PURPOSES: CASE STUDY	48
1. BACKGROUND	49
2. MATERIALS AND METHODS	50
3. RESULTS	54
4. DISCUSSION.....	63
5. CONCLUSION	65
CHAPTER III:	70
INFLUENCE OF CONCENTRATION OF A LOW MOLECULAR WEIGHT HYALURONIC ACID IN SCAR SKIN TREATMENT: CASE STUDY	70
1. BACKGROUND	71
2. MATERIALS AND METHODS	73
3. RESULTS	76
4. DISCUSSION	80
5. CONCLUSION	81
CHAPTER IV:	85
A NOVEL TRANSLATIONAL SYSTEM IN STEM CELL THERAPY: CASE STUDY	85
1. BACKGROUND	86
2. MATERIALS AND METHODS	87
3. RESULTS	92
4. DISCUSSION.....	100

5. CONCLUSION	102
FINAL REMARKS	108
DISCUSSION	109
FUTURE PERSPECTIVES	110

LIST OF FIGURES

INTRODUCTION

- Figure 1.** Publications related to Tissue Engineering through years. Analysis performed using Scopus Database tool (12). 19
- Figure 2.** Timeline of Tissue Engineering evolution. (Extracted from (14)). 20
- Figure 3.** Illustration of the key elements of Tissue Engineering and Regenerative Medicine. 20

CHAPTER I

- Figure 1.** Experimental plan for the *Vibrio alginolyticus* collagenase optimization method and comparison with commercial enzymes. 28
- Figure 2.** (A) Cellular yield, (B) clonogenic potential and (C) cellular growth of extracted cells after the enzymatic digestion with *V. alginolyticus* collagenase varying concentration and incubation time. The results are shown as the mean \pm standard error indicating the significant statistical differences (*: p-value <0.05, **: p \leq 0.01, ***: p \leq 0.001). 32
- Figure 3.** (A) Viability and (B) proliferation capacity of extracted cells after the enzymatic digestion with *V. alginolyticus* collagenase varying concentration and incubation time. The results are shown as the mean \pm standard error indicating the significant statistical differences (**: p \leq 0.01, ****: p \leq 0.0001). 33
- Figure 4.** Immunophenotyping of the extracted cells with the optimized protocol of *V. alginolyticus* collagenase after the adipose tissue enzymatic digestion (P0). 34
- Figure 5.** Immunophenotyping of extracted cells with the optimized protocol after culture procedure until reach passage 4 from the adipose digestion. 34
- Figure 6.** (A) Optical microscopy images of extracted cells with the optimized protocol compared with extracted cells with Col. Type 1 after being induced with differentiation medium (adipocytes present lipid droplets identify with black arrows, chondrocytes in blue and osteocytes in red) in comparison with not induced cells (CTRL-). Statistical graphs of semi-quantitative analysis of (B) lipid droplets number for adipogenic differentiation, (C) the cartilage-like matrix area for chondrogenic differentiation and (D) the Calcium deposits area for the osteogenic differentiation. The results are shown as the mean \pm standard error indicating the significant statistically differences (* p \leq 0,05 ** p \leq 0,01, *** p \leq 0,001, **** p \leq 0,0001). 35
- Figure 7.** (A) Cellular yield, (B) clonogenic potential and (C) cellular growth of extracted cells after the enzymatic digestion with the optimized *V. alginolyticus* collagenase compared with Collagenase Type I and *C. histolyticum* blend. The results are shown as the mean \pm standard error indicating the significant statistical differences (*: p-value <0.05). 37
- Figure 8.** (A) Viability and (B) proliferation capacity of extracted cells after the enzymatic digestion with the optimized *V. alginolyticus* collagenase compared with Collagenase Type I and *C. histolyticum* blend. There are no statistical differences among the data. 38
- Figure 9.** Viability percentage of expanded cells placed in contact with the optimized *V. alginolyticus* collagenase compared with Collagenase Type I and *C. Histolyticum* blend for 20 min evaluated with the (A) trypan blue exclusion test and (B) MTT test. The results are shown as the mean \pm standard error indicating the significant statistical differences (p \leq 0.01, ***, p \leq 0.001, ****: p \leq 0.0001). 38
- Figure 10.** Representative images of TEM analysis of P4 cells treated with the optimized *V. alginolyticus* collagenase compared with Collagenase Type I and *C. histolyticum* blend for 20 min and cells placed in agitation for 20 min as control group. 39

CHAPTER II

- Figure 1.** Morphological and physical characterization of the ACMs. a) SEM of ACMs in cross-view. The layered structure is identifiable for ACM1 and ACM2 (white bars indicates the different layers, Scale bar 200 μ m), while ACM3 is composed of a single layer (Scale bar 200 μ m) and are recognizable the elastic fibres (white square indicates the area of higher magnification, Scale bar 20 μ m). b) SEM images of ACMs at top view at two magnifications in dry and wet conditions (Scale bar: upper 200 μ m, bottom 5 μ m) show the surface porosity created by the crossed collagen fibres. c) The table summarizes the physical properties of ACMs (data reported as mean \pm standard deviation). CL: Compact layer; PL: Porous layer; EF: Elastic fibres. 56
- Figure 2.** SEM analysis of ASCs colonization capacity over ACMs at different magnifications. Some cytoplasmic flaps are appreciable on cells cultured with ACM1 and ACM2, while cells in

contact with ACM3 present a wrinkled plasmatic membrane. (Scale bar: upper 20 μm , middle 5 μm , bottom 10 μm) (ASCs: Adipose-derived stem cells on ACMs surface and spreading through their porous, CF: cytoplasmatic flaps on ASCs Surface, WPM: wrinkled plasmatic membrane)..... 57

Figure 3. *In vitro* biostimulation. ASCs after 7 and 14 days of contact with the evaluated ACMs were compared with ASCs cultured growth medium (negative control) and adipose differentiative medium (positive control). (Scale bar 20 μm) (Arrows indicate membrane debris, dotted arrows indicate vacuolization). 58

Figure 4. Elastosis formation after silicone prosthesis implantation. Magnetic Resonance images of control group are shown on the upper line after 7, 14 and 30 of follow-up. Histology images on the middle and bottom panels show H&E (Scale bar 100 μm) and MT (Scale bar 100 μm and 20 μm) staining of negative control group (uncovered silicone prosthesis) compared with positive control (healthy skin). (Arrow: silicone prosthesis; dotted arrow: fluid accumulation: black arrow: elastosis, White asterisks: inflammatory reaction, H&E: Hematoxylin/Eosin staining; MT: Mallory's Trichrome) 59

Figure 5. Evaluation of *in vivo* tissue integration. Magnetic resonance images performed after 7, 14, and 30 days of implantation of the evaluated ACMs allowed the calculation of the membrane's reabsorption degree and the surrounding fluid accumulation. (Arrow: ACMs, dotted arrow: fluid accumulation)..... 60

Figure 6. *Ex vivo* tissue integration after 14 days of study. The excised samples (ACMs with surrounding tissue) were stained with H&E and MT showed in upper panel (Scale bar 100 μm). Additionally, immunohistochemical analyses were performed with Coll. I and VEGF antibodies in bottom panel (Scale bar 30 μm). Asterisk indicates loss of fibre density; arrows indicate Coll. I positivity. CL: compact layer, PL: porous layer, H&E: Hematoxylin/Eosin staining, MT: Mallory's Trichrome, Coll. I: Collagen type I staining, VEGF: Vascular Endothelial Growth Factor staining 61

Figure 7. *Ex vivo* tissue integration after 30 days of study. The excised samples (ACMs with surrounding tissue) were stained with H&E and MT are shown in upper panel (Scale bar 100 μm). Additionally, immunohistochemical analyses were performed with Coll. I and VEGF antibodies in bottom panel (Scale bar 30 μm). Arrows identify positive responses for Coll. I. H&E: Hematoxylin/Eosin staining, MT: Mallory's Trichrome, Coll. I: Collagen type I staining, VEGF: Vascular Endothelial Growth Factor staining 62

Figure 8. Induced adipose biostimulation study. a) shows H&E of the evaluated membranes (ACM1, ACM2 and ACM3) revealing an adipogenic formation inside ACM1.b) MT staining of newly formed adipose tissue inside ACM1 (arrows delimited the membrane, scale bar 100 μm) and immunohistochemical analysis of newly formed adipose tissue for Coll. III and VEGF antibodies (scale bar 30 μm). H&E: Hematoxylin/Eosin staining, MT: Mallory's Trichrome, Coll. III: Collagen type III staining, VEGF: Vascular Endothelial Growth Factor staining..... 62

CHAPTER III

Figure 1. Schematic representation of a healthy skin morphology with the three main layers (Epidermis, dermis and hypodermis) clearly distributed..... 71

Figure 2. Representative scheme of the employed methodology for the *in vitro* evaluation of the evaluated LMW-HA..... 73

Figure 3. Schematic representation of the performed clinical study evaluating the LMW-HA at the commercial concentration. 76

Figure 4. Representative images of colored cells after 28 days of study. The evaluated concentrations are compared with negative and positive controls. The number of red spots in 2.5 mg/mL concentration is comparable with the positive control. 76

Figure 5. Statistical analysis for the rate of positive cells (up), amount of lipid droplets (down left) and the area of the lipid droplets (down right). It can be seen that the evaluated concentrations of 2.5 and 5 mg/mL are comparable with the positive control on three measured parameters. 77

Figure 6. Comparison of the CD44 expression of cells treated with the evaluated LMW-HA at two different concentrations (2.5 and 5 mg/mL) for 7, 14, 21 and 28 days compared with control cells. It can be seen that both treatments down regulate the CD44 expression 79

Figure 7. Representative images of a scar before and after the treatment with HA at two different magnifications (scale bars 100 μm (left) and 20 μm (right)) showing that after the treatment it is noticeable a papillary layer. 79

Figure 8. Representative images of a scar treated with saline solution pre and post injection at two magnifications (scale bars 100 μm (left) and 20 μm (right)) to evidence the presence of lymphocytic infiltrates after the treatment. 80

CHAPTER IV

Figure 1. Morphological analysis of Hy-Tissue Nanofat product. (A) Scheme of the Hy-Tissue Nanofat procedure; (B) Light microscopy of Hy-Tissue Nanofat product obtained with the whole-mount method. The square (in Figure 1B, left) indicates the location of the higher magnification (right). (Scale bar: (left) 300 μm , (right) 100 μm). The graph represents the size distribution of the lipid droplets. (C). Light microscopy of Hy-Tissue Nanofat product obtained with the whole-mount method after centrifugation. The square (in Figure 1C, left) indicates the location of the higher magnification (Figure 1C, right) (Scale bar: (left) 80 μm , (right) 40 μm). (D) Scanning electron microscopy of Hy-Tissue Nanofat product after centrifugation. The square (in Figure 1D, left) indicates the location of the higher magnification (Figure 1D, right), the elastic fibre, the connective tissue lamina and the single collagen fibre are showed with a dotted arrow, an asterisk and an arrow, respectively. (Scale bar: (left) 50 μm , (right) 5 μm). 93

Figure 2. Experimental methodology. The fat sample was divided into three portions to be processed in N-ASC, N-ED-ASC and ED-ASC and evaluated for cell proliferation capacity, CFU-F assay, immunophenotyping and differentiation potential. 94

Figure 3. Cellular yield and proliferation capacity obtained with the three evaluated procedures (A) Obtained nucleated cells after the three evaluated treatments. Cells yield (n° of cell/ml FAT) was evaluated considering the enzymatic digestion as 100%; (B, **left**) Proliferation capacity N-ASC, N-ED-ASC and ED-ASC in T25 flasks. The days required for the adherent cells to reach confluence (passage 1) were counted. (B, **right**) The PDT of N-ASC, N-ED-ASC and ED-ASC were analysed to evaluate the growth rate of adherent cells; (C) Microscopic images of adherent cells 3 days after the extraction. All the results are shown as mean \pm standard deviation represented by the error bars. Box and whisker plots represent the median. Significant statistical differences are indicated (p-value $<0.05=*$, $0.005<p\text{-value}<0.001=**$ or $p\text{-value}<0.001=***$). 95

Figure 4. Clonogenic potential of Hy-Tissue Nanofat product. (A) Representative light microscope of CFU-F assay stained with Toluidine Blue (scale bar 20 μm); (B) CFU-F yields of N-ASC, N-ED-ASC, and ED-ASC. (C) Percentage of CFU-F of N-ASC, N-ED-ASC, and ED-ASC. All the results are shown as mean \pm standard deviation represented by the error bars. Significant statistical differences are indicated (p-value $<0.05=*$, $0.005<p\text{-value}<0.001=* *$ or $p\text{-value}<0.001=***$). .. 96

Figure 5. Surface markers expression was detected by flow cytometric analysis of N-ASC. The percentage of positive cells for each marker was calculated after subtracting the non-specific fluorescence obtained with the control (unmarked). (A) Representative set of flow cytometry analysis for CD34, CD45, CD105, CD29, and CD73 markers performed on N-ASC. Percentage of positive cells to CD markers was indicated as an average of the samples; (B) Percentage of positive cells to CD markers (as an average of the samples) in N-ASC compared to N-ED-ASC and ED-ASC; (C) Percentage of positive cells to CD markers after *in vitro* cell expansion in N-ASC, N-ED-ASC, and ED-ASC. Results are presented as the mean \pm standard deviation portrayed with error bars. Significant statistical differences are indicated (p-value $<0.05=*$). 97

Figure 6. Multilineage differentiation assay. (A) Optical microscopy images of induced N-ASC, N-ED-ASC and ED-ASC and not induced (CTR) with differentiation medium at days 4 (Oil-Red O staining scale bar 10 μm ; Alzarín Red staining scale bar 20 μm ; Alcian blue staining scale bar 10 μm); (B) Optical microscopy images of induced N-ASC, N-ED-ASC and ED-ASC and not induced (CTR) with differentiation medium at days 9 (Oil-Red O staining scale bar 10 μm ; Alzarín Red staining scale bar 20 μm ; Alcian blue staining scale bar 10). Red spots indicated by the accumulation of neutral lipid vacuoles stained with Oil-Red-Oil; Alzarín Red staining reveals in red the extracellular matrix calcification; deposition of sulfated proteoglycan-rich matrix was marked in blue with Alcian Blue staining; (C) Graph represents the mean amount of lipid droplets of the induced ASC. After 9 days of the induction, N-ASC shows higher lipid droplets formation than ED-ASC, N-ED-ASC, and CTR. (D) The graph showed the extracellular matrix calcification area measurement (μm^2) of the induced ASC. After 9 days of treatment, N-ASC showed the highest calcium deposit formation. (E) The graph represents the area measurement of the generated cartilage-like matrix (μm^2). On the 9th day, N-ASC showed the larger cartilage deposit formation. In graphics C, D and E, the pink line represents N-ASC, the green line ED-ASC and the blue line N-ED-ASC. The data is presented as the mean \pm standard deviation, significant statistical differences

are indicated (p-value<0.05=*, 0.05<p-value<0.001= **, p-value<0.001= *** or p-value<0.0001= ****). 99

Figure 7. Multilineage differentiating stress enduring cells expression. A) Flow cytometry of N-ASC, N-ED-ASC, and ED-ASC to investigate the presence of MUSE cells. The percentage of positive cells to SEEA-3 and CD105 markers were indicated as an average of three samples, and the results are presented as the mean ± standard deviation. B) Immunofluorescence microscopy of MUSE cells. MUSE cells in N-ASC were detected as a positive cell for CD105 (left), SEEA3 (middle) and the simultaneous expression of CD105-SEEA3 (right). 100

FINAL REMARKS

Figure 1. Representative scheme of the proposed Regenerative Algorithm..... 28109

LIST OF TABLES

CHAPTER I

Table 1. Name code of the evaluated enzyme concentration of Fidia collagenase with the evaluated incubation time for each concentration. 27

CHAPTER III

Table 1. Statistical significance of % adipo-positive cells/tot among the treatments at each evaluated time. Significant statistical differences are indicated (p-value <0.05=*, 0.005<p-value <0.001=**, p-value <0.001=*** or p-value <0.0001=****). 78

CHAPTER IV

Table 1. Code names of the products obtained with the evaluated protocols for fat tissue digestion. 89

INTRODUCTION

PROLOGUE:

Shakespeare wrote, “Our bodies are our gardens...”; however, acute and chronic disorders that result in organ malfunction/failure have been a constant puzzle for humankind. This introductory chapter explains the concepts of Tissue Engineering and Regenerative Medicine that have been present since the prehistoric age. Additionally, it is proposed a novel approach for tissue regeneration by creating a methodological Regenerative Algorithm.

TISSUE ENGINEERING AND REGENERATIVE MEDICINE SHORT HISTORY AND FUTURE PERSPECTIVES

The human body is a beautiful design of nature that has evolved over time; however, damage to organs and tissues can occur from disease and accidents. Since ancient times, the health of people has been of great importance in society, which is why a large part of the scientific advances have been made in this area so that the quality of life of the people can be improved.

The concept of Organ Regeneration has been part of humankind since immemorial times. In the Book of Genesis in the Holy Bible, the story of the first woman Eve who was created from the rib of Adam presents the classical concept of a whole organism regeneration from a body part (1).

Ancient Greek mythology presents several examples of human creation without sexual reproduction. The myth of Prometheus, who was chained, spending his days at the mercy of an eagle that ate his liver, and at night his tissue regenerated, presented the concept of liver regeneration. This story suggests the knowledge of ancient Greeks of the regeneration capability of the liver, which is probably why they named it "*hepar*," which means "*repair itself*"(2).

The lack of organs has been a growing problem as accidents involving total or partial organ failure and the inability to meet the demand with existing donors increase (3)(4), and the option of autologous transplantation (tissue from the same patient, taken from another area of the body) is limited by the amount of tissue available and possible infections in situ (5). Due to this inconvenience, Tissue Engineering (TE) arose to help tissue cell regeneration using natural or synthetic materials that meet the necessary biocompatibility conditions. Today, the study of TE is increasingly promising in the medical field since it offers a new alternative in terms of using synthetic materials to promote cell growth (6). Thus, Cell Growth Platforms (Scaffolds) began to be created using biocompatible materials with similar characteristics to those of the tissue for which they were created.

The use of compatible materials dates from around 1500 B.C. with the use of wood in limb prostheses (7) or skins to cover naked bodies. In Capua, Italy, an artificial leg dating to approximately 300 B.C. made of iron and bronze, with a wooden core, was unearthed, which already demonstrates the use of natural materials in the manufacture of prostheses (7). The first prostheses were used for the replacement of a limb so that motor problems could be solved when a limb is missing; this is to some extent, an indication of bone replacement.

Biomaterials have been part of human evolution; however, TE became known in 1962 when scientists began to develop the first synthetic skin, being used as a successful therapy in the treatment of burns in the mid-1970s (8). Even so, TE as a field of study was defined in the late 1980s (9). By then, research in the field began to grow, as reflected in the number of articles published to date and which can be seen in Figure 1, where it is evident that since the 1960s, there had already been research related to TE, but it is since mid-'70s and early 80's when this field began to gain strength, defining itself as an interdisciplinary field in the mid-1980's and coining the term Tissue Engineering in 1987 (10)(11).

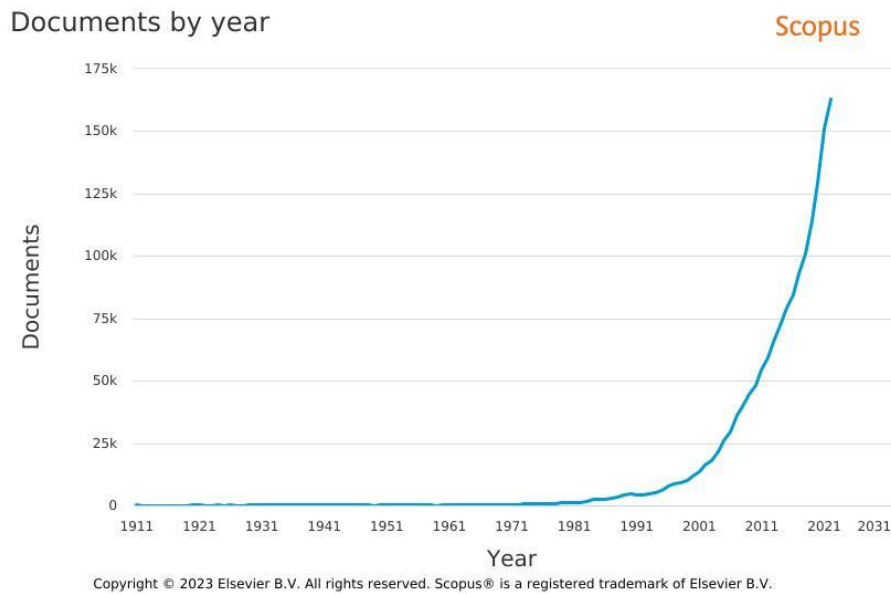


Figure 1. Publications related to Tissue Engineering through years. Analysis performed using Scopus Database tool (12).

During the early years, research focused on studying tissues and cells. In the early 70s, W.T. Green (11) carried out a series of experiments to regenerate cartilage using a chondrocyte culture in combination with a bone scaffold. Although he was unsuccessful in generating cartilage, his experiment laid the theoretical and practical foundation for the concept of connecting cells with cell growth matrices. The research conducted by Green led to promising work in TE focusing on skin regeneration using keratinocytes or fibroblasts in synthetic matrices to promote new tissue growth. The first functional synthetic leather was developed between the 1970s and 1980s; this was a starting point for what is now known as Tissue Engineering (8)(9). Following the study on skin regeneration using cells combined with cell growth matrices or scaffolds, a series of TE works began to be developed to regenerate different types of organs.

This is the case of Pro-Osteon, developed by Interpore International, a coral derivative used as bone implant material developed in 1993 (8). But it was in the year 1997 that the complete regeneration of cartilage tissue is achieved. The experiment developed by Charles Vacanti in 1997 (growing ear-shaped cartilage cells on the dermis of a mouse) (13) revolutionized TE in the musculoskeletal system.

However, it has only been possible to develop commercial products that allow the regeneration of skin and cartilage; such as Alloderm, Dermagraft, and TransCyte, among others (9); while for the other tissues, it has not yet been possible to advance from the laboratory stages.

The discovery of cell by Robert Hooke in 1665 marked a breakthrough in the history of Regenerative Medicine, but with the knowledge of the dynamic between cells and their micro niche for tissue development by Christian Pander in 1817 and the tissue regeneration guided by cell proliferation discovered by Rudolf Virchow in 1858 paved the development of a multidisciplinary approach for TE (1).

Figure 2 shows the timeline of greatest discoveries that have revolutionized the field of Tissue Engineering (14).

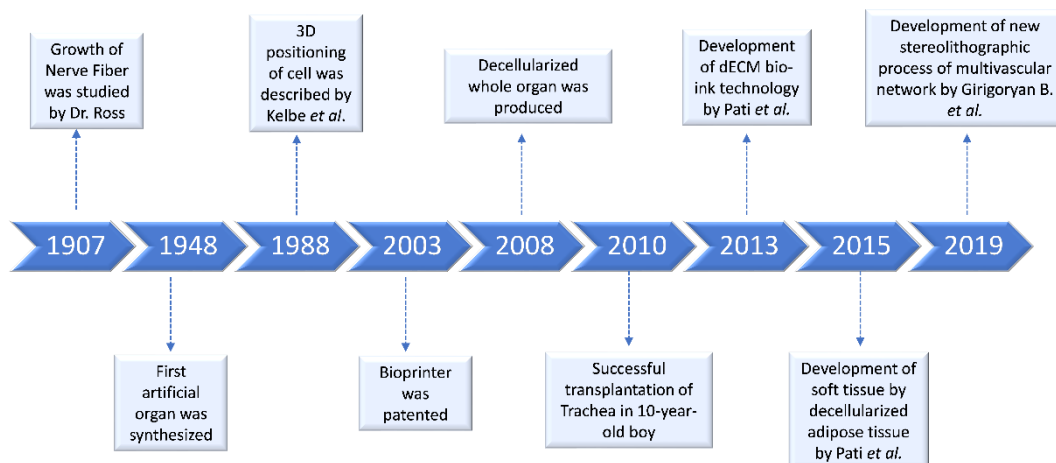


Figure 2. Timeline of Tissue Engineering evolution. (Extracted from (14))

Currently, TE uses three main components, the so call Tissue Engineering Triad (9): living cells, biocompatible materials and signaling factors (biochemical and physical elements as shown in Figure 3.

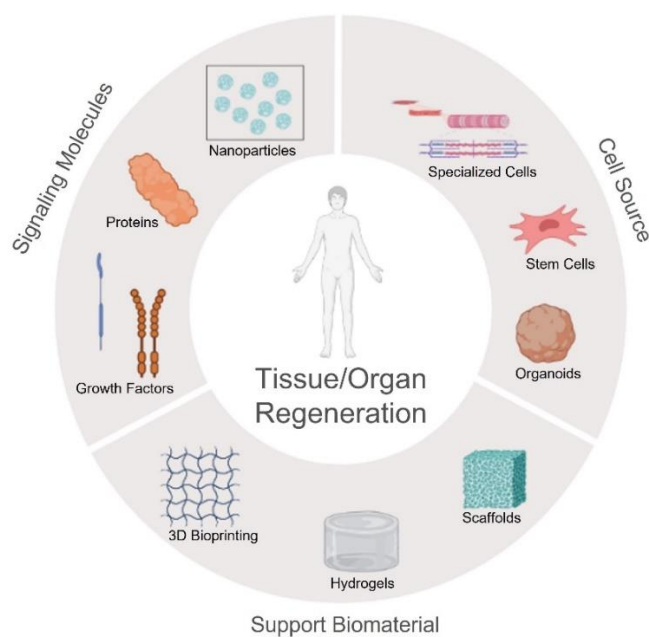


Figure 3. Illustration of the key elements of Tissue Engineering and Regenerative Medicine.

Tissue Engineering and Regenerative Medicine (TERM) is an extensively complex field that requires profound knowledge of the key actuators in developing and maintaining tissues and organs. In this regard, a novel approach is proposed in this study describing a methodological pathway to achieve the able tissue regeneration, named the Regenerative Algorithm.

As a common understanding in the construction field, it is important to remove all the compromised areas before repairing structural damages in buildings or other

infrastructures. After the removal of the damaged parts, it is required to generate a new supportive framework to finally be filled with new material.

In the case of TERM, following the previous analogy, the regeneration can only start after the appropriate removal of the damaged or altered tissue, known as a destructuring of the tissue. Then, the Regenerative Algorithm suggests creating a supporting material with similar physical characteristics to the damaged tissue that allows the conformation of favorable conditions for the last step of the algorithm, which is the promotion of tissue restructuring by using cells and signaling molecules that induce the regeneration, these last two steps are commonly known as the Tissue Regenerative Triad. Accordingly, the independent development of each mentioned step will contribute to consolidating the optimization of the final Regenerative Algorithm, which has as central target Tissue Regeneration.

This study presents four distinct research approaches focused on the stages proposed for the novel regenerative algorithm. Every chapter presents independent research focused on different pathologies of interest for Regenerative Medicine.

Chapter 1 highlights the first step of the proposed algorithm, which is the destructuring or removal of damaged tissue. The chapter presents the *in vitro* optimization for using a *Vibrio alginolyticus*-based collagenase and its comparison with commercial ones. In clinical practice, collagenases have been used in the treatment of necrotic tissue as a debriding instrument for the removal of damaged tissue.

Chapters 2 and 3 display two approaches for the second phase of the algorithm, which is the use of external supports that recreates the natural structure of the target tissue. Chapter 2 is focused on the *in vitro* and *in vivo* stimulation promoted by decellularized collagen membranes in a specific pathological case. On the other hand, chapter 3 shows the study on injectable hyaluronic acid and its effect on *in vitro* adipogenesis. Natural biomaterials have been widely used for their biocompatibility and the capacity to recreate the physical structure of tissues providing a sort of framework for the newly generated tissue to grow.

Finally, chapter 4 displays validation research of a novel kit for isolating the stromal vascular fraction (SVF) from adipose tissue, an excellent source of stem cells and connective tissue that enhance tissue restructuring. The use of SVF in clinical practice is gaining attention due to its regenerative effect attributable to the presence of stem cells, and endothelial cells, among others, and especially to the proliferative, pro-angiogenic, pro-differentiative and pro-antiapoptotic factors present in SVF secretome which are key factors in the regenerative process induction.

REFERENCES

1. Thankam FG, Sharma CP, Chandy T, Thomas V. Genesis and historic evolution of tissue engineering and regenerative medicine [Internet]. Tissue Engineering: Current Status and Challenges. Elsevier Inc.; 2022. 1–7 p. Available from: <https://doi.org/10.1016/B978-0-12-824064-9.00018-6>
2. Nandakumar A. Towards improved scaffolds for bone tissue engineering [Internet]. [Enschede, The Netherlands]: University of Twente; 2012. Available from:

<http://purl.org/utwente/doi/10.3990/1.9789036533416>

3. Estrada C, Paz AC, López LE. INGENIERÍA DE TEJIDO ÓSEO : Consideraciones Básicas. *Rev EIA*. 2006;5:93–100.
4. López R. Producción de materiales híbridos bioreabsorbibles para la regeneración ósea [Internet]. Universitat Politècnica de València; 2014. Available from: <http://hdl.handle.net/10251/39775>
5. Baldino L, Cardea S, De Marco I, Reverchon E. Chitosan scaffolds formation by a supercritical freeze extraction process. *J Supercrit Fluids* [Internet]. 2014;90:27–34. Available from: <http://linkinghub.elsevier.com/retrieve/pii/S0896844614000631>
6. Deville S, Saiz E, Tomsia AP. Freeze casting of hydroxyapatite scaffolds for bone tissue engineering. *Biomaterials* [Internet]. 2006;27(32):5480–9. Available from: <http://www.ncbi.nlm.nih.gov/pubmed/16857254>
7. Norton K. Un breve recorrido por la historia de la protésica. *inMotion*. 2007;17(7):5.
8. Nature America Inc. Tissue engineering. *Nat Biotech*. 2000;18.
9. Berthiaume F, Maguire TJ, Yarmush ML. Tissue Engineering and Regenerative Medicine: History, Progress, and Challenges. *Annu Rev Chem Biomol Eng* [Internet]. 2011 Jun 17;2(1):403–30. Available from: <http://dx.doi.org/10.1146/annurev-chembioeng-061010-114257>
10. Vacanti J, Vacanti CA. The History and Scope of Tissue Engineering. In: *Principles of Tissue Engineering*. Third Edit. Elsevier Inc.; 2007. p. 3–6.
11. Meyer U. The History of Tissue Engineering and Regenerative Medicine in Perspective. *Fundam Tissue Eng Regen Med* [Internet]. 2009;5–12. Available from: <http://www.springerlink.com/index/10.1007/978-3-540-77755-7>
12. Analyze search results. *Tissue Engineering* [Internet]. Scopus Database tool. 2023 [cited 2022 Oct 26]. Available from: [http://aplicacionesbiblioteca.udea.edu.co:2055/term/analyzer.uri?sid=40CC97A961AF03D178DEEFD1B47D4A44.FZg2ODcJC9ArCe8WOZPvA:10&origin=result_slist&src=s&s=TITLE-ABS-KEY\(tissue+engineering\)&sort=plf-f&sdt=b&sot=b&sl=33&count=101394&analyzeResults=Analyze+re](http://aplicacionesbiblioteca.udea.edu.co:2055/term/analyzer.uri?sid=40CC97A961AF03D178DEEFD1B47D4A44.FZg2ODcJC9ArCe8WOZPvA:10&origin=result_slist&src=s&s=TITLE-ABS-KEY(tissue+engineering)&sort=plf-f&sdt=b&sot=b&sl=33&count=101394&analyzeResults=Analyze+re)
13. Cao Y, Vacanti JP, Paige KT, Upton J, Vacanti CA. Transplantation of chondrocytes utilizing a polymer-cell construct to produce tissue-engineered cartilage in the shape of a human ear. *Plast Reconstr Surg* [Internet]. 1997 Aug;100(2):297–302; discussion 303-4. Available from: <http://content.wkhealth.com/linkback/openurl?sid=WKPTLP:landingpage&an=00>

006534-199708000-00001

14. UnivDatos (Market Insights) (2023). Tissue Engineering Market: Current Analysis and Forecast (2021-2027).

CHAPTER I:

ISOLATION OF ADIPOSE- DERIVED STEM CELLS USING *Vibrio alginolyticus*-based COLLAGENASE: CASE STUDY

PROLOGUE

Brene Brown wrote, “To fall in love with yourself is the first secret to happiness.” Personal interactions are highly ruled by how a person sees himself. Damage tissue, significantly damaged skin, affects not only the tissue itself but the psychological well-being of the person. This chapter presents a case study of the evaluation of a novel collagenase with future applications in wound debridement necessary for scar treatment.

1. BACKGROUND

Regenerative cell therapy, which passes on to the therapeutic accomplishment of stem cells to recover diseased or damaged tissue, has obtained strengthening consideration from scientists and clinicians (1,2). In this regard, the use of enzymatic treatments has been described as a good method in the remotion of lesioned tissue stimulating the endogen staminal regenerative niche to induce the self-healing capacity (3). However, it is important an initial *in vitro* approach to understand the enzymatic characteristics of new enzymes.

Mesenchymal Stem Cells (MSCs) are multipotent fibroblast-like cells capable of self-renewal and differentiate under adequate stimuli into different cell lineages such as adipocytes, chondrocytes, or neurons that can be harvested from diverse adult tissues (4–7). MSCs are responsible for maintaining the functionality of the body by substituting cells that can no longer accomplish their role in an organ or tissue (8). It has been found that MSCs not only present the capacity to differentiate into a variety of cell types but also possess the ability to secrete high quantities of cytokines and growth factors (fibroblast growth factor, keratinocyte growth factor, IL-6, IL-7, among others) increasing the MSCs effect in the reparative processes (9). MSCs carry considerable engagement for tissue regeneration due to their essential capability to supply a renewable contribution of progenitor cells that can build several cell varieties, whole tissue structures, and organs (10,11). The primary sources used to isolate MSCs are some adult and fetal tissues such as amniotic fluid, peripheral blood, bone marrow, adipose and so forth (12). Among these, adipose tissue stands out the most, given that it is an abundant and available supply of MSCs and is considered as a discarded tissue after procedures such as liposuction or abdominoplasty (13). For this reason, autologous adipose-derived stem cells (ASCs) have developed into highly interesting for the usage of regenerative cell therapy given the high availability and differentiation capability into different cellular lineages (14–19). The clinical use of ASCs is increasing rapidly because of their encouraging results across a wide range of clinical applications (20–22).

Optimizing the isolation of ASCs is essential not only to improve the extraction efficiency but also to correctly identify the physiological level of extracted ASCs, which determines their possible clinical applications (23). There have been studied different isolation methodologies of ASCs to optimize the extraction separating the highest possible amount of living ASCs from the lowest achievable quantity of adipose tissue in the shortest workable time. Some of these methods are focused on mechanical isolation using shear force, centrifugal force or turbulence force (24–32), and some others use enzymatic digestion (33,34). In this last regard, bacterial collagenase is the most conventional proteolytic enzyme used to disaggregate tissues (35). The most popular commercially available bacterial collagenase is a lyophilized extract of the anaerobic culture of *Clostridium histolyticum*. Among the best-known uses of *C. histolyticum* collagenase in the medical field are wound debridement (3,36), treatment of Dupuytren's disease (37–39), and treatment of collagen plaque in the tunica albuginea of Peyronie's disease (40,41). However, *C. histolyticum* collagenases present low collagen selectivity degrading other membrane proteins such as fibronectin and decorin, which are fundamental components of the extracellular matrix (42). The low selectivity of *C. histolyticum* collagenases is probably due to their proteolytic composition variability (43). On this regard, the study on collagenases derived from diverse bacteria strains has

gained attention. Those of the genus *Vibrio* are one of the most encouraging bacteria, a non-pathogenic strain well known as protease producers, praiseworthy of furthermore attention and investigation as a wellspring of enzymes (44,45). The first reported collagenolytic enzyme was the collagenase from *Vibrio alginolyticus* chemovar *iophagus* bacteria which was first named as *Achromobacter collagenase* or *achromase*, recently known as *Vibrio collagenase*. The *V. collagenase* is an 81875Da zinc metalloproteinase with a specific activity towards collagen substrates (42,44,46). Due to its low metabolic activity against fibronectin and decorin, the primary utility of *Vibrio collagenases* counts on their capability to perform the careful eradication of necrotic tissue (42,47) with the only minor implication of the peri-wound healthy tissues (48,49). The *V. collagenase* has established to be valuable and suitable as debriding instrument and is being favorably related to pharmaceutical uses (50). The value and accordance of collagenase has been a recurring changeable in the literature between batches and manufacturers (51). Moreover, at the present day, the use of enzymes implies high costs and might impact on safety and efficacy (52,53).

The translation of research-based methods into the process for large-scale preparation of clinical-grade ASCs contemplating the Good Manufacturing Practice rules is crucial and firmly based on the safety, purity, and efficacy of cells. The procedure demands rigorous Quality Control validation of all pivotal points during fabrication (54).

This study aimed to evaluate a novel *Vibrio* collagenase enzyme for the isolation of Adipose-derive Stem Cells, comparing cellular yield, cellular viability, and number of living cells per ml of lipoaspirate in comparison with the standard research-used *Clostridium* collagenase.

2. MATERIALS AND METHODS

2.1. Adipose tissue collection

The adipose samples were collected from 10 patients after an informed consent through a liposuction procedure. The samples collection followed the ethical guidelines established by the review committee for human studies. To obtain the adipose sample, it was injected Klein tumescence solution (2% Lidocaine solution: 0.8% w/v; Adrenaline 1mg/mL solution: 0.1% v/v in 0.9% saline) 10 min before the liposuction. Around 30mL of lipoaspirate was collected from the abdominal area of each donor with a cannula of 11 G, 6 holes, and a 20 mL Vac-Lock syringe.

2.2. Adipose tissue enzymatic digestion

The study was divided into two main parts. The first part consisted of the optimization of the adipose digestion using a novel *Vibrio alginolyticus*-based collagenase with an enzymatic activity of 1U/mL. For this purpose, it was selected as a control the standard enzymatic digestion consisting of 1mg/mL of enzyme and 45min of incubation time. Additionally, to optimize the Fidia collagenase process, the enzyme concentration and the incubation time were modified. The evaluated enzyme concentrations are displayed in Table 1 with the different evaluated incubation times for each concentration.

Table 1. Name code of the evaluated enzyme concentration of Fidia collagenase with the evaluated incubation time for each concentration.

Name code	Enzyme concentration (mg/mL)	Incubation time (min)
1x	0.9	45
2x	1.8	45, 30, 20
4x	3.6	30, 20

The lipoaspirate sample was divided into portions of 5 mL each for every evaluated combination of parameters. Every part was added into 5 mL of 1X PBS (Phosphate Base Solution) with the evaluated concentration of *V. alginolyticus* collagenase and 2% BSA (Bovine Serum Albumin) and placed in agitation at 37°C, evaluating different incubation times. Once the time passed, the digestion process was stopped with complete growth medium (DMEM supplemented with 10% Fetal Bovine Serum, 1% of 1:1 penicillin/streptomycin and 0,6% Amphotericin B) and centrifuged for 5 minutes at 3000 rpm.

The obtained pellet of each portion was resuspended in 1 mL of complete growth media and filtered with a cell strainer to be seeded in a T25 flask. The extracted cells were evaluated regarding cellular yield, clonogenic and proliferation capacity, and the optimized parameters were further characterized with flow cytometry and differentiation potential.

The second part of the study consisted of the confrontation of the previously optimized method with two commercial *Clostridium histolyticum*-based collagenases with an enzymatic activity of 250 U/mL: a commercial *C. histolyticum* blend and Collagenase Type I (GIBCO life technology, USA). Both commercial collagenases were prepared in 1mg/mL concentration in 1X HBSS (Hank's Balanced Salt Solution) with 2% of BSA. The adipose tissue was divided into portions of 5 mL and was enzymatically digested in 5mL of each commercial collagenase solution at 37°C for 45 min in agitation. The enzymatic action was blocked with complete growth medium, and the following steps were executed as previously described. The extracted cells with the optimized method and the commercial enzymes were compared in terms of *cellular yield*, *clonogenic* and *proliferation capacity*, and in terms of *cellular viability* on expanded cells.

Intra and inter-donor comparative analyses were performed. Figure 1 summarizes the followed methodology.

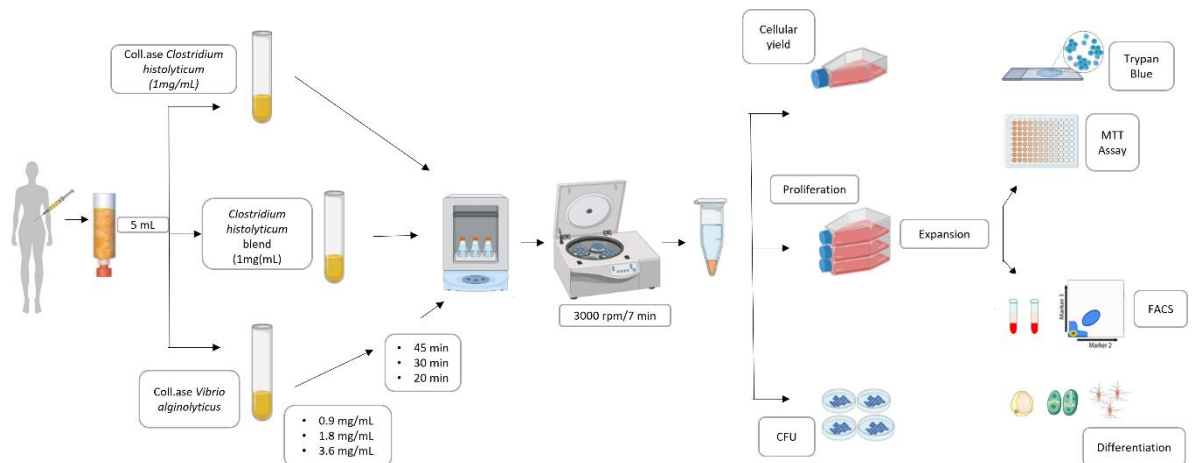


Figure 1. Experimental plan for the *V. alginolyticus* collagenase optimization method and comparison with commercial enzymes.

2.3. Cellular yield

The extracted cells were counted for cellular yield calculation considering the number of extracted free cells divided by the processed fat volume. The number of living cells was calculated using the Trypan Blue exclusion assay in a CytoSMART counter (Automated Image-Based Cell Counter, version 1.5.0.16380, CytoSMART Technologies B.V., Eindhoven, Netherlands).

2.4. Clonogenic capacity

To evaluate the clonogenic capacity of the extracted cells, they were plated in triplicate in a 12-well plate at a concentration of 1000 cells/mL. The cells were incubated in a humidified atmosphere with 5% CO₂ at 37°C for 14 days changing the medium every 48 h. The cells were stained with Toluidine Blue (Sigma-Aldrich, Milan, Italy) on the last study day to count the colonies. The colony former unit (CFU-F) was calculated as a percentage of the number of colonies divided by the number of seeded cells.

2.5. Proliferation capacity

The extracted cells were seeded on a 25 cm² T-flask with complete culture medium and incubated in a humidified atmosphere at 37°C with 5% CO₂. The first medium change was performed after 72 h from the enzymatic digestion, and the subsequent changes every 48 h. The proliferation capacity was determined considering the required days to reach 80% confluence.

2.6. Immunophenotyping

Collected cells with the optimized enzymatic digestion immediately after (Passage 0), as well as the subsequent subculture cells (Passage 4), were characterized by flow cytometry. The digested adipose tissue was centrifuged at 3000 rpm for 6 min. The cell pellet was incubated with 1 mL of erythrocyte lysis buffer 1X (Macs Miltenyi Biotec, Milan, Italy) for 10 min and filtered through a 70 µm cell-strainer. Subsequently, cells were washed with 1 mL in PBS (1X) and incubated (1×10^5 for

each tube) with conjugated antibodies on ice for 30 min. After incubation, the pellets were centrifuged (5000 rpm, 7 min) and resuspended in 100 μ L of PBS (1X). The antibodies used were: CD45 FITC conjugate (1:20 dilution), CD34 PE conjugate (1:5 dilution), CD90 PE conjugate (1:20 dilution), CD73 BV421 conjugate (1:5 dilution), CD34 APC conjugate (1:20 dilution), CD146 APC conjugate (1:5 dilution), CD105 PE conjugate (1:5 dilution), SEEA3 FITC conjugate (1:5). For cell viability, Propidium Iodide was used. All antibodies were purchased from BD Biosciences (Becton Dickinson Italy S.P.A., Milano, Italy). Immunophenotyping was performed through a chant II FACS (BD, Becton Dickinson, Milano, Italy).

2.7. Differentiation assay

To evaluate the differentiation potential of the extracted cells with the optimized parameters, cells from passage 4 (P4) were used for both treated and control stained compared with differentiated cells extracted with Collagenase Type I, each in triplicate. For adipogenic and osteogenic differentiation, 5000 cells were seeded in a 12-well plate in triplicate and incubated at 37°C with 5% CO₂. After 24 h of cell incubation, the complete culture medium was replaced with adipogenic and osteogenic medium, respectively (StemPro osteogenesis differentiation Kit–GIBCO Life Technology, Monza, Italy). For the adipogenic differentiation capability, cells were fixed after 14 days of study with Baker's fixative (Bio-Optica, Milan, Italy) for 10 min at 4°C as recommended by the fabricant, washed for 10 min with tap water, stained with Oil-Red-O ready-to-use solution (Bio-Optica, Milan, Italy) for 15 min and Mayer's Hematoxylin (Bio-Optica, Milan, Italy) for 5 min. Finally, the cells were washed with tap water for 5 min and mounted with Mount Quick aqueous solution (Bio-Optica, Milan, Italy).

After 14 days of incubation, the osteogenic differentiation capacity was evaluated by staining the cells with Alzarin Red solution (Merck KGaA, Darmstadt, Germany) for 3 min post-fixation with 4% formaldehyde (Bio-Optica, Milan, Italy) in PBS 0.05 M for 30 min at 4°C. The Alzarin Red was washed with distilled water, followed by immersion of the samples in Mayer's Hematoxylin for 30 s. Finally, the glass coverslips were dehydrated in an ethanol gradient concluding with two passages in xylene to be mounted with Entellan (Merck KGaA, Darmstadt, Germany).

The differentiation in the chondrogenic lineage was evaluated by resuspending 1 x 10⁶ cells in 5 μ L of complete culture medium in triplicate and incubating for 2 h in a 12-well plate. After time passed, the chondrogenic medium (StemPro chondrogenic differentiation Kit, GIBCO Life Technology, Monza, Italy) was added and changed every 3 days. After 21 days of study, the cells were fixed with 4% formaldehyde in PBS 0.05 M for 30 min at 4°C. The fixative was washed with distilled water, and the cells were stained with Alcian Blue solution (Merck KGaA, Darmstadt, Germany) for 40 min in slow agitation and later with Nuclear Fast Red (Bioptica, Milan, Italy) for 20 min. The samples were dehydrated and mounted with Entellan.

The same 4th passage cells with complete culture media were used as control, and they were seeded and stained following the same procedure for every lineage. Once the samples were completely dried, the cells were imaged in light microscopy using

an Olympus BX-51 microscope (Olympus, Tokyo, Japan) equipped with a digital camera (DKY-F58 CCD JVC, Yokohama, Japan) and connected to a PC endowed with Image-Pro Plus 7.0 software. The mounted samples were gently cleaned with ethanol, then placed on the microscope slides holder, and 5 images for each slide were acquired using a 20X objective for quantifying the lipid droplets, 10X objective for the osteogenic and 4X for chondrogenic quantification. Photoshop software (Adobe Photoshop CS6 v13.0 extended) was used for each quantification to isolate the specific differentiation staining color (red for lipid droplets and calcium deposits, blue for cartilage-like matrix). Successively, a custom-designed ImageJ plugin (U.S. National Institutes of Health), in blind condition, was used to make a binary image and quantify the differentiation-specific color previously isolated. The number of lipid droplets (referred to as red spot on the cell cytoplasm) was quantified for the adipogenic differentiation. For chondrogenic differentiation was considered the Area of the chondrogenic aggregates (marked by the Alcian blue staining), and for the osteogenic differentiation was quantified as the calcium deposit area (marked from the Alzarin Red staining). After the semi-quantification with ImageJ, the data was transferred into a PRISM file for the statistical analysis and graph creation.

2.8. Cellular viability test

To evaluate the potential cytotoxicity activity of the *V. alginolyticus* Collagenase at the optimized protocol, two viability tests were performed compared with Collagenase type I and *C. histolyticum* blend. The first viability test was the Trypan Blue Exclusion test. Expanded cells (P4) were detached and divided into three portions, one for each evaluated collagenase. The viability of each part was measured with Trypan Blue solution in a CytoSMART counter (Automated Image-Based Cell Counter, version 1.5.0.16380, CytoSMART Technologies B.V., Eindhoven, Netherlands) and named as Viability Pre-Treatment. The cells were then placed in contact with the evaluated collagenases at the optimized concentration for *V. alginolyticus* collagenase and 1mg/mL for Collagenase type I and *C. histolyticum* blend and incubated at 37°C for 20 min in agitation. As previously mentioned, the Viability Post-Treatment was measured with Trypan Blue at the end of the incubation time. The test was performed in triplicate.

The second viability test was the Methyl-thiazolyl-tetrazolium (MTT) colorimetric assay for metabolic activity. P4 cells were detached and divided into four portions, one with no treatment as control and the remaining three were treated with the evaluated enzymes at the optimized concentration for *V. alginolyticus* collagenase and 1mg/mL for Collagenase type I and *C. histolyticum* blend. All four portions were incubated at 37°C for 20 min in agitation. After the time passed, 1×10^4 cells were seeded in sextuplicate for each evaluated enzyme with 100 μ L of complete growth medium in a 96-well plate. The cells were incubated for 24 hours at 37°C and 5% CO₂. The medium was removed after the incubation time, and the cells were washed with 1X PBS. The cells were treated with 100 μ L of MTT (3-(4,5-dimethylthiazol-2-yl)2,5-diphenyltetrazolium bromide) at a concentration of 5mg/mL (Sigma, Italy) and incubated for 4 hours in the dark. Subsequently, the formed formazan crystals were dissolved in 100 μ L of dimethyl sulfoxide (DMSO) for 10 min. The optical density was measured in a microplate reader (HTX

Microplate Reader BioTek Instruments, Winooski, VT, USA) at a wavelength of 530 nm. The cell viability was calculated using equation 1 as a percentage of the absorbance of the treated cells in relation to the absorbance of control cells. All measurements were performed in triplicate for each treatment and control cell.

$$\%cells\ viability = \left(\frac{A_{Treatment}}{A_{Control}} \right) * 100$$

Finally, the expanded cells treated with the evaluated enzymes were morphologically analyzed through a Transmission Electron Microscope (TEM) to evaluate cell integrity. The expanded cell pellets obtained after enzymatic treatments were fixed for 1 h in 2% glutaraldehyde in 0.1 M phosphate buffer solution (PBS) and, after washed, postfixed for 1 h in 1% OsO₄ diluted in 0.2 M K₃Fe (CN)₆. After rinsing in 0.1 M PBS, the samples were dehydrated in graded acetone concentrations and embedded in a mixture of Epon and Araldite (Electron Microscopic Sciences, Fort Washington, PA, USA). Ultrathin sections were cut at 70 nm thickness on an Ultracut E ultramicrotome (Reichert-Jung, Heidelberg, Germany), placed on Cu/Rh grids and contrasted with lead citrate. Samples were observed with a Philips Morgagni 268 D electron microscope (Fei Company, Eindhoven, The Netherlands) equipped with a Megaview II camera to acquire digital images.

2.9. Statistical Analyses

Statistical analyses were performed using GraphPad Prism 7.03 for Windows (GraphPad Software, La Jolla, CA, USA). The data is reported as the mean ± standard error obtained after analyzing four consecutive patients. One-way analysis of variance (ANOVA) and the multiple comparisons tests (Tukey test) was employed. A confidence interval of 95% was contemplated to compare the evaluated experimental groups considering a *p*-value < 0.05 to indicate the differences were statistically significant.

3. RESULTS

3.1. Optimization of *V. alginolyticus* collagenase adipose tissue digestion process

3.1.1. Cellular yield, clonogenic potential and proliferation capacity

The extracted cells obtained after the enzymatic digestion with the *V. alginolyticus* Collagenase in different concentrations and incubation time were analyzed in cellular yield, viability, proliferation capacity, and clonogenic potential. Figure 2.A shows the number of nucleated cells for mL of fat of all the evaluated protocols being higher with the 4x / 20 min treatment compared to the other protocols. Considering the concentration of 1 mg/mL with an incubation time of 45 min as the "standard method" (cell yield 100%), the cellular yield of the method 4x / 20 min resulted in 235.49 ± 35.85%. However, there are no significant differences among the treatments. Figure 2.B shows the relative proportion of CFU-F (colony-forming unit fibroblast) evaluated 7 and 14 days after the seeding. The graphic shows that

the 2x / 45 min protocol presents the highest among the treatments to extract colony-forming units from adipose tissue. However, it can be seen from Figure 2.C that cells extracted with 4x / 20 min protocol present a faster population doubling time, which means that these cells required fewer days to reach confluence than the other methods.

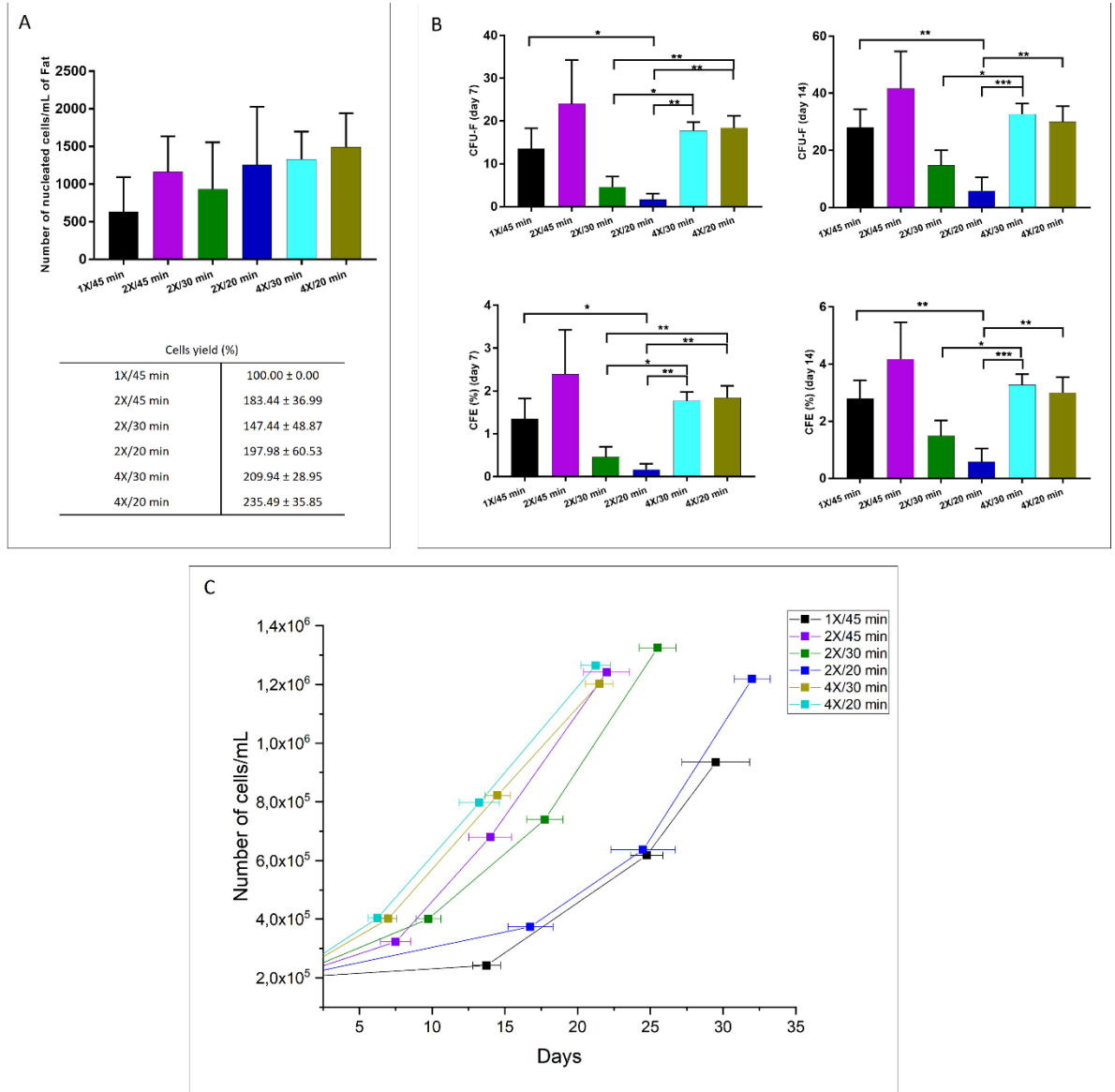


Figure 2. (A) Cellular yield, (B) clonogenic potential and (C) cellular growth of extracted cells after the enzymatic digestion with *V. alginolyticus* collagenase varying concentration and incubation time. The results are shown as the mean ± standard error indicating the significant statistical differences (*: p-value <0.05, **: p≤0.01, ***: p≤0.001).

Figure 3.A shows the percentage of cellular viability obtained with the studied methods. As seen, there is no significant difference among the treatments in terms of cell viability; for all the protocols, it was found to be over 96%. Additionally, Figure 3.B presents the proliferation capacity of the different evaluated protocols. From the graphic, the elevated proliferative function of the extracted cells is notorious after the 2x / 20 min methodology compared to the other procedures.

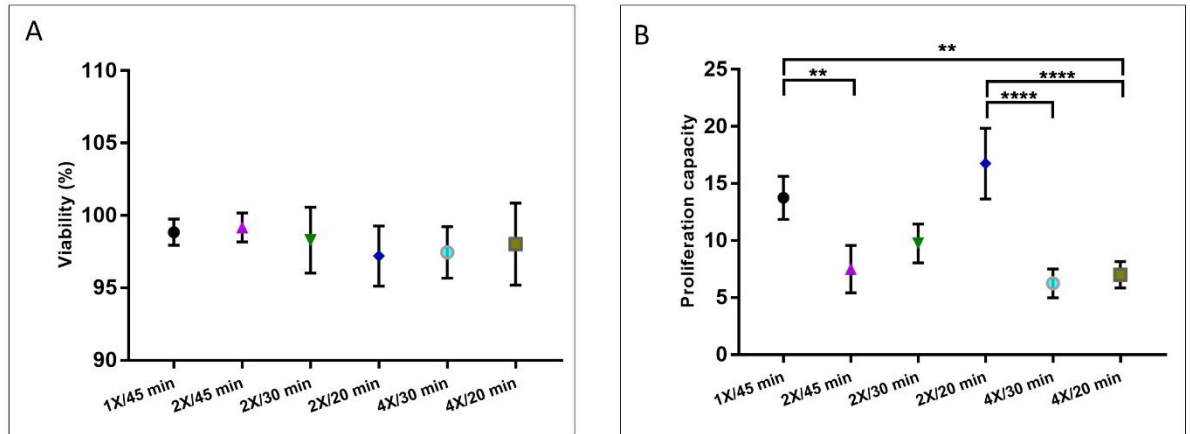


Figure 3. (A) Viability and (B) proliferation capacity of extracted cells after the enzymatic digestion with *V. alginolyticus* collagenase varying concentration and incubation time. The results are shown as the mean \pm standard error indicating the significant statistical differences (**: $p \leq 0.01$, ****: $p \leq 0.0001$).

Considering the obtained results, the selected optimized protocol was with a concentration of 4x with an incubation time of 20 min. The protocol was preferred given that its biological behavior is comparable to the other protocols but requires less time to digest adipose tissue.

3.1.2. Immunophenotyping of optimized *V. alginolyticus* collagenase method

The cells extracted with the optimized protocol were characterized to identify the cellular composition of the suspension after the extraction (passage 0; P0) and after being cultured them until passage 4 (P4). Figure 4 shows the FACS results at P0 for the different analyzed antibodies. It can be seen by the large cloud of data located on the negative side of the Propidium Iodide (PI) marker that most of the evaluated cells (approximately 99.8 %) were alive, which indicates that the results for the different antigens accurately represent the cellular population on the sample. Firstly, it was analyzed the CD45 antibody of the total evaluated cells, 6.4% were positive for CD45, representing a population of leucocytes. The remaining cells were negative for this marker which, alongside the positive expression of CD90, CD73, CD34 and CD105, characterize mesenchymal stem cells and cells of hematopoietic origin. On the same CD45 negative population, the positive expression of CD146 represents pericytes on the cellular suspension. Additionally, it was characterized by the presence of another subpopulation, the Multilineage-differentiating stress-enduring cells (MUSE), by the simultaneous expression of CD105 and SEEA3.

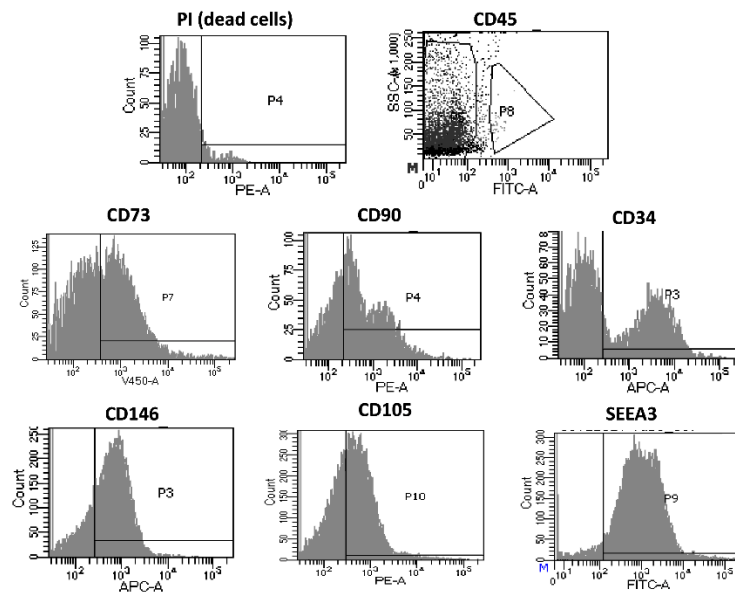


Figure 4. Immunophenotyping of the extracted cells with the optimized protocol of Fidia collagenase after the adipose tissue enzymatic digestion (P0).

On the other hand, Figure 5 shows the cellular characterization of the extracted cells with the optimized protocol after being cultured until passage 4. As seen with the P0 analysis, most of the evaluated cells were alive during the study. It can be seen that the cell expressed the typical markers for mesenchymal stem cells with a reduced presence of other subpopulations, as seen with the almost non-existent positive result for CD45 and CD34, markers for leucocytes and hematopoietic stem cells, respectively. Moreover, the cells maintain their multipotency, proven by the simultaneous positive response for CD105 and SEEA3 markers.

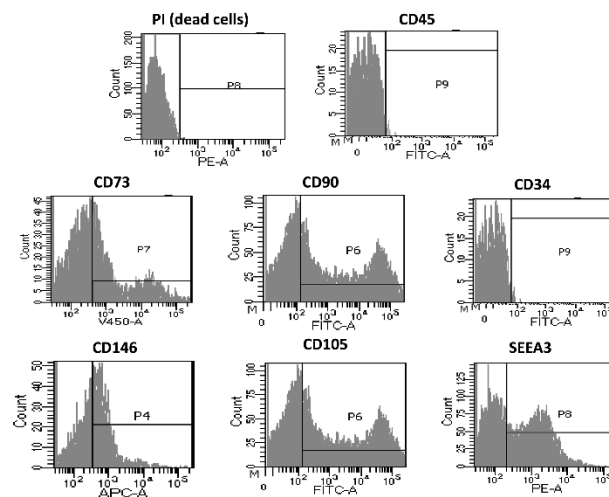


Figure 5. Immunophenotyping of extracted cells with the optimized protocol after culture procedure until reach passage 4 from the adipose digestion.

3.1.3. Analysis of multipotency

The extracted cells show a differentiative capacity in the three evaluated cellular lineages after being seeded in the differentiative culture medium in the evaluated

time. Figure 6.A shows representative images of the differentiation process compared with the differentiated cells extracted with collagenase type I and control (cells cultured in complete growth medium). The semi-quantification analysis of lipid droplets presented in figure 6.B showed comparable adipogenic differentiation between *V. alginolyticus* collagenase ($215,3 \pm 17,5$, n=3) and Collagenase Type 1 ($227,1 \pm 29,7$, n=3), while negative control resulted in $3,867 \pm 1,348$, n=3. Otherwise, *V. alginolyticus* collagenase resulted in a statistically significantly higher differentiation potential for chondrogenic ($313114 \mu\text{m}^2 \pm 79755 \mu\text{m}^2$, n=3) and osteogenic ($185119 \mu\text{m}^2 \pm 8431 \mu\text{m}^2$, n=3) lineages when compared to Col. Type 1 ($124643 \mu\text{m}^2 \pm 8240 \mu\text{m}^2$, n=3, $75572 \mu\text{m}^2 \pm 13652 \mu\text{m}^2$, n=3) and negative controls (0 ± 0 , n=3, $31,73 \pm 18,67$, n=3) as seen in figures 6.C and 6.D respectively. The results showed that the extracted cells with the optimized treatment present the capacity to proliferate in adipocytes, osteocytes, and chondrocytes.

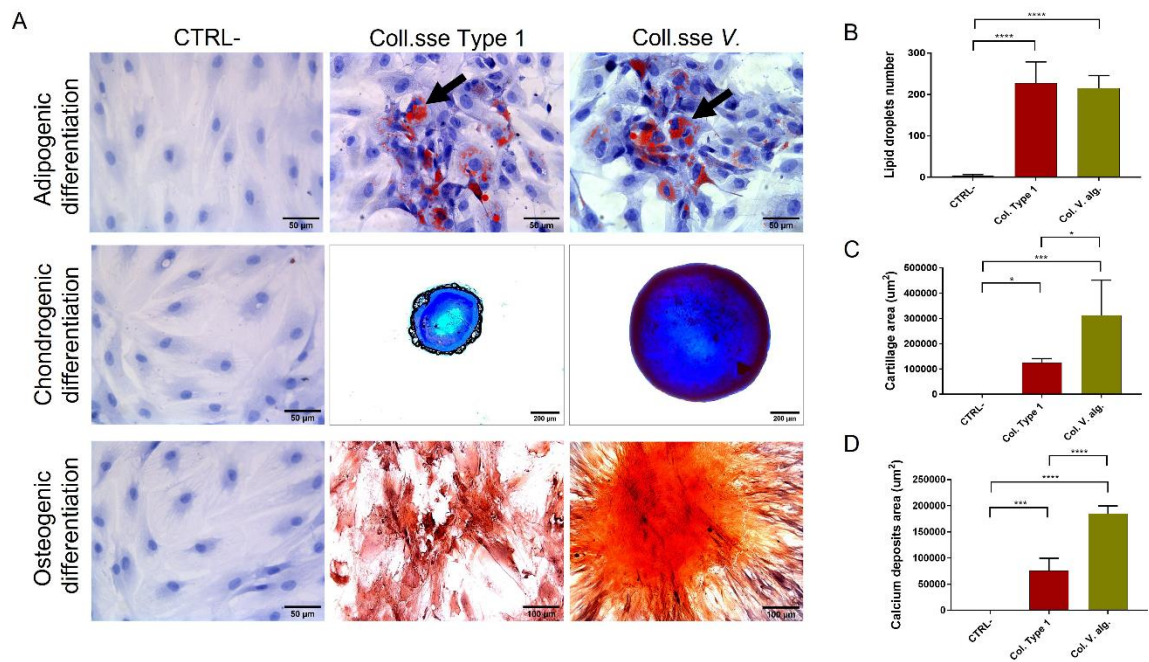


Figure 6. (A) Optical microscopy images of extracted cells with the optimized protocol compared with extracted cells with Col. Type I after being induced with differentiation medium (adipocytes present lipid droplets identified with black arrows, chondrocytes in blue and osteocytes in red) in comparison with not induced cells (CTRL-). Statistical graphs of semi-quantitative analysis of (B) lipid droplets number for adipogenic differentiation, (C) the cartilage-like matrix area for chondrogenic differentiation and (D) the Calcium deposits area for the osteogenic differentiation. The results are shown as the mean \pm standard error indicating the significant statistical differences (* $p \leq 0,05$ ** $p \leq 0,01$, *** $p \leq 0,001$, **** $p \leq 0,0001$).

3.2. Comparison of the optimized protocol with commercial collagenases

3.2.1. Cellular yield, clonogenic potential and proliferation capacity

Figure 7.A. shows the number of cells obtained after the three enzymatic treatments in the study. As seen in the graphic, an average of $1.49 \times 10^3 \pm 2.27 \times 10^2$ cells are obtained with *V. alginolyticus* collagenase 4x/20 min, while in the case of the two control treatments, the average of cell number was $9.64 \times 10^2 \pm 3 \times 10^2$ and $9.51 \times 10^2 \pm 1.75 \times 10^2$ for Collagenase Type I and *C. histolyticum* blend, respectively. Considering Collagenase Type I as the "gold standard," and therefore with a cellular

yield of 100% in terms of the number of extracted cells per mL of processed adipose tissue, the cellular yield percentage of *V. alginolyticus* collagenase 4x/20 min was 154.96 ± 23.59 proving to be more efficient, whereas for *C. histolyticum* blend the cellular yield percentage was of 98.70 ± 18.12 . However, there was no statistical significance among the data. Figure 7.B. reports the number of Fibroblasts-like Colony Forming Units (CFU-F) for the evaluated enzymatic treatments counted 7 and 14 days after the enzymatic digestion. The average CFU-F obtained with *V. alginolyticus* collagenase 4x/20 min was 18.42 ± 1.40 and 30 ± 2.74 after 7 and 14 days, respectively. In the case of both control collagenases, the average number of CFU-F after 7 days was 21.25 ± 2.66 and 25.75 ± 3.40 for Collagenase Type I and *C. histolyticum* blend, respectively. Even though the number of CFU-F for *V. alginolyticus* collagenase after 7 days is lower than the other two treatments, there is no statistical significance among the data. Notwithstanding, after 14 days, the number of CFU-F for *C. histolyticum* blend (45.25 ± 3.20) is statistically higher than the one reported for Fidia collagenase but with no difference from the average number for Collagenase Type I (36.50 ± 3.52). The graph also shows the clonogenic efficiency (CFE) at 7 and 14 days. *V. alginolyticus* collagenase 4x/20 min reports a CFE lower than Liberase at 7 days and even lower after 14 days. Figure 7.C. shows the cell growth curve of the evaluated enzymatic treatments. To assess the proliferative capacity of each product, after the enzymatic digestion, 2×10^5 cells were seeded for every treatment, and the time and number of cells were evaluated once the plates reached confluence. The proliferative capacity is comparable between the three methods with no statistical differences.

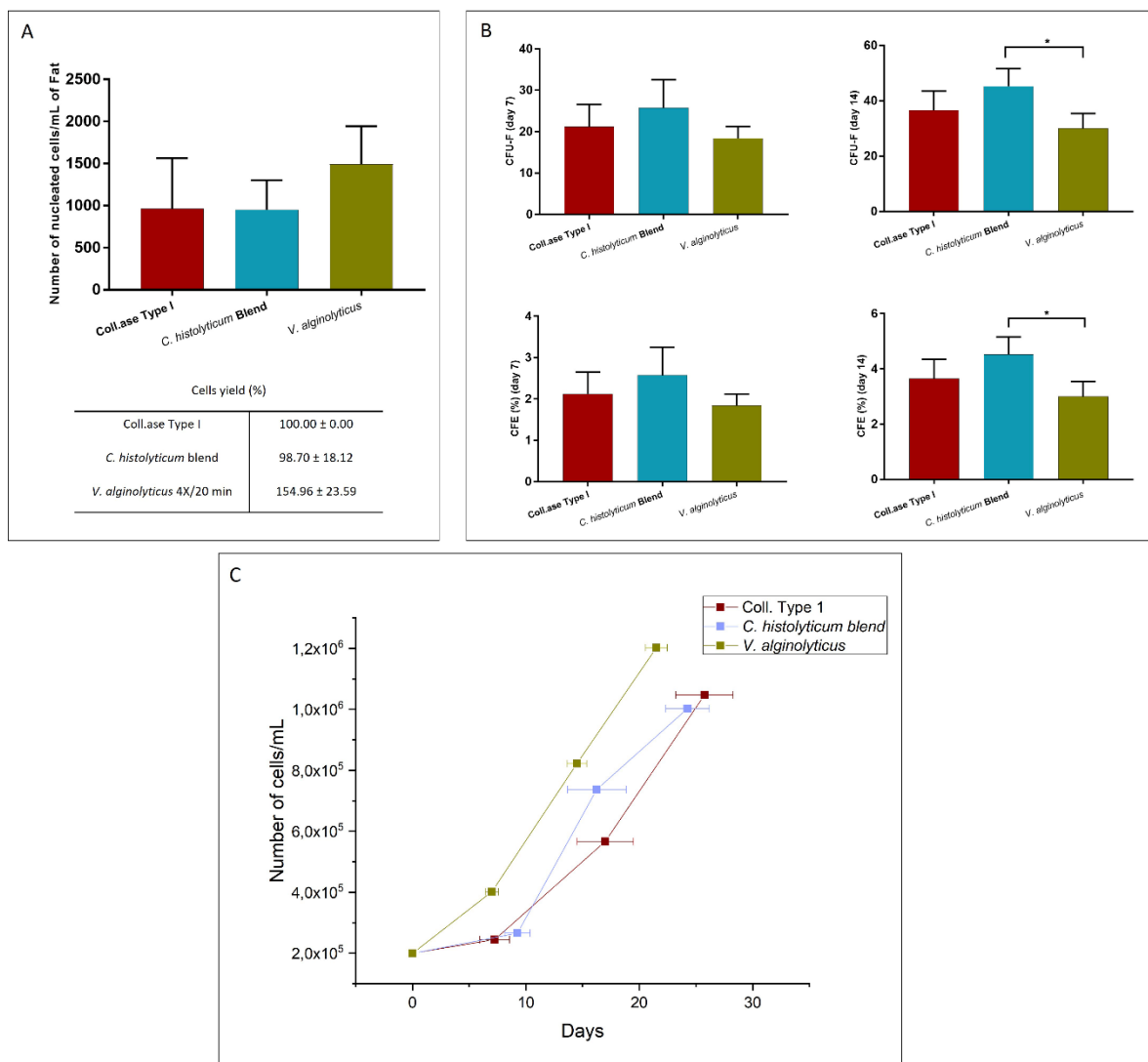


Figure 7. (A) Cellular yield, (B) clonogenic potential and (C) cellular growth of extracted cells after the enzymatic digestion with the optimized *V. alginolyticus* collagenase compared with Collagenase Type I and *C. histolyticum* blend. The results are shown as the mean \pm standard error indicating the significant statistical differences (*: p-value <0.05).

Figure 8 shows the cellular viability and proliferation capacity of the products extracted with the three enzymatic methods. It can be seen from the figure that there is no significant difference among the treatments. In terms of cell viability, all the evaluated methods present a viability percentage over 95%, while the proliferative capacity is over 5 days to confluence.

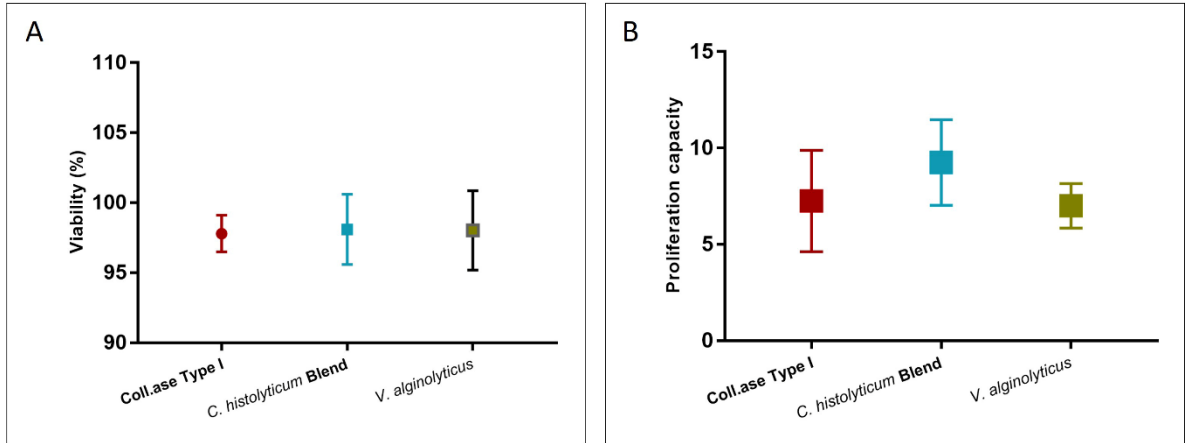


Figure 8. (A) Viability and (B) proliferation capacity of extracted cells after the enzymatic digestion with the optimized *V. alginolyticus* collagenase compared with Collagenase Type I and *C. histolyticum* blend. There are no statistical differences among the data.

3.2.2. Cellular integrity assay

To evaluate whether the studied collagenases preserve the integrity of the cell membrane, expanded ASCs were subjected to treatment with the three enzymes being assessed (*V. alginolyticus* collagenase 4x/20 min, Collagenase Type I and *C. histolyticum* blend) for 20 min.

The cellular viability was measured with the Trypan Blue mortality test before (pre) and after (post) the treatment with the collagenases. Figure 9.A. shows the mean percentage value of viability where it is noticeable that there is no difference between pre and post-treatment for *V. alginolyticus* collagenase 4x/20 min and Collagenase Type I, but a decrease in viability for cells treated with *C. histolyticum* blend is appreciable (pre-viability 97.81±0.92%, post-viability 82.03±1.69%).

Figure 9.B. shows the viability percentage of cells treated with the evaluated enzymes after 24 h of treatment assessed with the MTT test compared with control cells (cells not subjected to enzyme exposure). The cells treated with *V. alginolyticus* collagenase 4x/20 min and Collagenase Type I present viability of 94.88±17.88% and 86.46±6.06%, respectively. *C. histolyticum* blend, on the other hand, shows a viability percentage of 46.16±2.59%, which is nearly half of that for *V. alginolyticus* collagenase.

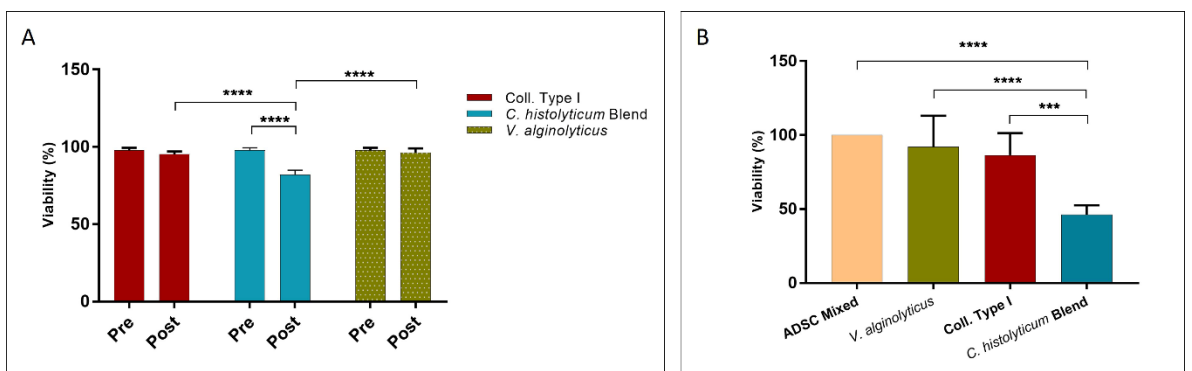


Figure 9. Viability percentage of expanded cells placed in contact with the optimized *V. alginolyticus* collagenase compared with Collagenase Type I and *C. histolyticum* blend for 20 min evaluated with the (A)

trypan blue exclusion test and (B) MTT test. The results are shown as the mean \pm standard error indicating the significant statistical differences ($p \leq 0.01$, ***: $p \leq 0.001$, ****: $p \leq 0.0001$).

Finally, the cells were morphologically evaluated through transmission electron microscopy. Figure 10 shows some TEM-selected images of P4 cells treated with the evaluated collagenases. The cells treated with the *V. alginolyticus* collagenase present a regular profile with characteristics of cellular activation and polarization; in fact, many cytoplasmic membrane extroversions are noted. The same aspects can be seen in the cells treated with Collagenase type I. Both treatments allow the release of extracellular vesicles following the formation of sessile and pedunculated bubbles on the cytoplasmic membrane. On the other hand, the cells treated with the *C. histolyticum* blend collagenase show irregularities of shape and size, with most of the cells characterized by diffuse cytoplasmic vacuolization and autophagosomes, which indicate cellular degenerative processes. Finally, the control cells present a rounded morphology consistent with the literature. The cytoplasm is well conserved with smooth endoplasmic reticulum activation, and the plasmalemma shows short microvillar protrusions.

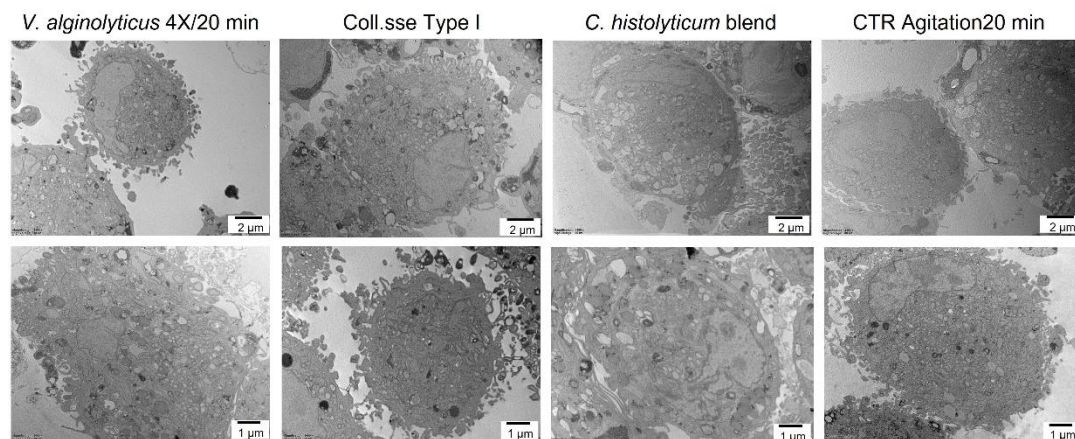


Figure 10. Representative images of TEM analysis of P4 cells treated with the optimized *V. alginolyticus* collagenase compared with Collagenase Type I and *C. histolyticum* blend for 20 min and cells placed in agitation for 20 min as control group.

4. DISCUSSION

Bacterial collagenases are a usual proteolytic family of enzymes for the disintegration of tissue; among these the most recognized in the medical practice is the lyophilized extract of *Clostridium histolyticum* (55). However, collagenases extracted from *C. histolyticum* possess reduced protein selectivity degrading not only collagen but other essential proteins (42). Though the *C. histolyticum* collagenase has been used for over four decades in laboratory, it is not suited for clinical practice given its long-lasting and non-standardized procedure (30,56). Collagenases extracted from *Vibrio alginolyticus* are primarily unexplored and understudied. Nevertheless, their uses are different and highly effective in the wound fields. This manuscript aimed to clarify the effects of a novel collagenase blend from *V. alginolyticus* strain, compared with standard collagenases regarding cell isolation, cellular yield, cell viability and number of extracted living cells from human adipose tissue.

The *V. alginolyticus*-based collagenase was evaluated at different concentrations and with different incubation periods. It was found that all evaluated protocols presented no statistical differences with respect to number of extracted cells, cellular viability, and cellular growth. However, regarding cellular growth, the mean necessary days to the confluence was lower for the concentration of 3.6 mg/mL with an incubation time of 30 and 20 min than the rest of the protocols, indicating a faster replication capacity that might influence cell behavior *in vivo*. Even though both protocols presented similar results for all the evaluated parameters, the one with the faster enzymatic reaction is preferable. The optimized method based on a concentration of 3.6 mg/mL of *V. alginolyticus* collagenase, and 20 min of incubation was used for further characterization. The FACS data showed that the extracted cells presented the stem cells characteristics preserving the distinctive phenotype. Additionally, these cells can differentiate in three mesodermal cellular lineages (adipocytes, chondrocytes, osteocytes) and are comparable with the extracted cells after collagenase Type 1 enzymatic reaction. The higher chondrogenic and osteogenic potential showed by *V. alginolyticus* collagenase in the multipotency analysis could be due to the higher integrity of extracellular and membrane proteins, and cellular receptors, essentials for signaling and differentiation processes.

Additionally, the optimized protocol was compared with the standard enzyme for laboratory procedures and a commercial blend of *C. histolyticum*-based collagenase. It was found that, in terms of cellular yield, clonogenic potential and proliferation capacity, there are no differences among the optimized *V. alginolyticus* collagenase and the standard ones. Even though there were not statistical differences among the data, the results showed that the mean value for the optimized protocol cellular yield was higher than those reported for both of the *C. histolyticum*-based collagenases. Furthermore, it was demonstrated with the cellular growth curve that the extracted cells with the *V. alginolyticus* collagenase reach confluence faster than the other two evaluated enzymes.

Finally, it was seen that the evaluated enzymes in direct contact with stem cells provoke different reactions affecting cellular vitality. It was found that cells in contact with *C. histolyticum* blend enzyme presented a considerably vitality reduction after 45 min of treatment, meanwhile cells in contact with the optimized method presented the highest vitality among the treatments.

These findings show that while the *V. alginolyticus* collagenase has a comparable enzymatic function than those *C. histolyticum* based, it does not affect additional structures that might be of vital importance in tissue regeneration applications. The enzymatic characteristics of *V. alginolyticus* collagenase are gentle on extracellular matrix structures as they are selective in their degradation capacity (44).

5. CONCLUSION

Using the *V. alginolyticus*-based Collagenase at a concentration of 3.6 mg/mL for 20 min of incubation time at 37°C, the highest enzymatic efficiency with the low incubation time was found compared with the other evaluated parameters. Additionally, the selected method showed comparable efficiency with two commercial collagenases, Collagenase Type I (GIBCO life technology) and *C. histolyticum* blend, but without affecting cellular integrity when used on expanded cells.

The cells extracted with *V. alginolyticus* collagenase at a 3.6 mg/mL concentration presented the phenotypic characteristic of stem cells and can differentiate into three mesenchymal lineages showing the potential applications of this enzyme in different areas of regenerative medicine.

REFERENCES

1. Koch TG, Berg LC, Betts DH. Current and future regenerative medicine-Principles, concepts, and therapeutic use of stem cell therapy and tissue engineering in equine medicine. *Can Vet J*. 2009;50(2):155–65.
2. Alzate-Correa D, Lawrence WR, Salazar-Puerta A, Higuera-Castro N, Gallego-Perez D. Nanotechnology-Driven Cell-Based Therapies in Regenerative Medicine. *AAPS J* [Internet]. 2022 Mar 15;24(2):43. Available from: <https://link.springer.com/10.1208/s12248-022-00692-3>
3. Ramundo J, Gray M. Enzymatic Wound Debridement. *J Wound, Ostomy Cont Nurs* [Internet]. 2008 May;35(3):273–80. Available from: <http://journals.lww.com/00152192-200805000-00005>
4. Rodríguez-Fuentes DE, Fernández-Garza LE, Samia-Meza JA, Barrera-Barrera SA, Caplan AI, Barrera-Saldaña HA. Mesenchymal Stem Cells Current Clinical Applications: A Systematic Review. *Arch Med Res*. 2021;52(1):93–101.
5. Samsonraj RM, Raghunath M, Nurcombe V, Hui JH, van Wijnen AJ, Cool SM. Concise Review: Multifaceted Characterization of Human Mesenchymal Stem Cells for Use in Regenerative Medicine. *Stem Cells Transl Med*. 2017;6(12):2173–85.
6. Wang J, Chen Z, Sun M, Xu H, Gao Y, Liu J, et al. Characterization and therapeutic applications of mesenchymal stem cells for regenerative medicine. *Tissue Cell* [Internet]. 2020;64(126):101330. Available from: <https://doi.org/10.1016/j.tice.2020.101330>
7. Ghorbani A, Jalali SA, Varedi M. Isolation of adipose tissue mesenchymal stem cells without tissue destruction: A non-enzymatic method. *Tissue Cell* [Internet]. 2014;46(1):54–8. Available from: <http://dx.doi.org/10.1016/j.tice.2013.11.002>
8. Vasanthan J, Gurusamy N, Rajasingh S, Sigamani V, Kirankumar S, Thomas EL, et al. Role of human mesenchymal stem cells in regenerative therapy. *Cells*. 2021;10(1):1–14.

9. Prasai A, El Ayadi A, Mifflin RC, Wetzel MD, Andersen CR, Redl H, et al. Characterization of Adipose-Derived Stem Cells Following Burn Injury. *Stem Cell Rev Reports* [Internet]. 2017 Dec 23;13(6):781–92. Available from: <http://link.springer.com/10.1007/s12015-017-9721-9>
10. Bernardo ME, Pagliara D, Locatelli F. Mesenchymal stromal cell therapy: a revolution in Regenerative Medicine? *Bone Marrow Transplant* [Internet]. 2012 Feb 11;47(2):164–71. Available from: <https://www.nature.com/articles/bmt201181>
11. Jovic D, Yu Y, Wang D, Wang K, Li H, Xu F, et al. A Brief Overview of Global Trends in MSC-Based Cell Therapy. *Stem Cell Rev Reports* [Internet]. 2022 Mar 28; Available from: <https://link.springer.com/10.1007/s12015-022-10369-1>
12. Murphy MB, Moncivais K, Caplan AI. Mesenchymal stem cells: Environmentally responsive therapeutics for regenerative medicine. *Exp Mol Med* [Internet]. 2013;45(11):e54-16. Available from: <http://dx.doi.org/10.1038/emm.2013.94>
13. Sherman LS, Condé-Green A, Naaldijk Y, Lee ES, Rameshwar P. An enzyme-free method for isolation and expansion of human adipose-derived mesenchymal stem cells. *J Vis Exp*. 2019;2019(154):1–5.
14. De Francesco F, Gravina P, Busato A, Farinelli L, Soranzo C, Vidal L, et al. Stem Cells in Autologous Microfragmented Adipose Tissue: Current Perspectives in Osteoarthritis Disease. *Int J Mol Sci* [Internet]. 2021 Sep 22;22(19):10197. Available from: <https://www.mdpi.com/1422-0067/22/19/10197>
15. Zuk PA, Zhu M, Mizuno H, Huang J, Futrell JW, Katz AJ, et al. Multilineage Cells from Human Adipose Tissue: Implications for Cell-Based Therapies. *Tissue Eng* [Internet]. 2001 Apr;7(2):211–28. Available from: <https://www.liebertpub.com/doi/10.1089/107632701300062859>
16. Zuk PA, Zhu M, Ashjian P, De Ugarte DA, Huang JI, Mizuno H, et al. Human Adipose Tissue Is a Source of Multipotent Stem Cells. Raff M, editor. *Mol Biol Cell* [Internet]. 2002 Dec;13(12):4279–95. Available from: <https://www.molbiolcell.org/doi/10.1091/mbc.e02-02-0105>
17. De Ugarte DA, Morizono K, Elbarbary A, Alfonso Z, Zuk PA, Zhu M, et al. Comparison of Multi-Lineage Cells from Human Adipose Tissue and Bone Marrow. *Cells Tissues Organs* [Internet]. 2003;174(3):101–9. Available from: <https://www.karger.com/Article/FullText/71150>

18. Nakagami H, Morishita R, Maeda K, Kikuchi Y, Ogihara T, Kaneda Y. Adipose Tissue-Derived Stromal Cells as a Novel Option for Regenerative Cell Therapy. *J Atheroscler Thromb* [Internet]. 2006;13(2):77–81. Available from: http://www.jstage.jst.go.jp/article/jat/13/2/13_2_77/_article
19. De Francesco F, Ricci G, D’Andrea F, Nicoletti GF, Ferraro GA. Human Adipose Stem Cells: From Bench to Bedside. *Tissue Eng Part B Rev* [Internet]. 2015 Dec;21(6):572–84. Available from: <https://www.liebertpub.com/doi/10.1089/ten.teb.2014.0608>
20. Hassani N, Taurin S, Alshammary S. Meta-Analysis: The Clinical Application of Autologous Adult Stem Cells in the Treatment of Stroke. *Stem Cells Cloning Adv Appl* [Internet]. 2021 Dec;Volume 14:81–91. Available from: <https://www.dovepress.com/meta-analysis-the-clinical-application-of-autologous-adult-stem-cells--peer-reviewed-fulltext-article-SCCAA>
21. Han Y, Li X, Zhang Y, Han Y, Chang F, Ding J. Mesenchymal Stem Cells for Regenerative Medicine. *Cells* [Internet]. 2019 Aug 13;8(8):886. Available from: <https://www.mdpi.com/2073-4409/8/8/886>
22. Zhuang W-Z, Lin Y-H, Su L-J, Wu M-S, Jeng H-Y, Chang H-C, et al. Mesenchymal stem/stromal cell-based therapy: mechanism, systemic safety and biodistribution for precision clinical applications. *J Biomed Sci* [Internet]. 2021 Dec 14;28(1):28. Available from: <https://jbiomedsci.biomedcentral.com/articles/10.1186/s12929-021-00725-7>
23. Alstrup T, Eijken M, Bohn AB, Møller B, Damsgaard TE. Isolation of Adipose Tissue-Derived Stem Cells: Enzymatic Digestion in Combination with Mechanical Distortion to Increase Adipose Tissue-Derived Stem Cell Yield from Human Aspirated Fat. *Curr Protoc Stem Cell Biol* [Internet]. 2019 Feb;48(1):e68. Available from: <http://doi.wiley.com/10.1002/cpsc.68>
24. Busato A, De Francesco F, Biswas R, Mannucci S, Conti G, Fracasso G, et al. Simple and Rapid Non-Enzymatic Procedure Allows the Isolation of Structurally Preserved Connective Tissue Micro-Fragments Enriched with SVF. *Cells* [Internet]. 2020 Dec 29;10(1):36. Available from: <https://www.mdpi.com/2073-4409/10/1/36>
25. Domenis R, Lazzaro L, Calabrese S, Mangoni D, Gallelli A, Bourkoula E, et al. Adipose tissue derived stem cells: in vitro and in vivo analysis of a standard and

- three commercially available cell-assisted lipotransfer techniques. *Stem Cell Res Ther* [Internet]. 2015 Dec 5;6(1):2. Available from: <https://stemcellres.biomedcentral.com/articles/10.1186/scrt536>
26. Purpura V, Bondioli E, Melandri D, Parodi PC, Valenti L, Riccio M. The Collection of Adipose Derived Stem Cells using Water–Jet Assisted Lipoplasty for their Use in Plastic and Reconstructive Surgery: A Preliminary Study. *Front Cell Dev Biol* [Internet]. 2016 Nov 22;4. Available from: <http://journal.frontiersin.org/article/10.3389/fcell.2016.00136/full>
 27. Raposio E, Bertozzi N. How to isolate a ready-to-use adipose-derived stem cells pellet for clinical application. *Eur Rev Med Pharmacol Sci*. 2017;21(18):4252–60.
 28. Coccè V, Brini A, Gianni AB, Sordi V, Berenzi A, Alessandri G, et al. A Nonenzymatic and Automated Closed-Cycle Process for the Isolation of Mesenchymal Stromal Cells in Drug Delivery Applications. *Stem Cells Int* [Internet]. 2018;2018:1–10. Available from: <https://www.hindawi.com/journals/sci/2018/4098140/>
 29. De Francesco F, Mannucci S, Conti G, Prè ED, Sbarbati A, Riccio M. A Non-Enzymatic Method to Obtain a Fat Tissue Derivative Highly Enriched in Adipose Stem Cells (ASCs) from Human Lipoaspirates: Preliminary Results. *Int J Mol Sci* [Internet]. 2018 Jul 15;19(7):2061. Available from: <http://www.mdpi.com/1422-0067/19/7/2061>
 30. Dai Prè E, Busato A, Mannucci S, Vurro F, De Francesco F, Riccio V, et al. In Vitro Characterization of Adipose Stem Cells Non-Enzymatically Extracted from the Thigh and Abdomen. *Int J Mol Sci* [Internet]. 2020 Apr 27;21(9):3081. Available from: <https://www.mdpi.com/1422-0067/21/9/3081>
 31. De Francesco F, Riccio V, Biswas R, Busato A, Di Bella C, Serri E, et al. Correction: De Francesco et al. In Vitro Characterization of Canine Microfragmented Adipose Tissue Non-Enzymatically Extracted from the Thigh and Lumbar Regions. *Animals* 2021, 11, 3231. *Animals* [Internet]. 2022 Mar 8;12(6):673. Available from: <https://www.mdpi.com/2076-2615/12/6/673>
 32. De Francesco F, Guastafierro A, Nicoletti G, Razzano S, Riccio M, Ferraro G. The Selective Centrifugation Ensures a Better In Vitro Isolation of ASCs and Restores a Soft Tissue Regeneration In Vivo. *Int J Mol Sci* [Internet]. 2017 May

- 12;18(5):1038. Available from: <http://www.mdpi.com/1422-0067/18/5/1038>
33. Gentile P, Scioli MG, Orlandi A, Cervelli V. Breast Reconstruction with Enhanced Stromal Vascular Fraction Fat Grafting. *Plast Reconstr Surg - Glob Open* [Internet]. 2015 Jun;3(6):e406. Available from: <http://journals.lww.com/01720096-201506000-00003>
 34. Grasys J, Kim B-S, Pallua N. Content of Soluble Factors and Characteristics of Stromal Vascular Fraction Cells in Lipoaspirates from Different Subcutaneous Adipose Tissue Depots. *Aesthetic Surg J* [Internet]. 2016 Jul;36(7):831–41. Available from: <https://academic.oup.com/asj/article-lookup/doi/10.1093/asj/sjw022>
 35. Daboor SM, Budge SM, Ghaly AE, Brooks S-L, Dave D. Extraction and Purification of Collagenase Enzymes: A Critical Review. *Am J Biochem Biotechnol* [Internet]. 2010 Apr 1;6(4):239–63. Available from: <http://www.thescipub.com/abstract/10.3844/ajbbbsp.2010.239.263>
 36. Kirshen C, Woo K, Ayello EA, Sibbald RG. Debridement: a vital component of wound bed preparation. *Adv Skin Wound Care* [Internet]. 2006 Nov;19(9):506–17. Available from: <http://journals.lww.com/00129334-200611000-00011>
 37. Hurst LC, Badalamente MA, Hentz VR, Hotchkiss RN, Kaplan FTD, Meals RA, et al. Injectable Collagenase Clostridium Histolyticum for Dupuytren’s Contracture. *N Engl J Med* [Internet]. 2009 Sep 3;361(10):968–79. Available from: <http://www.nejm.org/doi/abs/10.1056/NEJMoa0810866>
 38. Syed F, Thomas AN, Singh S, Kolluru V, Emeigh Hart SG, Bayat A. In Vitro Study of Novel Collagenase (XIAFLEX®) on Dupuytren’s Disease Fibroblasts Displays Unique Drug Related Properties. Deli MA, editor. *PLoS One* [Internet]. 2012 Feb 24;7(2):e31430. Available from: <https://dx.plos.org/10.1371/journal.pone.0031430>
 39. Martín-Ferrero MÁ, Simón-Pérez C, Rodríguez-Mateos JI, García-Medrano B, Hernández-Ramajo R, Brotat-García M. Tratamiento de la enfermedad de Dupuytren mediante la colagenasa del Clostridium histolyticum. *Rev Esp Cir Ortop Traumatol* [Internet]. 2013 Nov;57(6):398–402. Available from: <https://linkinghub.elsevier.com/retrieve/pii/S1888441513001094>
 40. Gelbard M, Lipshultz LI, Tursi J, Smith T, Kaufman G, Levine LA. Phase 2b Study of the Clinical Efficacy and Safety of Collagenase Clostridium Histolyticum in

- Patients With Peyronie Disease. *J Urol* [Internet]. 2012 Jun;187(6):2268–74. Available from: <http://www.jurology.com/doi/10.1016/j.juro.2012.01.032>
41. El-Khatib FM, Towe M, Yafi FA. Management of Peyronie’s disease with collagenase *Clostridium histolyticum* in the acute phase. *World J Urol* [Internet]. 2020 Feb 15;38(2):299–304. Available from: <http://link.springer.com/10.1007/s00345-019-02791-x>
 42. Di Pasquale R, Vaccaro S, Caputo M, Cuppari C, Caruso S, Catania A, et al. Collagenase-assisted wound bed preparation: An in vitro comparison between *Vibrio alginolyticus* and *Clostridium histolyticum* collagenases on substrate specificity. *Int Wound J*. 2019;16(4):1013–23.
 43. Van Wart HE. *Clostridium* Collagenases. In: *Handbook of Proteolytic Enzymes* [Internet]. Elsevier; 2013. p. 607–11. Available from: <https://linkinghub.elsevier.com/retrieve/pii/B9780123822192001265>
 44. Fukushima J, Shimura Y, Okuda K. *Vibrio* Collagenase. In: *Handbook of Proteolytic Enzymes* [Internet]. Elsevier; 2013. p. 604–6. Available from: <https://linkinghub.elsevier.com/retrieve/pii/B9780123822192001253>
 45. Salamone M, Nicosia A, Ghersi G, Tagliavia M. *Vibrio* Proteases for Biomedical Applications: Modulating the Proteolytic Secretome of *V. alginolyticus* and *V. parahaemolyticus* for Improved Enzymes Production. *Microorganisms* [Internet]. 2019 Sep 24;7(10):387. Available from: <https://www.mdpi.com/2076-2607/7/10/387>
 46. Rawlings ND, Barrett AJ, Finn R. Twenty years of the MEROPS database of proteolytic enzymes, their substrates and inhibitors. *Nucleic Acids Res* [Internet]. 2016 Jan 4;44(D1):D343–50. Available from: <https://academic.oup.com/nar/article-lookup/doi/10.1093/nar/gkv1118>
 47. Onesti MG, Fioramonti P, Carella S, Fino P, Sorvillo V, Scuderi N. A new association between hyaluronic acid and collagenase in wound repair: An open study. *Eur Rev Med Pharmacol Sci*. 2013;17(2):210–6.
 48. Riley KN, Herman IM. Collagenase promotes the cellular responses to injury and wound healing in vivo. *J Burns Wounds* [Internet]. 2005;4:e8. Available from: <http://www.ncbi.nlm.nih.gov/pubmed/16921413%0Ahttp://www.pubmedcentral.nih.gov/articlerender.fcgi?artid=PMC1501117>

49. De Francesco F, De Francesco M, Riccio M. Hyaluronic Acid/Collagenase Ointment in the Treatment of Chronic Hard-to-Heal Wounds: An Observational and Retrospective Study. *J Clin Med* [Internet]. 2022 Jan 21;11(3):537. Available from: <https://www.mdpi.com/2077-0383/11/3/537>
50. Bassetto F, Maschio N, Abatangelo G, Zavan B, Scarpa C, Vindigni V. Collagenase From *Vibrio alginolyticus* Cultures: Experimental Study and Clinical Perspectives. *Surg Innov* [Internet]. 2016 Dec 27;23(6):557–62. Available from: <http://journals.sagepub.com/doi/10.1177/1553350616660630>
51. Williams SK, Mckenney S, Jarrell BE. Collagenase Lot Selection and Purification for Adipose Tissue Digestion. *Cell Transplant* [Internet]. 1995 May 22;4(3):281–9. Available from: <http://journals.sagepub.com/doi/10.1177/096368979500400306>
52. Carvalho PP, Gimble JM, Dias IR, Gomes ME, Reis RL. Xenofree Enzymatic Products for the Isolation of Human Adipose-Derived Stromal/Stem Cells. *Tissue Eng Part C Methods* [Internet]. 2013 Jun;19(6):473–8. Available from: <https://www.liebertpub.com/doi/10.1089/ten.tec.2012.0465>
53. Agostini F, Rossi FM, Aldinucci D, Battiston M, Lombardi E, Zanolin S, et al. Improved GMP compliant approach to manipulate lipoaspirates, to cryopreserve stromal vascular fraction, and to expand adipose stem cells in xeno-free media. *Stem Cell Res Ther* [Internet]. 2018 Dec 11;9(1):130. Available from: <https://stemcellres.biomedcentral.com/articles/10.1186/s13287-018-0886-1>
54. Sensebé L, Bourin P, Tarte K. Good manufacturing practices production of mesenchymal stem/stromal cells. *Hum Gene Ther*. 2011;22(1):19–26.
55. Frederick RE, Bearden R, Jovanovic A, Jacobson N, Sood R, Dhall S. Clostridium Collagenase Impact on Zone of Stasis Stabilization and Transition to Healthy Tissue in Burns. *Int J Mol Sci* [Internet]. 2021 Aug 11;22(16):8643. Available from: <https://www.mdpi.com/1422-0067/22/16/8643>
56. Raposio E, Ciliberti R. Clinical use of adipose-derived stem cells: European legislative issues. *Ann Med Surg* [Internet]. 2017 Dec;24:61–4. Available from: <https://linkinghub.elsevier.com/retrieve/pii/S2049080117303953>

CHAPTER II:

COLLAGEN MEMBRANES FOR RECONSTRUCTIVE PURPOSES: CASE STUDY

PROLOGUE

The use of collagen membranes in regenerative medicine has been increasing since its beginnings in the mid-80s as an evolution of barrier membranes for regenerative applications. This chapter presents a case study where three different collagen membranes were evaluated to avoid capsular contracture during breast reconstruction/augmentation surgery.

1. BACKGROUND

After introducing breast prostheses in 1962, the number of these surgical procedures increased over the years, with an estimated 1'841,049 procedures worldwide in 2018 only for cosmetic purposes (1)(2). The growing incidence of breast cancer is the main reason for the rise of mastectomy interventions, which ultimately increase the number of reconstructive breasts surgery. In accordance to the World Cancer Research Fund, the most typical type of cancer in women is breast cancer, that reached over 2 million new cases in 2018, with European countries accounting for the highest proportion (3). The number of women undergoing breast reconstruction surgery after mastectomy through silicone implant-based procedures is steadily increasing (4). The formation of the peri-prosthetic capsule (PPC) is considered part of the local reparative process against the foreign material (implant), which involves a diversity of inflammatory cells (5–7). The PPC formation can become a problematic response when it contracts around the inserted material, causing hardness and deformity to the breast, known as capsular contracture (CC). The CC is an inflammatory reaction characterized by fibrosis surrounding the implant due to the action of excessive collagen production, which provokes hard and painful breasts (8). According to Atlan *et al.* (2018) (9), collagen fibre alignment presents a significant role in CC, which means that disrupting this orientation may reduce the incidence and severity of the contracture. The differences among the surfaces of mammary implants may influence the CC. In contrast, smooth surfaces allow the proper collagen fibre alignment; the texturized ones interfere with the fibre growth protecting against the CC (9)(10).

The CC formation is one of the most commonly reported complications after implant-based breast augmentation and represents an important and persistent cause of women morbidity (11). More than 10% of cases of CC report a noticeable and painful deformity (12). Its etiology and a proper strategy to prevent its formation must be ascertained. Different hypotheses about the formation of capsular contracture have been formulated, such as the activation of a cascade of biochemical events due to the movement of the prostheses (7). The pathogenesis of capsular contracture has been described as a multifactorial process: fibrotic reaction and recruitment of different cellular elements under pro-inflammatory stimulation (8). This fibrotic reaction is beneficial to support the implant by maintaining it in its position; however, if this fibrosis is excessive, it can cause pain and deformity to the breast (13). According to extensive studies, the capsular contracture pathogenesis seems to be due to an elevated recruitment of immune system cells such as macrophages, lymphocytes and fibroblasts, the predominant cell types within the capsule (14). It has been reported that the number of fibroblasts accumulated at the place of contact between the implant and the capsule is correlated with a high degree of pain and deformity (8). Fibroblasts regulate the secretion and orientation of collagen fiber during the contracture formation. During the formation of capsular contracture, the thickness of collagen bundles is increased, and the orientation of fibers appears regulated directly by fibroblasts (15). Another important type of cells involved in the development of capsule contracture are myofibroblasts which are contractile fibroblasts that are believed to furnish a contractile force reducing the capsule surface area, while the matrix of collagen remodels and gives support to the contracture (8)(16). Other cell types,

like lymphocytes and macrophages, have been described as having a role during the formation of capsular contracture due to the secretion of cytokines by myofibroblasts and fibroblasts (5). Regrettably, no successful preventive therapies are currently developed, and the conventional treatment requires surgical intervention for capsular remotion (11).

Since their introduction in the mid-80s as barrier cover, collagen membranes have been widely spread to be used as highly biocompatible and versatile scaffolds for tissue engineering applications due to native components that enhance cell migration, differentiation, and proliferation (17)(18). The use of acellular matrices (ACMs), the main element of the extra-cellular matrix (ECM) structure, has been gaining attention. They are obtained from human or animal tissues, properly treated, and deprived of any resident cell population (19)(20).

ACMs can be used to treat difficult-to-heal wounds, deep burn closure, and as a scaffold for organ parts and tissue reconstruction due to their capacity to support host tissue cell colonization and promote their differentiation (18)(21)(22). ACMs healing ability is regarding their capacity to induce wound repair by amplifying the collagen secretion and deposition and adjusting the reparative healing phases (23)(24). ACMs have been used as a coating material for silicone breast implants to prevent PPC contracture and the recruitment of macrophages, neutrophils, and cellular elements responsible for contracture formation (myofibroblast). It is considered that there is a high possibility that ACMs can attenuate the inflammatory response of tissue (25).

Due to ACMs being considered scaffolds, they must accomplish the same characteristics, such as promoting the healing process, progenitor cell differentiation, and mimicking the extra-cellular environment (26). Some researchers have described the influence of materials in stem cell differentiation, where the type of material directly affects the final differentiated cell (27).

Restoring the damaged tissue requires different types of cells, appropriate ECM components, and the collaboration of cytokines. Among these cells, adipocytes, which are the primary energy storage location, have a regenerative role due to the production of different adipocytokines involved in repair and regeneration processes (28)(29).

This study aimed to investigate three natural ACMs, two porcine-derived and one bovine-derived membrane, with different physical structures, such as porosity, thickness, and stratification, both *in vitro* and *in vivo*. *In vitro* cell-biomaterial interaction was analyzed through colonization capacity of adipose-derived stem cells (ASCs) in direct contact with the ACMs. Subcutaneous implantation of ACMs in mice was assessed to evaluate the tissue integration and biostimulation membrane-induced.

2. MATERIALS AND METHODS

2.1. *In vitro* evaluation

2.1.1. *Acellular collagen membranes*

In this study, three xenogeneic non-crosslinked membranes provided by DECO med S.r.l. (Venice, Italy) were evaluated:

- 0.6 mm thick porcine acellular dermis, without additional chemicals, manufactured by ADIPOMATRIX[®] processes (subjected to industrial secrecy) named ACM1.
- 0.6 mm thick porcine-derived dermal membrane prepared with a common enzymatic deantigenation named ACM2.
- 0.4 mm thick bovine-derived acellular pericardium membrane with a common enzymatic deantigenation named ACM3.

2.1.2. Morphological and Physical properties of membranes

Scanning Electron Microscopy (SEM) was performed to evaluate the membranes in dry and wet conditions. Each piece was fixed for 4 hours with glutaraldehyde 2% (Sigma Aldrich, Milan, Italy) in 0.1 M Phosphate Buffer Solution (PBS), postfixed in 1% osmium tetroxide (Sigma Aldrich, Milan, Italy) in PBS 0.1 M for 1 hour. Then, the samples were dehydrated in a graded concentration of ethanol (Sigma Aldrich, Milan, Italy), followed by a critical point dryer (CPD 030, Balzers, Vaduz, Liechtenstein), fixed to stubs with colloidal silver and sputtered with gold by a MED 010 coater (Balzers), to be imaged with FEI XL30 scanning electron microscope (FEI Company, Eindhoven, Netherlands). The increment of mean porous size of membranes due to the embedding in culture growth media was calculated using Image-J Software using 10 SEM images taken before and after the embedding process at the same magnification. In addition, the swelling ratio of the evaluated membranes was measured using Equation 1, where W_i is the initial weight of the membrane under dry conditions and W_w the weight after submerging the membrane in PBS for 24 hours at room temperature (30)(31).

$$S(\%) = \left(\frac{W_w - W_i}{W_i} \right) * 100 \quad \text{Equation 1.}$$

The porosity percentage was evaluated according to Archimedes principle and the procedure suggested by Lou T. *et al.* (2014 and 2016) (30)(31) using pure ethanol (Sigma-Aldrich, Milan, Italy) as displacement liquid. Membranes were weighed in dry (W) and subsequently soaked in 70% ethanol (Sigma-Aldrich, Milan, Italy) for 1 hour in vacuum conditions. After the time passed, wet membranes were submerged in a known volume (V_1) and weight (W_1) of pure ethanol. The system weight (W_2) and the displaced volume (V_2) were measured. The porosity percentage (ε) was calculated using Equation 2, considering pure ethanol density (ρ) at 20°C.

$$\varepsilon = \frac{(W_2 - W_1 - W) / \rho}{(V_2 - V_1)} \quad \text{Equation 2.}$$

2.1.3. Isolation and seeding of Adipose-derived Stem Cell

ASCs were isolated from human lipoaspirate of healthy donors (women of ages between 35 and 45 years) after informed consent, following the protocol described by Peroni *et al.* (2018) and Busato *et al.* (2020), using an enzymatic method (32)(33). The lipoaspirate samples were incubated in 1 mg/mL of Collagenase type

I (GIBCO life technology, Monza, Italy) dissolved in Hank's Balanced Salt Solution (HBSS, GIBCO Life Technology, Monza, Italy) with 2% of Bovine Serum Albumin (BSA, GIBCO Life Technology, Monza, Italy). Complete growth medium (Dulbecco's Modified Eagle's Medium (DMEM), Sigma-Aldrich, Italy) supplemented with 10% of Fetal Bovine Serum (FBS, GIBCO Life Technology, Monza, Italy), 1% of 1:1 penicillin/streptomycin (P/S, GIBCO Life Technology, Monza, Italy) solution, and 0.6% of Amphotericin B (GIBCO Life Technologies, Monza, Italy) was added to neutralise the enzymatic action. The extracted cells were incubated in a humidified atmosphere with 5% CO₂ at 37°C in a 25 cm² flask with complete growth medium. The cells were detached after reaching between 70 and 80% confluence by incubation with 0.25% trypsin (GIBCO Life Technology, Monza, Italy) at 37°C for 5 min, centrifuged at 3000 rpm for 7 minutes, and the cell pellet was re-plated in a 25 cm² flask. The cells were cultured until passage four (P4), following the procedure mentioned above.

2.1.4. ASCs colonization capacity and *in vitro* biostimulation

For each ACM, two 6-well plates were prepared for *in vitro* test, consisting of the incubation of a 1 cm² of the membrane with P4 cultured ASCs, for 7 and 14 days. For this aim, a glass was positioned at the bottom of the wells and simultaneously 1x10⁴ cells were seeded in each well, covered with 2 ml of complete growth medium and incubated at 37°C, 5% of CO₂ for 24 hours. After incubation, 1 cm² of each ACM was positioned in the wells (with both layers facing the bottom of the well) and incubated for 24 hours with complete growth medium (DMEM supplemented with 10% FBS, 1% P/S and 0.6% Amphotericin B). After 24 hours, ASCs were homogeneously seeded above and over the membranes. All the conditions were performed in triplicates. For all the wells, complete growth medium was replaced every 72 hours.

After 7 and 14 days, the medium was discarded and, both membranes and cells were processed for SEM (with the protocol reported above) and Oil-Red-Oil staining, respectively. Briefly, once the membranes were removed from the 6-well plate, the coverslips with adherent ASC were washed with PBS 0.1 M pH 7.4 and fixed for 30 min with 4% formalin (Bio-Optica, Milan, Italy) in PBS 0.05 M. The adherent cells were washed with PBS 0.1 M three times and stained with Oil Red Oil ready-to-use solution (Bio-Optica, Milan, Italy) for 30 minutes at room temperature. Samples were washed with PBS and stained with Mayer's Hematoxylin ready-to-use solution (Bio-Optica, Milan, Italy) for 2 minutes, at room temperature, and washed with tap water. The coverslips were mounted on a microscopy glass with a Mount Quick aqueous solution (Bio-Optica, Milan, Italy). Once the microscopy glasses were dried under the cabinet, samples were observed in light microscopy using an Olympus BX-51 microscope (Olympus, Tokyo, Japan) equipped with a DKY-F58 CCD JVC digital camera (Yokohama, Japan) with Magnification 20X. ASCs cultured with complete growth medium (without ACMs) were used as a negative control. Instead, ASCs cultured with specific adipogenic media (Sigma-Aldrich, Milan, Italy) were used as a positive control.

2.2. *In vivo* evaluation

2.2.1. *Membranes subcutaneous implant in mice*

For *in vivo* study were used n=30 Balb/c female mouse strain of 10-weeks old purchased from Envigo (Envigo, Milan, Italy) implanted in the left flank, 10 mice for each evaluated membrane. Animals were housed in a controlled environment, as indicated by the Interdepartmental Center for Animal Study and Research of Verona University (CIRSAL), with free access to food and water. The protocol of membrane implant was approved by CIRSAL and by the Italian Ministry of Health (protocol number 56DC9.38). For the subcutaneous implant, animals were anaesthetized using a face mask by inhalation of 2% isoflurane for 5 minutes and left at 1% for the duration of surgery. Moreover, animals were positioned on a heated bed to maintain a stable temperature during surgical procedures.

A subcutaneous pocket was made at the dorsal region, and 1 cm² of each membrane was implanted above the muscular fascia followed by a suture using a non-absorbable silk 3/8 13 mm 4.0 suture-thread. At the end of the surgery, animals were housed following the CIRSAL guidelines. Three mice for each group were sacrificed 7 days after surgery, three after 14 days, and the remaining mice were sacrificed at 30 days.

In addition, silicone prostheses were implanted in a group of n=3 animals (positive control) using the previously described protocol, and the animals were sacrificed 30 days after surgery.

2.2.2. *Magnetic resonance imaging (MRI) acquisition*

MRI was performed at different time points (7, 14, and 30 days after subcutaneous implantation) to evaluate the membranes and silicone prosthesis localisation and integration. Magnetic resonance images were acquired with a Bruker system operating at 7 T (Bruker Biospin, Ettlingen, Germany). T₂ weighted 3D RARE (Rapid Acquisition Refocused Echo) sequence was performed with the following parameters: echo time (TE) = 4 ms, repetition time (TR) = 1200 ms, field of view (FOV) = 25 x 25 x 30 mm, number of averages = 16, flip angle = 180 degrees, slice thickness = 0.350 mm, and matrix size (MTX) = 256 x 128 x 32 pixels. During the procedure, mice were anaesthetized by inhaling a mixture of O₂ and air containing 1–1.5% of isoflurane, placed in a prone position in the heated animal bed in a 3.5 cm diameter bird-cage coil. The acquisition parameters were maintained during the time of observation for all the animals. Moreover, the volume of each subcutaneous implant was determined with the MRI acquisition to quantify the reabsorption degree at different time points. The area occupied by the subcutaneous implant was manually selected, drawing a Region of Interest (ROI) in every slice, and the volume was calculated with Equation 3.

$$V = (\sum_{i=1}^n \rho u_i) * image\ resolution \quad \text{Equation 3.}$$

where ρu_i represents the number of pixels manually selected.

The percentage of membrane reabsorption was calculated at each time point using Equation 4:

$$\text{Reabsorption} = \left(\frac{V_t - V_0}{V_0} \right) * 100 \quad \text{Equation 4.}$$

where V_t is the volume at a time t and V_0 is the initial volume.

2.2.3. *Ex vivo evaluations*

After MRI acquisition at 14 and 30 days from subcutaneous implantation, mice were sacrificed, and ACMs with surrounding tissue was excised. The explanted samples were fixed in 10% formalin for 24 hours, paraffin-embedded and cut with a microtome to obtain sections of 7 μ m. For the histological evaluation, the slices were deparaffinised and stained with Mayer's Hematoxylin and Eosin (H&E, Bio-Optica, Milan, Italy) and Mallory's trichrome (MT, Bio-Optica, Milan, Italy). The same histological stainings were performed for the excised tissue exposed to the silicone prostheses after 30 days of implantation.

In addition, the samples were processed with Collagen type I (Coll. I) and Vascular Endothelial Growth Factor (VEGF) for immunohistochemical analysis to evaluate the tissue-ACMs integration. The slides were deparaffinized in xylene for 20 minutes, rehydrated and incubated with Sodium Citrate Buffer (10 mM Sodium Citrate and 0.05% of Tween 20, pH 6.0) for 20 minutes at 95-100°C to promote the antigen retrieval procedure. After slow cooling, the slices were incubated in hydrogen peroxide (3% in methanol) (Sigma Aldrich, Milan, Italy) for 30 minutes to cease the endogenous peroxidase activity. The slices were washed in phosphate-buffered saline (pH 7.4) and incubated with blocking solution (10 g/L BSA, 3 mL/L Triton X-100 and 10 mL/L normal goat serum) for 30 minutes. The samples were incubated with the following primary antibodies overnight at 4°C: rabbit anti-collagen type I, dilution 1:500 (GTX41286; GeneTex, Irvine, CA, USA); mouse anti-VEGF, dilution 1:100 (GTX83426; GeneTex). After a short washing in phosphate-buffered saline (pH 7.4), the slices were covered with biotinylated secondary antibody (anti-rabbit antibody diluted 1:400 for collagen type I; anti-mouse antibody diluted 1:400 for VEGF) for 1 hour at room temperature. The samples were then incubated with avidin-biotin complex (VECTASTAIN Elite ABC-HRP Kit, Vector Laboratories, Burlingame, CA, USA) for 45 minutes at room temperature, and the immunoreaction was identified adding 3,3'-diaminobenzidine tetrahydrochloride (Dako, Santa Clara, CA, USA) for 5 to 10 minutes. Finally, the sections were re-dehydrated and mounted with Entellan (Merck, Kenilworth, NJ, USA). The glasses were examined by light microscopy using an Olympus BX-51 microscope, equipped with a DKY-F58 CCD JVC digital camera.

To characterize the adipogenic biostimulation, the newly formed adipose tissue was analysed at 30 days for mouse anti-collagen type III (Coll. III), dilution 1:1000 (GTX26310; GeneTex) and VEGF using the same protocol previously described.

3. RESULTS

3.1. *In vitro* evaluation

3.1.1. *Morphological and physical characterization*

Structural and physical properties of the evaluated membranes were measured in order to analyse the morphological characteristics and the porosity in dry and wet conditions in culture growth media.

Figure 1.a shows the SEM images at cross-view in dry conditions of the ACMs. The stratification is noticeable due to the different pressing grades of ACM1 and ACM2, which present two and three layers, respectively. While ACM3 results composed by a single stratum where the elastic fibres (EF) are clearly identifiable, as indicated in the higher magnification reported in figure 1.a. ACM1 presents a two-layer structure, one is highly porous (porous layer: PL), while the other appears more compact (compact layer: CL). SEM images reveal that ACM2 is composed of three layers; both external layers are thinner and more compact (CL), while the middle one results porous (PL).

Figure 1.b presents the top view of the membranes in dry and wet conditions at two different magnifications. ACM1 exhibits a porous surface composed of crossed collagen fibres forming an irregular porosity through 3D structure with a mean porous size near 2 μm as reported in Figure 1.c. After the embedding procedure in culture growth media, it can be seen that the lamellar organization is more noticeable, and the size of the porous is increased. In the case of ACM2, the surface displays a porous configuration when analysed dry with a mean porous size ranging between 4 and 5 μm (Figure 1.c). After embedding in culture growth media, the lamellar structure appears non-homogenous, and the porous size of the membrane surface increases (from 4.5 ± 1.1 to 8.3 ± 1.8 μm), as reported in Figure 1.c.

Likewise, ACM3 was analysed before and after embedding in culture growth media. Under dry conditions, the membrane surface is highly dense and smooth, composed of a compact fibre structure that creates porous (0.2 ± 0.1 μm) as reported in Figure 1.c. After the embedding process, the membrane is characterised by a more irregular surface and the porous results closed due to the liquid uptake.

The table in Figure 1.c reports the swelling ratio and the porosity percentage. It is appreciable that liquid absorption capacity influences the porosity and, therefore, the increment of porous size. For ACM1, the increment of mean porous size is higher than the reported for the other two evaluated membranes (88.9%) with a porosity percentage of ($56.50\pm 6.84\%$). On the contrary, for ACM2, the swelling ratio is higher, which probably increases the size of the fibres that might affect the increase of the porous size (45.6%), and in addition, its porosity percentage is increased ($71.77\pm 6.01\%$). The same effect is reported for ACM3, which loses its porosity due to liquid uptake (swelling ratio of $100\pm 6.65\%$), affecting its porosity percentage ($17.22\pm 6.56\%$).

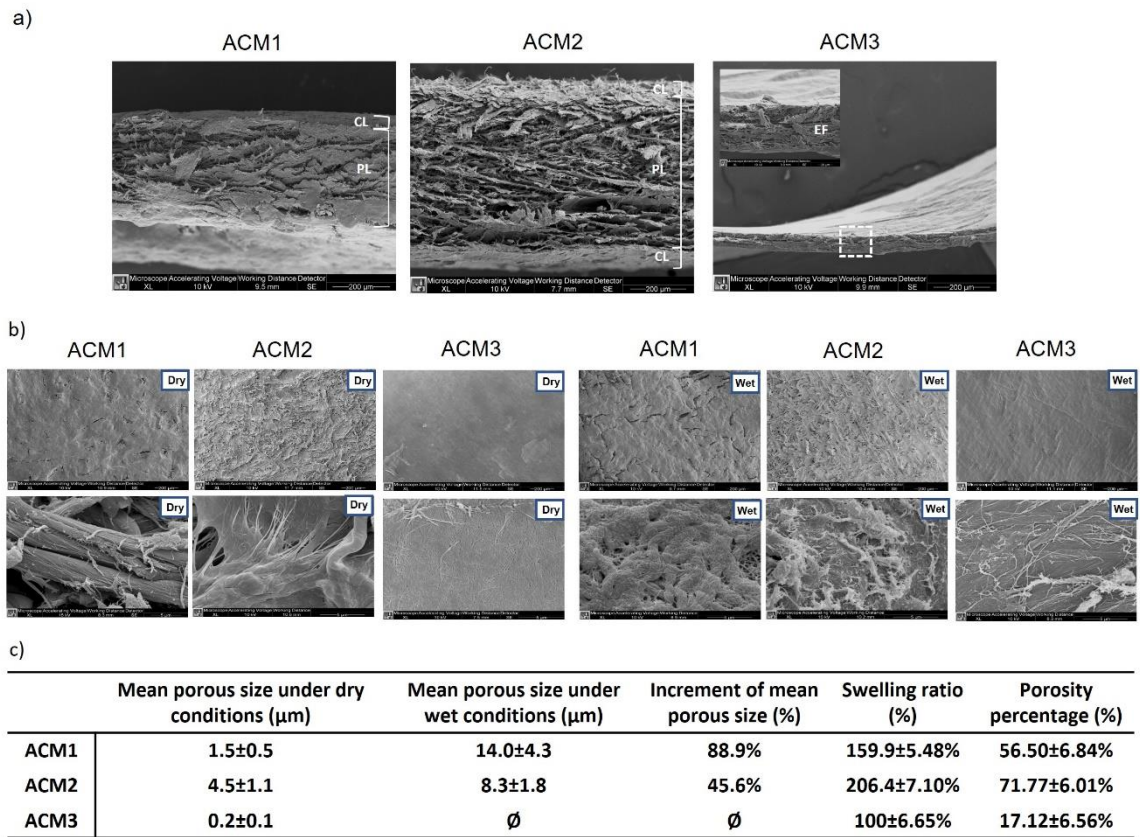


Figure 1. Morphological and physical characterization of the ACMs. a) SEM of ACMs in cross-view. The layered structure is identifiable for ACM1 and ACM2 (white bars indicates the different layers, Scale bar 200 μm), while ACM3 is composed of a single layer (Scale bar 200 μm) and are recognizable the elastic fibres (white square indicates the area of higher magnification, Scale bar 20 μm). b) SEM images of ACMs at top view at two magnifications in dry and wet conditions (Scale bar: upper 200 μm , bottom 5 μm) show the surface porosity created by the crossed collagen fibres. c) The table summarizes the physical properties of ACMs (data reported as mean \pm standard deviation). CL: Compact layer; PL: Porous layer; EF: Elastic fibres.

3.1.2. ASCs colonization capacity

To evaluate the colonization capacity of ASCs on ACMs surfaces, the cells were cultured over the membranes for 7 days and subsequently were studied with SEM images. Figure 2 shows on the upper panel the membranes surface colonized by cultured cells. It is appreciable that for ACM1 and ACM2, the surface is covered with ASCs with elongated filopodia, while for ACM3 cells are hardly detectable. Seeing the middle panel, cells in contact with ACM1 reveal the presence of numerous cytoplasmic flaps (CF) over the surface, which indicates strict adherence with the membrane. The CF detectable on the ASCs surface in contact with ACM2 appears scarce. The cells in contact with ACM3 present a non-conventional shape with a wrinkled plasmatic membrane (WPM). Furthermore, the adhesion between cells and the membrane is reduced.

The last panel shows the cells growing and spreading through the porous of ACMs colonizing the 3D structure. Those cells seeded over ACM1 and ACM2 generate connections between them; while, in the case of ACM3, the cells are not adherent to the surface and are not characterised by the presence of filipodia.

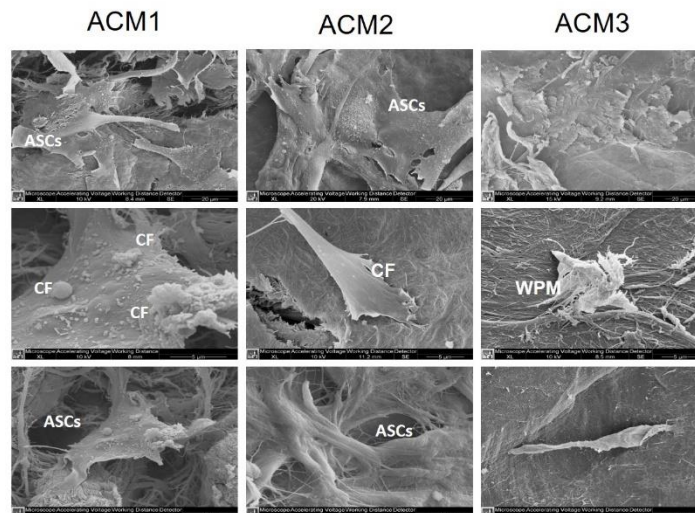


Figure 2. SEM analysis of ASCs colonization capacity over ACMs at different magnifications. Some cytoplasmic flaps are appreciable on cells cultured with ACM1 and ACM2, while cells in contact with ACM3 present a wrinkled plasmatic membrane. (Scale bar: upper 20 μm , middle 5 μm , bottom 10 μm) (ASCs: Adipose-derived stem cells on ACMs surface and spreading through their porous, CF: cytoplasmic flaps on ASCs Surface, WPM: wrinkled plasmatic membrane).

3.1.3. *In vitro* biostimulation

ASCs attached to the bottom of wells in which the ACMs were placed for 7 and 14 days were stained with Oil-Red-Oil solution and compared with positive and negative controls at the same time points. Figure 3 shows the images of the stained cells at the same magnification. On day 7, ASCs in contact with ACM1 started to internalise lipid droplets seen as red spots on the cytoplasm. The amount and size of the lipid droplets indicate an early stage of differentiation compared with the positive control. Additionally, small amounts of membrane debris around the cells can be seen in the culture medium (Figure 3, black arrows). On the other hand, ASCs in contact with ACM2 do not present lipid droplets on their cytoplasm, appearing with the typical morphology of stem cells as compared with the negative control. Moreover, a high quantity of membrane debris is detectably dispersed among the cells, probably due to the elevated degradation rate of the membrane. The cells cultured with ACM3 are reduced in number and appear stressed with a suffering morphology.

After 14 days of study, ASCs exposed to ACM1 show their capacity to duplicate actively, reaching the confluence and with a visible increment of lipid droplets, indicating the progression in adipogenic differentiation similar to the reported for positive control. ASCs growing in the presence of ACM2 starts to accumulate lipid droplets in the cytoplasm, indicating a slow ASCs differentiation into adipocytes compared to the positive control and cells in contact with ACM1. Finally, for ACM3, the behaviour found on the 7th day continues in time, showing that the membrane affects both the growth, the shape, and the vacuolization (Figure 3, dotted arrows) of ASCs. No adipose differentiation is visible.

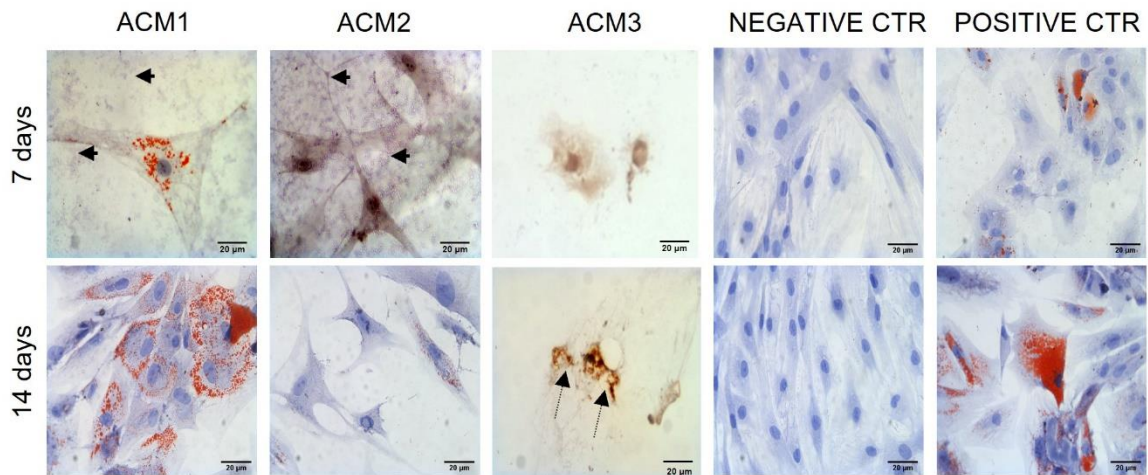


Figure 3. *In vitro* biostimulation. ASCs after 7 and 14 days of contact with the evaluated ACMs were compared with ASCs cultured growth medium (negative control) and adipose differentiative medium (positive control). (Scale bar 20 μm) (Arrows indicate membrane debris, dotted arrows indicate vacuolization).

3.2. *In vivo* and *ex vivo* evaluation

3.2.1. *Tissue integration*

In order to evaluate how silicone prosthesis affects the tissue, MR images and histological analysis were performed on mice subcutaneously implanted with silicone prosthesis. The MRI was performed for 7, 14 and 30 days after the silicone implantation. The images clearly identify the area of the silicone graft (Figure 4, arrow) surrounded by an area of fluid accumulation (Figure 4, dotted arrow) that appears stable over time. The *ex vivo* findings display an altered tissue morphology in the area of silicone prosthesis insertion (Figure 4, H&E) compared to the positive control (Figure 4, healthy skin H&E). Analysing the tissue with MT is possible to identify an accumulation of elastic fibres (Figure 4, MT black arrows) surrounded by an inflammatory infiltration (Figure 4, MT white asterisks) on the site of contact with the silicone implant. MT staining of healthy skin shows the physiological and non-altered subcutaneous structure.

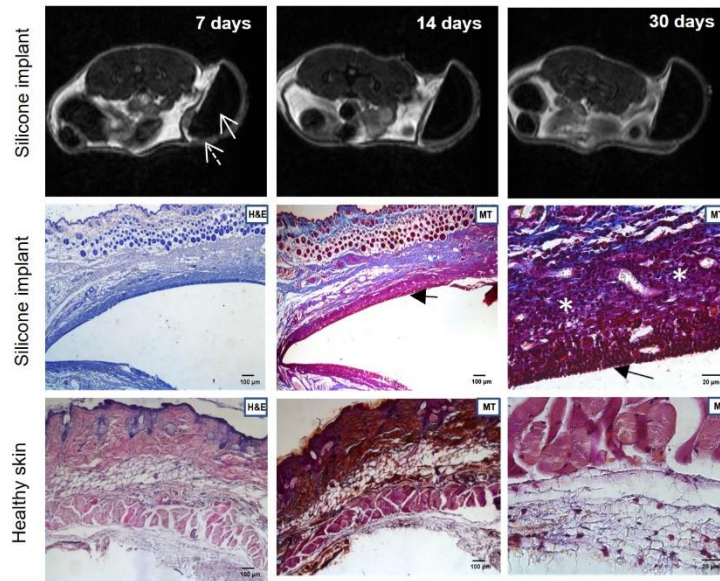


Figure 4. Elastosis formation after silicone prosthesis implantation. Magnetic Resonance images of control group are shown on the upper line after 7, 14 and 30 of follow-up. Histology images on the middle and bottom panels show H&E (Scale bar 100 μm) and MT (Scale bar 100 μm and 20 μm) staining of negative control group (uncovered silicone prosthesis) compared with positive control (healthy skin). (Arrow: silicone prosthesis; dotted arrow: fluid accumulation; black arrow: elastosis, White asterisks: inflammatory reaction, H&E: Hematoxylin/Eosin staining; MT: Mallory's Trichrome)

The *in vivo* tissue integration induced by the evaluated membranes was assessed after the subcutaneous implantation in mice of the ACMs. Figure 5 shows the MRI acquisitions after 7, 14 and 30 days from the surgery. On day 7th of study, the membranes are completely visible (Figure 5, arrows), and a fluid accumulation (Figure 5, dotted arrows) is observed in the subcutaneous region adjacent to all the evaluated grafts. After 14 days of study, the membranes reabsorption degree was calculated (Figure 5, reabsorption degree tables). Images reveal minimal reabsorption of ACM1 (12.21 ± 5.5), while the reabsorption rate of ACM2 and ACM3 results faster (67.28 ± 3.4 and 72.82 ± 8.1 , respectively). On the contrary, the fluid accumulation bordering the ACM1 seems to be reabsorbed faster than ACM2 and ACM3 (64.23 ± 10.30 , 37.13 ± 16.70 and 36.36 ± 14.20 , for ACM1, ACM2 and ACM3, respectively).

On the 30th day of follow-up, the fluid accumulation is not already visible in the surroundings of ACM1 with a reabsorption degree of $93.40 \pm 4.8\%$, while only $53.75 \pm 5.3\%$ of the membrane was reabsorbed. At the same time point, both ACM2 and the fluid accumulation around the membrane were almost entirely reabsorbed with a reabsorption degree of $94.60 \pm 2.7\%$ and $97.13 \pm 6.5\%$, respectively. In the case of ACM3, while the fluid accumulation is still present (reabsorption degree of $79.84 \pm 6.9\%$), the membrane appears highly reabsorbed (reabsorption degree of $92.59 \pm 4.3\%$), and the remains appear adherent to the muscular tissue of the animal.

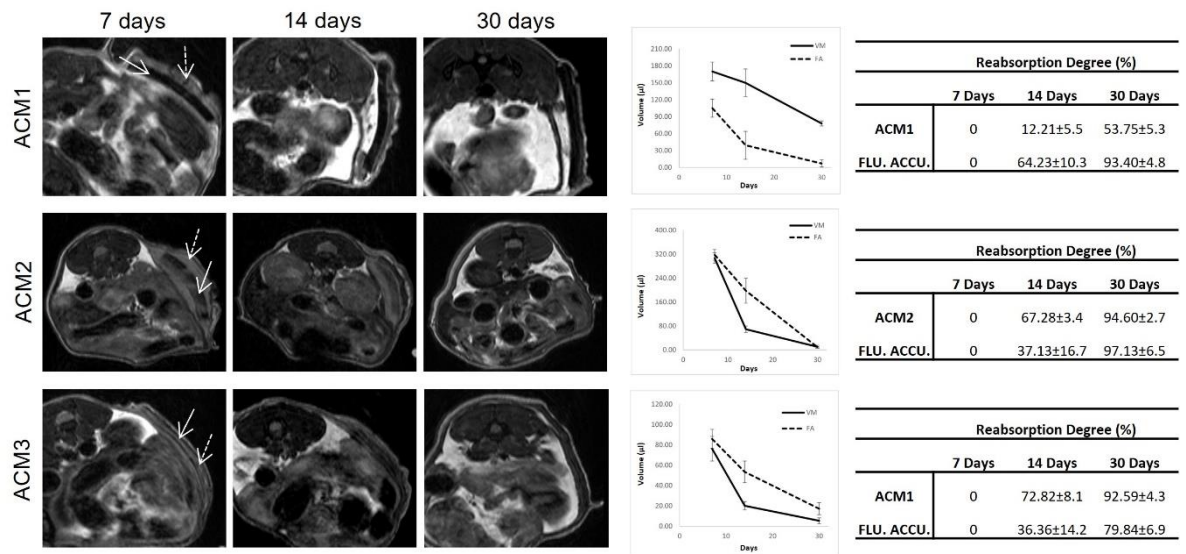


Figure 5. Evaluation of *in vivo* tissue integration. Magnetic resonance images performed after 7, 14, and 30 days of implantation of the evaluated ACMs allowed the calculation of the membrane's reabsorption degree and the surrounding fluid accumulation. (Arrow: ACMs, dotted arrow: fluid accumulation)

After 14 and 30 days from implantation, the *ex vivo* examinations were performed to analyse the morphological structure modifications of ACMs (H&E and MT staining) and tissue integration and colonization (Coll. I and VEGF) as shown in Figure 6.

After 14 days of surgery, histological examinations confirm the MRI results, and all the ACMs are still distinguishable. ACM1 appears well preserved, and the three-layer results are non-altered, as shown in Figure 6 (H&E and MT). As confirmed with the immunohistochemical analysis. Mallory's staining revealed that the membrane was colonised by resident cells and collagen fibre (Figure 6, Coll. I). Indeed, the positive result for the collagen type I antibody suggests an early integration between the autologous connective tissue and the membrane (Figure 6, Coll. I, arrows). No positive expression of VEGF was found.

Regarding ACM2, the membrane is well visible, and it is possible to recognise the layered structure (Figure 6, H&E and MT): CL has been positioned immediately after the reticular dermis, and PL is placed on the opposite side (Figure 6, MT). The immunohistochemical analysis shows no migration of native collagen fibres nor new vessels formation in the membrane (Figure 6, Coll. I and VEGF). However, the membrane results highly infiltrated by cells, probably due to an inflammatory reaction. For ACM3, the membrane appeared dense and compact (Figure 6, H&E and MT) except in the central portion in which the fluid accumulation has caused the loss of fibres density (Figure 6, MT, asterisk). Moreover, thanks to MT staining, the architecture of ACM3 is clearly visible: the elastic fibres that typically compose the pericardium are detectable as the red fibres in Figure 6. No evidence of cells colonisation (Figure 6, H&E), resident collagen fibres infiltration (Figure 6, Coll. I), and neovascularization (Figure 6, VEGF) are detectable.

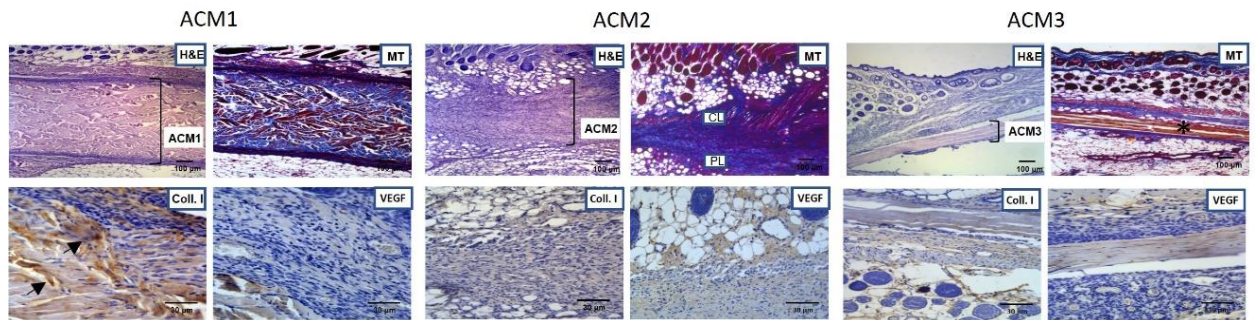


Figure 6. *Ex vivo* tissue integration after 14 days of study. The excised samples (ACMs with surrounding tissue) were stained with H&E and MT showed in upper panel (Scale bar 100 µm). Additionally, immunohistochemical analyses were performed with Coll. I and VEGF antibodies in bottom panel (Scale bar 30 µm). Asterisk indicates loss of fibre density; arrows indicate Coll. I positivity. CL: compact layer, PL: porous layer, H&E: Hematoxylin/Eosin staining, MT: Mallory's Trichrome, Coll. I: Collagen type I staining, VEGF: Vascular Endothelial Growth Factor staining.

At 30 days after the surgery, the ACM1 shows a reduced stratification and results partially reabsorbed, in accordance with MRI findings (Figure 7, H&E and MT). Moreover, the membrane appears compact with a well-structured collagen fibre (Figure 7, MT). Comparing the results with those at 14 days, ACM1 seems homogeneously colonized by resident cells and collagen fibres (Figure 7, Coll. I, arrows) but with no new vessel formation identified (Figure 7, VEGF).

In the case of ACM2, the dermis of the mice shows a physiological organisation while the membrane is hardly detectable (Figure 7, H&E and MT), probably due to the high degree of reabsorption as reported by MRI investigation. Moreover, an organically structured layer of resident collagen fibres (Figure 7, Coll. I, arrows) is detectable near the ACM2 implantation site, suggesting that the dermal compartment is fully restored, but the membrane results less colonized by collagen fibres than ACM1. Immunohistochemical analysis for neo-vascularization reveals no positive response for ACM2 (Figure 7, VEGF).

Finally, histological analysis of ACM3 confirms that the membrane is completely adherent at the muscular tissue and an unfolded, not compact, and disorganized structure is clearly identifiable (Figure 7, H&E and MT), justifying the high reabsorption degree obtained with MRI images. Immunohistochemical analysis reveals a partial integration between the membrane and the surrounding tissue. Native collagen fibres (Figure 7, Coll. I, arrows) and resident cells start to migrate through the ACM3. VEGF analysis reveals no signal of neo-angiogenesis surrounding the ACM3 after 30 days.

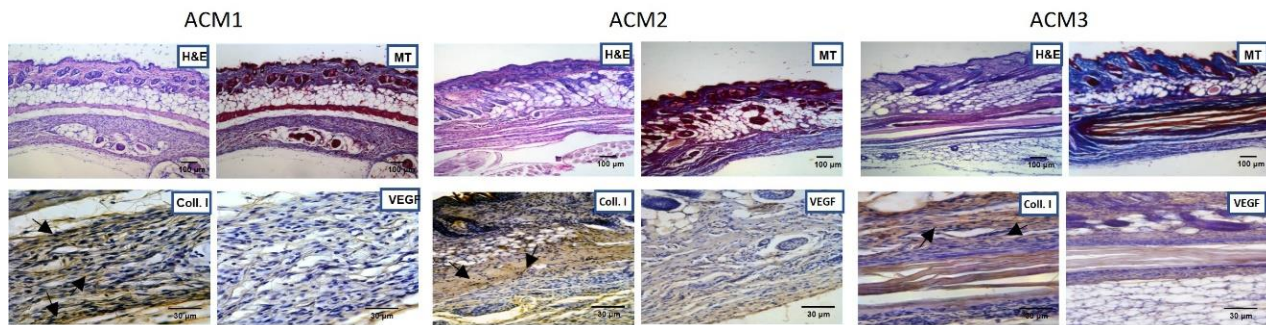


Figure 7. *Ex vivo* tissue integration after 30 days of study. The excised samples (ACMs with surrounding tissue) were stained with H&E and MT are shown in upper panel (Scale bar 100 µm). Additionally, immunohistochemical analyses were performed with Coll. I and VEGF antibodies in bottom panel (Scale bar 30 µm). Arrows identify positive responses for Coll. I. H&E: Hematoxylin/Eosin staining, MT: Mallory's Trichrome, Coll. I: Collagen type I staining, VEGF: Vascular Endothelial Growth Factor staining.

3.2.2. *In vivo* adipogenic biostimulation

Analysing the ACMs-induced biostimulation after 30 days of study, histological examination reveals an adipogenic induction thanks to ACM1, but no signs were found on ACM2 and ACM3 (Figure 8.a., H&E). Mallory's trichrome shows a well-organised adipose tissue deposition inside the membrane (Figure 8.b., MT, arrow indicating ACM1). Mature adipocytes resulted connected through a thin extracellular matrix of newly formed collagen fibre (Figure 8.b., Coll. III, arrows), and immunohistochemical analysis for VEGF detects the formation of new vessels distributed in the adipose tissue (Figure 8.b., VEGF, arrows).

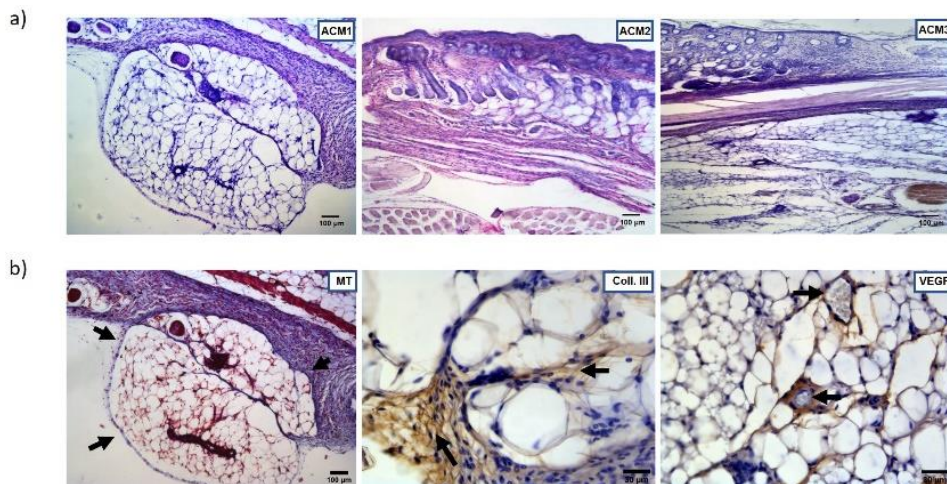


Figure 8. Induced adipose biostimulation study. a) shows H&E of the evaluated membranes (ACM1, ACM2 and ACM3) revealing an adipogenic formation inside ACM1. b) MT staining of newly formed adipose tissue inside ACM1 (arrows delimited the membrane, scale bar 100 µm) and immunohistochemical analysis of newly formed adipose tissue for Coll. III and VEGF antibodies (scale bar 30 µm). H&E: Hematoxylin/Eosin staining, MT: Mallory's Trichrome, Coll. III: Collagen type III staining, VEGF: Vascular Endothelial Growth Factor staining.

4. DISCUSSION

The number of women undergoing breast reconstruction surgery after mastectomy through silicone implant-based procedure is steadily increasing; however, silicone or polyurethane prostheses are associated with foreign body response which results in the PPC formation (6)(7). An unsolved issue is the elevated frequency of CC, in particular, related to breast irradiation. The CC is an inflammatory reaction characterised by fibrosis surrounding the implant due to the action of excessive collagen production, which provokes painful deformity (8).

To date, the standard treatment for CC is surgical remotion which is a highly invasive procedure. For this reason, the development of non-invasive approaches to prevent CC is necessary. Many positive reports are emerging about using biological materials to improve alloplastic breast reconstruction (7). In this study, ACMs different in morphology and physical structure have been evaluated *in vitro* and after subcutaneous implant in mice. Firstly, ACMs were incubated with ASCs to assess the interaction between the acellular scaffold and mesenchymal stem cells, representing one of the cellular elements involved in regeneration and repair pathways (34). According to the literature, the stimulation and differentiation of ASCs increase wound repair and regeneration ability by intensifying collagen secretion and deposition (21)(26). Recent studies have demonstrated a link between adipocytes and wound healing, given that adipocytes also act as key regulators of skin health (35). Collected data showed that *in vitro* colonisation capacity and adipogenic differentiation potential of ASCs are membrane dependent. Our results show that the ASCs in contact with the three evaluated ACMs have different behaviour. In particular, the high swelling ratio (more than 200%) of ACM2 improves the surface ASCs colonisation, but the non-homogenous lamellar structure and the pores mean diameter (about 8 μm) after the embedding procedure reduce the ability of ASCs to move across the 3D structure. Additionally, the cells in contact with ACM2 exhibit few cytoplasmic flaps indicating a poor activation capability. In the case of ACM3, the direct contact of ASCs with this material leads to cell stress. Indeed, SEM and optical microscopy evaluation showed a non-conventional shape of ASCs with a wrinkled and damaged cytoplasmic membrane. On the contrary, ACM1 presented an appropriate swelling ratio (about 160%) that increases the mean porous diameter (88.9%), allowing the complete colonisation of cells through the 3D structure. The numerous cytoplasmic flaps found on the ASCs surface reveal that ACM1 is able to stimulate and activates the cells. Indeed, Dasgupta S *et al* reports that an increased number of cytoplasmatic processes positively affects the attachment and the spreading of cells on biomaterial surfaces (36). Moreover, ASCs resulted stimulated by ACM1 improving their differentiation capacity into adipose-like cells.

The ACMs physical properties also influenced the degree of integration with the resident tissue and biostimulation (such as adipogenic stimulation, angiogenesis, or new collagen fibres deposition) *in vivo*. The control group implanted with the silicone prosthesis showed the formation of a high elastosis in the surroundings of the implant. On the contrary, ACMs presented a different tissue response. This suggests that using biological materials as implant beds avoiding direct contact between the silicone prosthesis and the resident tissue could favour a physiological integration (37). Schmitz M. *et al.* (2013) reported that the implantation of an

acellular dermal matrix covering a silicone prosthesis reduced the rate of inflammation in rats (7).

Our analysis reported an initial reaction of the resident subcutaneous tissue to the membrane implantation. Indeed, a different degree of membrane architecture modification and a consequent fluid accumulation surrounding the ACMs were reported. On day 14, the membrane structure of ACM1 appeared unaltered, and longitudinal MRI results revealed that it is still present until day 30, indicating a slow reabsorption rate. Moreover, the fluid accumulation appeared almost completely reabsorbed, indicating the high biocompatibility of ACM1 with the surrounding tissue. The slow reabsorption rate of ACM1 could be due to the two layers with different thicknesses and porosity that constitute the membrane. Low reabsorption could be advantageous for materials used as breast prosthesis coating due to a higher possibility of breast prosthesis integration that could reduce the PPC formation. A slow degradation rate allows the material to maintain its mechanical structure during tissue regeneration (38). Instead, the volume of ACM2 and ACM3 decreased about 70% from 7 to 14 days after implantation, indicating a faster reabsorption degree than ACM1. On the other hand, the fluid accumulation remains elevated (of about 75%), allowing the development of oedema and recruitment of inflammatory cells.

The integration between ACMs and subcutaneous tissue was evaluated by analysing the membrane colonisation by resident cells and collagen fibres matrix. While ACM2 and ACM3 resulted poorly infiltrated, ACM1 appeared highly colonised, and native collagen fibres spread within the membrane starting from day 14. As suggested by histological evaluation, the integration process of ACM3 was detectable from day 30, indicating a later migration of endogenous extra-cellular matrix components through the membrane compared to ACM1. These results are supported by previous *in vitro* experiments, in which ASCs culture with ACM3 appeared suffering. A different behaviour was observed for ACM2. At 30 days, the membrane was not detectable by MRI or histological analysis, suggesting a rapid degradation and absorption process. This phenomenon could be attributable to an immune-inflammatory response induced by oedema visible at day 14.

Finally, adipogenic biostimulation was also evaluated. Only ACM1 showed positive results at the last evaluated time point. Specifically, a deposition of adipose tissue inside the membrane was clearly visible. The newly formed adipocytes appeared surrounded by extra-cellular matrix components. Collagen fibres, which constitute the major matrix component, resulted positive for collagen type III antibody by immunohistochemical analysis. Moreover, the angiogenesis phenomenon was detectable, and new vessels were found inside the adipose tissue. Since mature adipose tissue is composed of multiple components (such as adipocytes, extra-cellular matrix, vessels) (39), our findings suggest a multiple functional biostimulation induced by ACM1, which stimulated the formation of new well-structured adipose tissue. Indeed, ECM is responsible for providing growth factors for signalling, immunological response and modulation of structure properties of the tissue leading to its restoration and maintaining homeostasis (40). The activation of adipogenesis after ACMs implantation hypothesises that adipocytes could improve the interaction between membrane and tissue, favouring the regeneration and repair processes. Another aspect that positively influences the regeneration is the angiogenesis by which resident mesenchymal stem cells could

migrate into the damage site with growth factors and cytokines. In different models and clinical protocols, the implant of ACMs restores the physiologic vascularisation (41). The stimulation of adipogenesis and the restoration of physiologic angiogenesis could ensure a *restitution ad integrum* of the dermis and subcutis (41).

5. CONCLUSION

This study evaluated three acellular matrices to be used as possible coating of breast silicone prosthesis. The results have shown that subcutaneously implanted natural membranes can induce biological activation in the surrounding tissue. Specifically, the induction of adipogenic stimulation is morphological-dependent on the porosity, thickness and swelling ratio of the membrane. The deposition of newly formed adipose tissue could play a key role in forming a well-organised tissue architecture preventing capsular contracture formation.

REFERENCES

1. Pool SMW, Wolthuisen R, Mouës-Vink CM. Silicone breast prostheses: A cohort study of complaints, complications, and explantations between 2003 and 2015. *J Plast Reconstr Aesthetic Surg*. 2018;71(11):1563–9.
2. ISAPS. International Survey on Aesthetic/Cosmetic Procedures performed in 2018. *ISAPS Int Surv Aesthetic/Cosmetic Proced* [Internet]. 2018;1–49. Available from: <https://www.isaps.org/wp-content/uploads/2019/12/ISAPS-Global-Survey-Results-2018-new.pdf>
3. Bray F, Ferlay J, Soerjomataram I, Siegel R, Torre L, Jemal A. Breast cancer statistics [Internet]. World Cancer Research Fund International. 2018 [cited 2020 Oct 20]. Available from: <https://www.wcrf.org/dietandcancer/cancer-trends/breast-cancer-statistics>
4. Baxter RA. Acellular Dermal Matrices in Breast Implant Surgery: Defining the Problem and Proof of Concept. *Clin Plast Surg*. 2012;39(2):103–12.
5. Britez MEM, Llano CC, Chaux A. Periprosthetic breast capsules and immunophenotypes of inflammatory cells. *Eur J Plast Surg*. 2012;35(9):647–51.
6. Thrusfield M. Observational studies. *Vet Epidemiol* Fourth Ed. 2017;319–38.
7. Schmitz M, Bertram M, Kneser U, Keller AK, Horch RE. Experimental total wrapping of breast implants with acellular dermal matrix: A preventive tool against capsular contracture in breast surgery? *J Plast Reconstr Aesthetic Surg* [Internet]. 2013;66(10):1382–9. Available from: <http://dx.doi.org/10.1016/j.bjps.2013.05.020>
8. Headon H, Kasem A, Mokbel K. Capsular contracture after breast augmentation: An update for clinical practice. *Arch Plast Surg*. 2015;42(5):532–43.

9. Atlan M, Nuti G, Wang H, Decker S, Perry TA. Breast implant surface texture impacts host tissue response. *J Mech Behav Biomed Mater* [Internet]. 2018;88(May):377–85. Available from: <https://doi.org/10.1016/j.jmbbm.2018.08.035>
10. Brown T. Surface areas of textured breast implants: Implications for the biofilm theory of capsule formation. *Plast Reconstr Surg - Glob Open*. 2018;6(3):1–5.
11. Wright MA, Samadi A, Lin AJ, Lara DO, Harper AD, Zhao R, et al. Periprosthetic Capsule Formation and Contracture in a Rodent Model of Implant-Based Breast Reconstruction With Delayed Radiotherapy. *Ann Plast Surg*. 2019;82(4S Suppl 3):S264–70.
12. Tevlin R, Borrelli MR, Irizarry D, Nguyen D, Wan DC, Momeni A. Acellular Dermal Matrix Reduces Myofibroblast Presence in the Breast Capsule. *Plast Reconstr Surg - Glob Open*. 2019;7(5):e2213.
13. Steiert AE, Boyce M, Sorg H. Capsular contracture by silicone breast implants: Possible causes, biocompatibility, and prophylactic strategies. *Med Devices Evid Res*. 2013;6(1):211–8.
14. Prantl L, Angele P, Schreml S, Ulrich D, Pöppel N, Eisenmann-Klein M. Determination of serum fibrosis indexes in patients with capsular contracture after augmentation with smooth silicone gel implants. *Plast Reconstr Surg*. 2006;118(1):224–9.
15. Moyer KE, Ehrlich HP. Capsular contracture after breast reconstruction: Collagen fiber orientation and organization. *Plast Reconstr Surg*. 2013;131(4):680–5.
16. Persichetti P, Segreto F, Carotti S, Marangi GF, Tosi D, Morini S. Oestrogen receptor-alpha and -beta expression in breast implant capsules: Experimental findings and clinical correlates. *J Plast Reconstr Aesthetic Surg* [Internet]. 2014;67(3):308–15. Available from: <http://dx.doi.org/10.1016/j.bjps.2013.12.002>
17. Sbricoli L, Guazzo R, Annunziata M, Gobbato L, Bressan E, Nastri L. Selection of collagen membranes for bone regeneration: A literature review. *Materials (Basel)*. 2020;13(3):1–16.
18. Brouki Milan P, Pazouki A, Joghataei MT, Mozafari M, Amini N, Kargozar S, et al. Decellularization and preservation of human skin: A platform for tissue engineering and reconstructive surgery. *Methods*. 2019;(July).
19. Liu M, Zeng X, Ma C, Yi H, Ali Z, Mou X, et al. Injectable hydrogels for cartilage and bone tissue engineering. Vol. 5, *Bone Research*. 2017.
20. Kornmuller A, Brown CFC, Yu C, Flynn LE. Fabrication of extracellular matrix-

- derived foams and microcarriers as tissue-specific cell culture and delivery platforms. *J Vis Exp*. 2017;2017(122):1–11.
21. Qi Y, Dong Z, Chu H, Zhao Q, Wang X, Jiao Y, et al. Denatured acellular dermal matrix seeded with bone marrow mesenchymal stem cells for wound healing in mice. *Burns* [Internet]. 2019;45(7):1685–94. Available from: <https://doi.org/10.1016/j.burns.2019.04.017>
 22. Freytes DO, Tullius RS, Valentin JE, Stewart-Akers AM, Badylak SF. Hydrated versus lyophilized forms of porcine extracellular matrix derived from the urinary bladder. *J Biomed Mater Res - Part A*. 2008;87(4):862–72.
 23. Gadelkarim M, Abushouk AI, Ghanem E, Hamaad AM, Saad AM, Abdel-Daim MM. Adipose-derived stem cells: Effectiveness and advances in delivery in diabetic wound healing. *Biomed Pharmacother*. 2018;107(July):625–33.
 24. Bush K, Gertzman AA. Process Development and Manufacturing of Human and Animal Acellular Dermal Matrices [Internet]. *Skin Tissue Engineering and Regenerative Medicine*. Elsevier Inc.; 2016. 83–108 p. Available from: <http://dx.doi.org/10.1016/B978-0-12-801654-1.00005-X>
 25. Carlsson AH, Gronet EM, Rose LF, Chan R. Clinical Applications of Acellular Dermal Matrices in Reconstructive Surgery [Internet]. *Skin Tissue Engineering and Regenerative Medicine*. Elsevier Inc.; 2016. 109–124 p. Available from: <http://dx.doi.org/10.1016/B978-0-12-801654-1.00006-1>
 26. Storti G, Scioli MG, Kim BS, Orlandi A, Cervelli V, De Francesco F. Adipose-Derived Stem Cells in Bone Tissue Engineering: Useful Tools with New Applications. *Stem Cells Int*. 2019;2019.
 27. Wu S, Liu X, Yeung KWK, Liu C, Yang X. Biomimetic porous scaffolds for bone tissue engineering. *Mater Sci Eng R Reports* [Internet]. 2014;80(1):1–36. Available from: <http://dx.doi.org/10.1016/j.mser.2014.04.001>
 28. Tan QW, Tang SL, Zhang Y, Yang JQ, Wang Z Le, Xie HQ, et al. Hydrogel from Acellular Porcine Adipose Tissue Accelerates Wound Healing by Inducing Intradermal Adipocyte Regeneration. *J Invest Dermatol* [Internet]. 2019;139(2):455–63. Available from: <https://doi.org/10.1016/j.jid.2018.08.013>
 29. Hoerst K, van den Broek L, Sachse C, Klein O, von Fritschen U, Gibbs S, et al. Regenerative potential of adipocytes in hypertrophic scars is mediated by myofibroblast reprogramming. *J Mol Med*. 2019;97(6):761–75.
 30. Lou T, Wang X, Song G, Gu Z, Yang Z. Fabrication of PLLA/??-TCP nanocomposite scaffolds with hierarchical porosity for bone tissue engineering. *Int*

- J Biol Macromol. 2014;69:464–70.
31. Lou T, Wang X, Yan X, Miao Y, Long YZ, Yin HL, et al. Fabrication and biocompatibility of poly(l-lactic acid) and chitosan composite scaffolds with hierarchical microstructures. *Mater Sci Eng C* [Internet]. 2016;64:341–5. Available from: <http://dx.doi.org/10.1016/j.msec.2016.03.107>
 32. Peroni D, Scambi I, Pasini A, Lisi V, Bifari F, Krampera M, et al. Stem molecular signature of adipose-derived stromal cells. *Exp Cell Res*. 2008;314:603–15.
 33. Busato A, De Francesco F, Biswas R, Mannucci S, Conti G, Fracasso G, et al. Simple and Rapid Non-Enzymatic Procedure Allows the Isolation of Structurally Preserved Connective Tissue Micro-Fragments Enriched with SVF. *Cells* [Internet]. 2020 Dec 29;10(1):36. Available from: <https://www.mdpi.com/2073-4409/10/1/36>
 34. Bukowska J, Szóstek-Mioduchowska AZ, Kopcewicz M, Walendzik K, Machcińska S, Gawrońska-Kozak B. Adipose-Derived Stromal/Stem Cells from Large Animal Models: from Basic to Applied Science. *Stem Cell Rev Reports*. 2021;17(3):719–38.
 35. Polotto S, Bergamini ML, Pedrazzi G, Arcuri MF, Gussago F, Cattelani L. One-step prepectoral breast reconstruction with porcine dermal matrix-covered implant: A protective technique improving the outcome in post-mastectomy radiation therapy setting. *Gland Surg*. 2020;9(2):219–28.
 36. Dasgupta S, Maji K, Nandi SK. Investigating the mechanical, physiochemical and osteogenic properties in gelatin-chitosan-bioactive nanoceramic composite scaffolds for bone tissue regeneration: In vitro and in vivo. *Mater Sci Eng C* [Internet]. 2019;94(October 2018):713–28. Available from: <https://doi.org/10.1016/j.msec.2018.10.022>
 37. Uzunismail A, Perk C, Fındık H, Beyhan G, Dinçler M. Effect of a fascial tissue interface on silicone implant capsule formation – a preliminary experimental study. *J Plast Reconstr Aesthetic Surg* [Internet]. 2008 Oct;61(10):1199–204. Available from: <https://linkinghub.elsevier.com/retrieve/pii/S1748681507003634>
 38. Abdulghani S, Mitchell GR. Biomaterials for in situ tissue regeneration: A review. *Biomolecules*. 2019;9(11).
 39. Carswell KA, Lee M-J, Fried SK. Culture of Isolated Human Adipocytes and Isolated Adipose Tissue. In 2012. p. 203–14. Available from: <http://www.springerlink.com/index/10.1007/978-1-61779-367-7>
 40. Sharath SS, Ramu J, Nair SV, Iyer S, Mony U, Rangasamy J. Human Adipose Tissue Derivatives as a Potent Native Biomaterial for Tissue Regenerative

Therapies. *Tissue Eng Regen Med* [Internet]. 2020 Apr 17;17(2):123–40. Available from: <http://link.springer.com/10.1007/s13770-019-00230-x>

41. Chen X, Yang R, Wang J, Ruan S, Lin Z, Xin Q, et al. Porcine acellular dermal matrix accelerates wound healing through miR-124-3p.1 and miR-139-5p. *Cytotherapy* [Internet]. 2020;22(9):494–502. Available from: <https://doi.org/10.1016/j.jcyt.2020.04.042>

CHAPTER III:

INFLUENCE OF CONCENTRATION OF A LOW MOLECULAR WEIGHT HYALURONIC ACID IN SCAR SKIN TREATMENT: CASE STUDY

PROLOGUE:

Mark Twain wrote, “The finest clothing made is a person’s own skin, but, of course, society demands something more than this.” With these words, the author highlights the importance of skin in a personal and social context. The overall well-being of the skin highly influences personal interactions and relations. This chapter presents an evaluation of a hyaluronic acid with the potential to improve aberrant scar treatment.

1. BACKGROUND

Although Skin is only a few centimeters thick, it is the largest organ of the body, with an average surface area of 2 m² and 3.6 kg in adults (1). It is a highly organized organ that functions as the first barrier against chemicals, diseases, UV light and physical damage by covering the external portion of the body and acting as a waterproof insulated shield (1)(2). The skin is composed of three layers that are different (3)(2) as represented in Figure 1:

- The epidermis is the external layer composed mainly of keratinocytes and melanocytes. It is the main barrier against environmental damage, protecting against pathogens, dehydration, UV radiation and pollution.
- Under the epidermis is the dermis, mostly composed of an extracellular matrix (ECM) that provides mechanical support to the tissue. The dermis also plays a vital role in hosting relevant structures such as sensory nerve cells, cutaneous vasculature and organelles.
- The inner layer is the hypodermis, which serves as a deposit of fat that helps in thermoregulation, isolation, storing nutrition and protecting inner soft tissues from injuries.

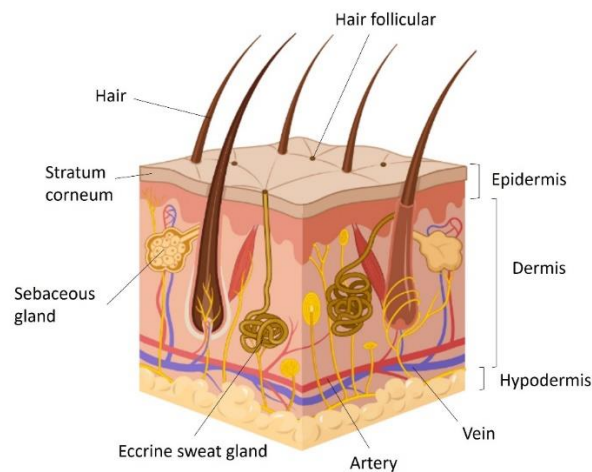


Figure 1. Schematic representation of a healthy skin morphology with the three main layers (Epidermis, dermis and hypodermis) clearly distributed.

This barrier could be destroyed if a person suffers from a major skin loss which may be produced either by external damage or by a secondary effect of some diseases (4)(5). In humans, an optimal healing process involves an overlapping sequence of four stages: coagulation, inflammation, proliferation and remodeling (6)(7). However, the sequence can be interrupted before completing the stages, leading to undesired results such as severe scar formation or organ-encompassing fibrosis (6). Those results produce malfunction of the tissue or even chronic wounds that will affect patients quality of life (7).

Due to the dynamic and complex process of natural wound healing, skin wound repair is still a challenging problem especially in the repair of burns, severe cutaneous trauma or diabetic foot ulcers (5) and even more laborious if this process is under low-hydration conditions that require additional time to tissue restoration (4). Therefore, how to promote complete wound healing is an increasing research

topic in the medical field. Although several treatments have been used to improve scarring in different stages, all of these approaches have yet to be successful. Different approaches have been proposed for scar treatment from pharmaceutical products, biomaterial-based dressing, cell therapy, and tissue-engineered substitutes that provide good results in scar reduction, such as honey, pycnogenol, microbial cellulose, or the use of Stem Cells (8). Some studies have demonstrated the influence of mechanical forces in the skin regeneration alongside hydration and chemical signaling (9). For this reason, studies are focused on biomaterials that allow moisture maintenance while providing mechanical support during tissue restoration. Among these biomaterials, natural polymers represent an essential group given their biocompatibility, biodegradability and availability (10). In recent years, scar treatment research has focused the attention on the production of wound dressings. A wound dressing is designed to be in contact with the wound, different from a bandage used to hold the dressing in place (11). The wound dressing characteristics have overcome the traditional wound dressing system to improve wound regeneration. Modern wound dressing made of synthetic materials can be classified as passive, which are non-occlusive materials used to cover the wound to restore the functionality of damaged tissue (ex., gauze). Another type of dressing is interactive ones that could be semi-occlusive or occlusive in the forms of hydrogels, foams, films or hydrocolloids. Finally, bioactive dressings, which are designed with biocompatible materials, make cells improve the healing process (11). Even though hydrogel dressings protect against microorganisms while maintaining a moist environment at the wound site, injectable hydrogels can adopt the shape of the defect, encapsulate molecules *in situ* and adhere to the wound (7)(12). Among the materials used for bioactive injectable hydrogels production, Hyaluronic Acid (HA) stands out as an attractive material due to its ability to self-assemble that provides a space to deliver encapsulated drugs or even living cells actively (7).

HA is a non-sulfated glycosaminoglycan belonging to the extracellular matrix (ECM) consisting of repeating disaccharide units of d-glucuronic and N-acetyl-d-glucosamine involved in skin moisture (13)(14). HA has been frequently used as a filler in aesthetic medicine or as significant component in scaffolds for regenerative applications due to its biocompatibility and remarkable capacity to promote cell proliferation and migration (15). It has been demonstrated that HA functions are primarily dictated by its size ranging between 5,000 to 20,000,000 Da *in vivo* (13). Moreover, this biomaterial has been used in aesthetic medicine to treat wrinkles, and scars, among others (15)(16). Several studies have suggested that HA promotes adipogenesis *in vitro* and *in vivo*, especially those with molecular weights over 60 kDa (13). However, the concentration and molecular weight influence in the adipose differentiation process is unclear.

The HA interacts with the cell through its binding with the type I transmembrane glycoprotein CD44 antigen (17)(18). The CD44 is a receptor found on the surface of most cell types of the dermis and plays an essential role in the cell-cell and cell-ECM interactions; it is also involved in cellular differentiation, migration and angiogenesis (17). Some studies have suggested that HA alone does not induce cellular migration nor stimulate wound healing (19). HA combined with the CD44 are involved in cell guidance, inducing the expression of genes related to differentiation, inflammation, and wound healing, among others (20)(21), suggesting the important role of the combined role of HA and CD44 receptor in the

tissue regeneration. However, this interaction can be modified by changing the physicochemical characteristics of the employed HA, as usually occurs when producing hydrogels (22).

This study aimed to evaluate the influence of concentration in the *in vitro* adipogenesis differentiation of a Low Molecular Weight Hyaluronic Acid (LMW-HA) in contact with Adipose-derived Stem Cells (ASC) and its capacity to bind with the CD44 receptor. In addition, the HA potential influence in the regeneration of different types of skin scars was studied in a clinical study due to the direct role in tissue remodelling when anchored to the cell surface through the CD44 receptor.

2. MATERIALS AND METHODS

2.1. Materials

In this study was evaluated a Low Molecular Weight Hyaluronic Acid (LMW-HA) of 200 kDa at a concentration of 15 mg/mL in 1X Phosphate Buffer Solution (PBS) provided by Fidia Pharmaceuticals (Abano Terme, Italy).

2.2. *In vitro* evaluation

2.2.1. Isolation and seeding of Adipose-derived Stem Cell

ASCs were isolated from human lipoaspirate of healthy donors (women of ages between 35 and 45 years) after informed consent, following the protocol described by Peroni *et al.* (2018) and Busato *et al.* (2020), using an enzymatic method [18,19]. The lipoaspirate samples were incubated in 1 mg/mL of Collagenase type I (GIBCO life technology, Monza, Italy) dissolved in Hank's Balanced Salt Solution (HBSS, GIBCO Life Technology, Monza, Italy) with 2% of Bovine Serum Albumin (BSA, GIBCO Life Technology, Monza, Italy). Complete growth medium (Dulbecco's Modified Eagle's Medium (DMEM), Sigma-Aldrich, Italy) supplemented with 10% of Fetal Bovine Serum (FBS, GIBCO Life Technology, Monza, Italy), 1% of 1:1 penicillin/streptomycin (P/S, GIBCO Life Technology, Monza, Italy) solution, and 0.6% of Amphotericin B (GIBCO Life Technologies, Monza, Italy) was added to neutralize the enzymatic action. The extracted cells were incubated in a humidified atmosphere with 5% CO₂ at 37°C in a 25 cm² flask with complete growth medium. The cells were detached after reaching between 70 and 80% confluence by incubation with 0.25% trypsin (GIBCO Life Technology, Monza, Italy) at 37°C for 5 min, centrifuged at 3000 rpm for 7 minutes, and the cell pellet was re-plated in a 25 cm² flask. The cells were cultured until passage four (P4), following the above procedure for the following studies, as represented in Figure 2.

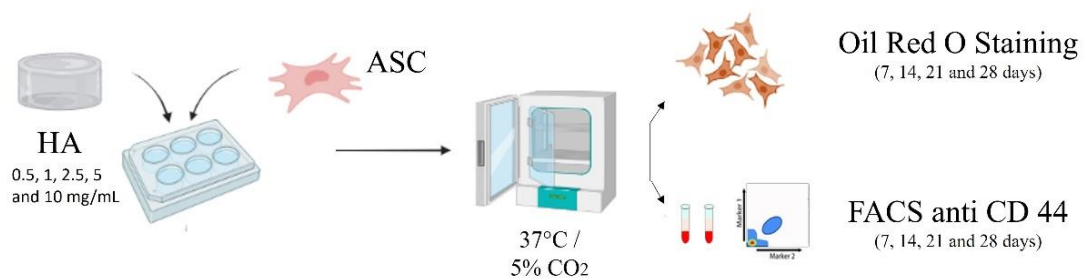


Figure 2. Representative scheme of the employed methodology for the *in vitro* evaluation of the evaluated LMW-HA.

2.2.2. *In vitro* biostimulation

The evaluated hyaluronic acid was mixed with the complete culture media in different concentrations (0.5, 1, 2.5, 5 and 10 mg/mL in triplicate) to evaluate the amount of hyaluronic acid in the differentiative stimulation of stem cells for 7, 14, 21 and 28 days. At each time point, it was studied the ability to induce adipose differentiation of the HA at the evaluated concentrations comparing with the positive control (cells in adipose-inductive media) and negative control (cells with standard growth media), all in triplicate for each time point. Initially, the cells were seeded in 12-well plates and incubated in complete culture medium at 37°C and 5% CO₂ for 24 hours. Once the cells were attached, the culture medium was replaced with the mixture of HA and medium at the evaluated concentrations. For both the controls, complete culture medium and adipose inductive medium were used. For all the conditions, the medium was replaced every 72 hours.

At each time point, the medium was discarded, and the cells were stained with Oil-Red-Oil solution. Briefly, the coverslips with adherent ASC were washed with PBS 0.1 M pH 7.4 and fixed for 10 min with Baker's fixative (Bio-Optica, Milan, Italy) at 4°C. The adherent cells were washed in tap water for 10 min and stained with Oil Red Oil ready-to-use solution (Bio-Optica, Milan, Italy) for 15 minutes at room temperature. Samples were washed in tap water for 10 min followed by a short rinse in distilled water and stained with Mayer's Hematoxylin ready-to-use solution (Bio-Optica, Milan, Italy) for 5 minutes, at room temperature, and washed with tap water. The coverslips were mounted on a microscopy glass with a Mount Quick aqueous solution (Bio-Optica, Milan, Italy). Once the microscopy glasses were dried under the cabinet, samples were observed in light microscopy using an Olympus BX-51 microscope (Olympus, Tokyo, Japan) equipped with a DKY-F58 CCD JVC digital camera (Yokohama, Japan) with Magnification 20X. The Oil-Red-Oil solution stains the lipid droplets in the cytoplasm, while the nuclei are colored in blue by the Hematoxylin solution. Lipid droplets are an accumulation of lipids that characterize the differentiation into adipose cells.

For a statistical evaluation, 10 images of each sample were acquired and processed with a custom-made script for Image J software and the statistical analysis with Graph Prism. The response variables were the number of lipid droplets, the area of the lipid droplets and the rate of positive cells.

ASCs cultured with complete growth medium (without ACMs) were used as a negative control. Instead, ASCs cultured with specific adipogenic media (Sigma-Aldrich, Milan, Italy) were used as a positive control.

2.2.3. *Antibody expression analysis*

Additionally, to identify the activated pathway of the cells while in contact with the HA, a flow cytometry assay was performed to examine the CD44 expression, which is a hyaluronic acid receptor. It has been discovered that the possible regulatory role of CD44 in metabolic syndrome during obesity. An increment of CD44 expression is related to an increase in lipid accumulation. Passage 3 ASCs were seeded in T25 flasks at the different confluence to have an amount of 100000 cells at each evaluated time point. The cells were treated with HA at the two concentrations with the highest performance during the biostimulation assay. Additionally, there were

cultured cells without HA as a control group. Once the cells reached the evaluated time points, they were characterized by flow cytometry. The cells were detached with 0.25% trypsin (GIBCO Life Technology, Monza, Italy) at 37°C for 5 min, centrifuged at 3000 rpm for 7 minutes, and the cell pellet was resuspended in 1mL of 1X PBS. The cells were counted, and 1×10^5 cells were placed in 15mL Falcon tubes and centrifuge to obtain a pellet. According to datasheet, the cells were resuspended and incubated in 100 μ L of conjugated antibody diluted in 1X PBS for 30 min on ice. After incubation, the pellets were centrifuged (5000 rpm, 7 min) and resuspended in 100 μ L of 1X PBS.

The antibodies used were: CD44 FITC conjugate (1:100 dilution) for the HA-treated cells and one non-treated cells as CD44 baseline; Rat IgG2b kappa Isotype Control was used in non-treated cells as isotype control. Both the CD44 antibody and the isotype were purchased from Invitrogen (ThermoFisher). Propidium Iodide was used in non-treated cells for cell viability, purchased from BD Biosciences (Becton Dickinson Italy S.P.A., Milano, Italy). Immunophenotyping was performed through a chant II FACS (BD, Becton Dickinson, Milano, Italy).

2.3.Clinical study

To evaluate the regenerative capacities of the evaluated HA, a double blinded clinical study was conducted in the aberrant scar treatment executed by the medical team of Cesena and Udine hospitals (Italy). For this purpose, four patients with visible skin scars were selected to be treated either with HA or saline solution. After the informed consent, a small biopsy of the scar for each patient was excised before and after 30 days of the treatment. The samples were paraffin-embedded and stained with Hematoxylin/eosin for histological analysis. The samples were imaged at light microscopy and were considered 4 main parameters for the analysis (aspect and size of the stratum corneum, epidermis size, aspect of the dermal-epidermal junction, and aspect of the epidermis). Given that it was a double blinded study, 4 different researchers independently evaluated the sample measuring and classifying the parameters mentioned above to analyzed them together to identify the samples treated with the HA and those treated with saline solution (control group). Figure 3 shows a representative scheme of the employed methodology during the clinical study.

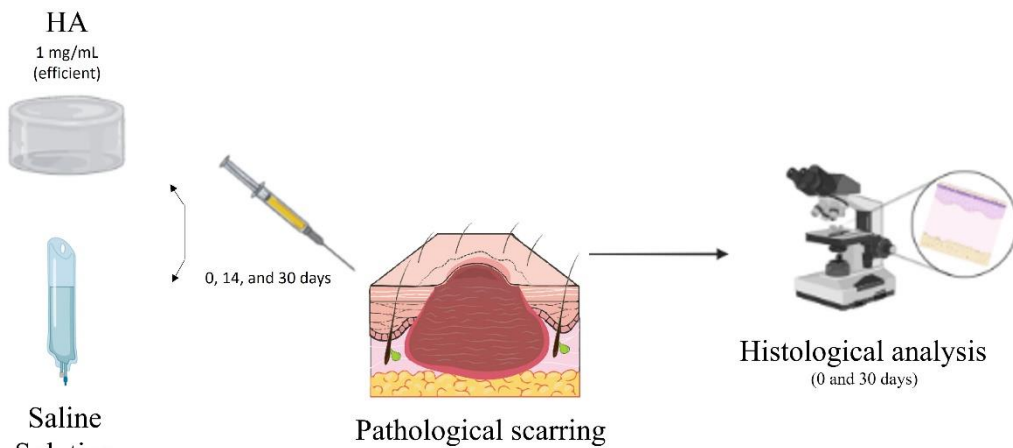


Figure 3. Schematic representation of the performed clinical study evaluating the LMW-HA at the commercial concentration.

3. RESULTS

3.1. *In vitro* evaluation

3.1.1. *Adipose stimulation*

After an initial visual evaluation, it was determined that from the 7th day of study, it was observable adipose-like cells in the presence of the HA at a concentration of 2.5 and 5 mg/mL, less for the concentration of 1 mg/mL and none for the remaining ones. After 14 days of study, the cells in contact with the concentration of 0.5 mg/mL started to differentiate. This differentiation process continued increasing for the concentrations of 0.5, a, 2.5 and 5 mg/mL until the 28th day. In the case of 10 mg/mL concentration, the cells subjected to this concentration started to differentiate only after 28 days of study. Figure 4 is a comparative example of imaged cells after 28 days of study at each evaluated concentration.

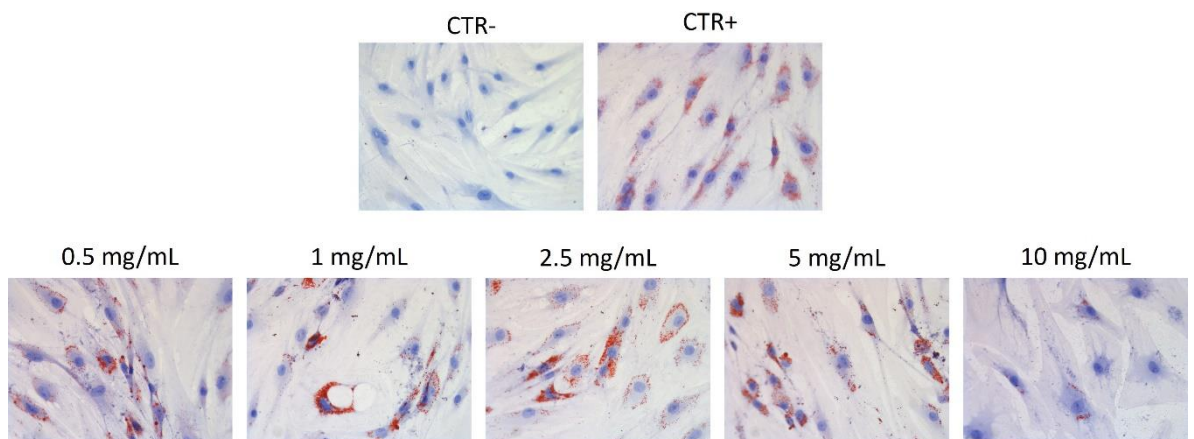


Figure 4. Representative images of colored cells after 28 days of study. The evaluated concentrations are compared with negative and positive controls. The number of red spots in 2.5 mg/mL concentration is comparable with the positive control.

The statistical analysis confirmed the visual study showing that hyaluronic acid at a concentration of 2.5 and 5 mg/mL stimulates an adipose differentiation faster than the other evaluated concentration and the positive control. However, after 28 days of study, the results are similar for the concentrations of 1, 2.5 and 5 mg/mL and the positive control. Figure 5 shows the statistical analysis for each response variable.

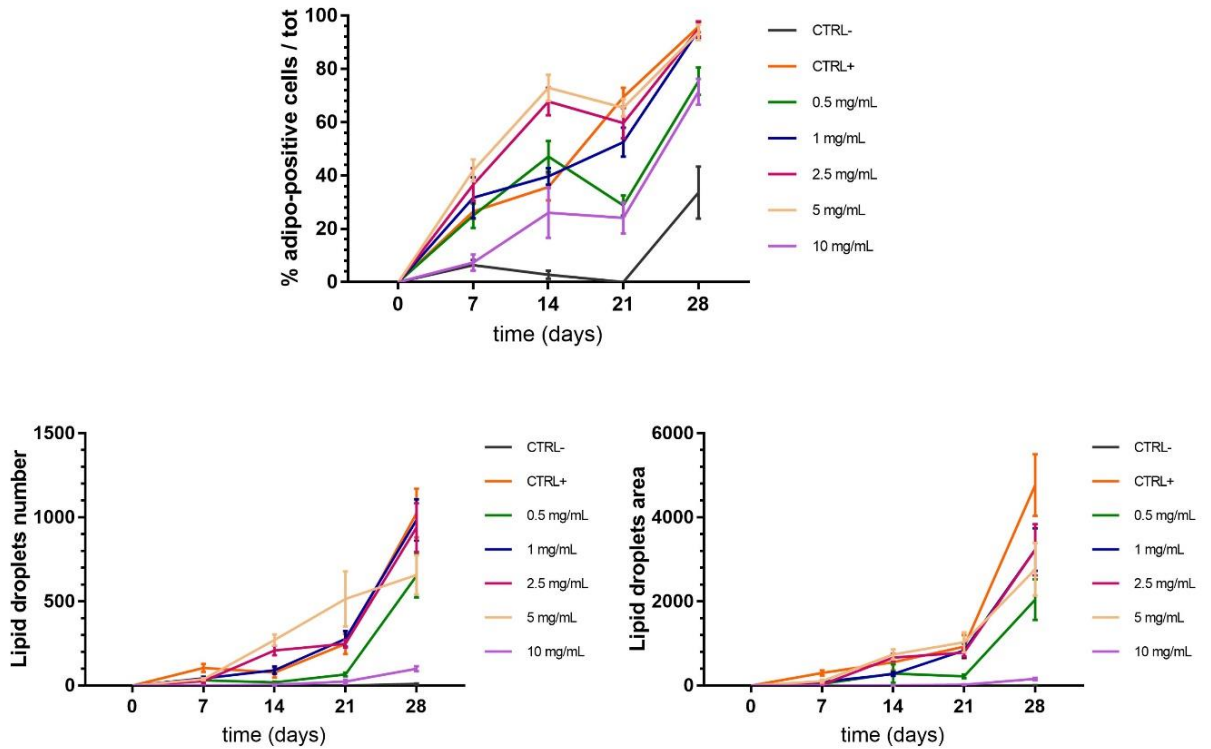


Figure 5. Statistical analysis for the rate of positive cells (up), amount of lipid droplets (down left) and the area of the lipid droplets (down right). It can be seen that the evaluated concentrations of 2.5 and 5 mg/mL are comparable with the positive control on three measured parameters.

Table 1. summarizes the statistical significance among the data for the percentage of positive cells parameter during the different days of evaluation. The analysis has been performed with Graph Prism performing a Two-Way Anova.

Table 1. Statistical significance of % adipo-positive cells/tot among the treatments at each evaluated time. Significant statistical differences are indicated (p-value <0.05=*, 0.005<p-value <0.001=**, p-value <0.001=*** or p-value <0.0001=****).

	0 days	7 days	14 days	21 days	28 days
CTR- : CTR+		*	****	****	****
CTR- : 0.5		*	****	***	****
CTR- : 1		**	****	****	****
CTR- : 2.5		****	****	****	****
CTR- : 5		****	****	****	****
CTR- : 10			**	**	****
CTR+ : 0.5				****	*
CTR+ : 1					
CTR+ : 2.5			****		
CTR+ : 5			****		
CTR+ : 10		*		****	**
0.5 : 1				**	*
0.5 : 2.5			*	****	*
0.5 : 5			***	****	
0.5 : 10			*		
1 : 2.5			***		
1 : 5			****		
1 : 10		**	**		**
2.5 : 5					
2.5 : 10		****	****	****	**
5 : 10		****	****	****	**

3.1.2. Analysis of antibody expression

Considering the results of the previous study for adipose stimulation, for the evaluation of the CD44 expression were selected the concentrations of 2.5 and 5 mg/ml to be evaluated. Figure 6 shows a graphic of the measured percentage of the CD44 antibody during the different evaluated time points comparing the selected concentrations and the control. It can be seen in the figure that the percentage of active CD44 gene in the control group remained almost stable during the days of study with a light decrement. On the other hand, the percentages of the treated cells decreased considerably from 7 to 14 days of study, with a more significant reduction for the cells treated with the HA at 5 mg/ml. The percentage continued decreasing for both treatments but with a reduced variability during the remaining days of the study. This behavior could be due to a downregulation mechanism of the cells that provoke the internalization of the CD44 antigen in the presence of an HA saturated medium.

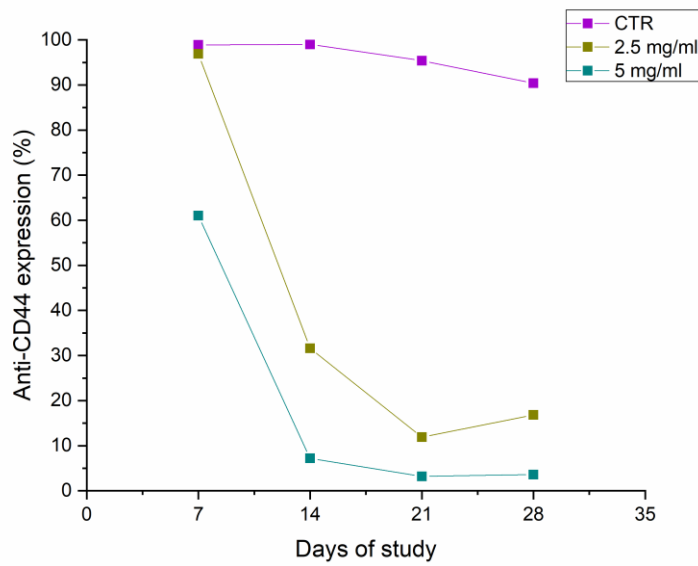


Figure 6. Comparison of the CD44 expression of cells treated with the evaluated LMW-HA at two different concentrations (2.5 and 5 mg/mL) for 7, 14, 21 and 28 days compared with control cells. It can be seen that both treatments down regulate the CD44 expression.

3.2.Clinical evaluation

The clinical results showed, among the 4 received samples, two of them presented improvements in the general aspect of the skin tissue with an increase in papillary and microvessels formation. After deeper analysis, it was found that LMW-HA at a concentration of 1mg/mL starts to repair the tissue after 30 days of treatment. Figure 7 shows representative images of the sample treated with the HA pre and post-treatment. The scar after 30 days presented a smoother and vascularized appearance indicating an initial restructuration of the tissue with a noticeable papillary layer.

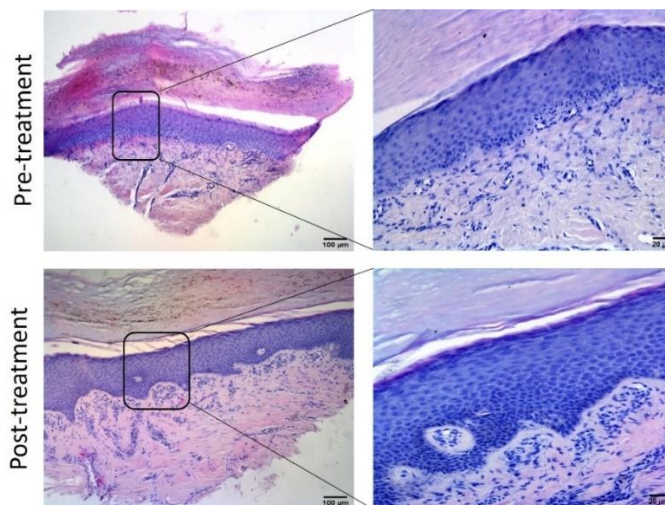


Figure 7. Representative images of a scar before and after the treatment with HA at two different magnifications (scale bars 100 µm (left) and 20 µm (right)) showing that after the treatment it is noticeable a papillary layer.

On the other hand, the samples treated with the saline solution displayed a compact structure with few vessels, disorganized collagen fibers and lymphocytic infiltrates. Additionally, after 30 days of study, the control samples do not present papilla formation. Figure 8 shows some representative images of a scar before and after the treatment with saline solution.

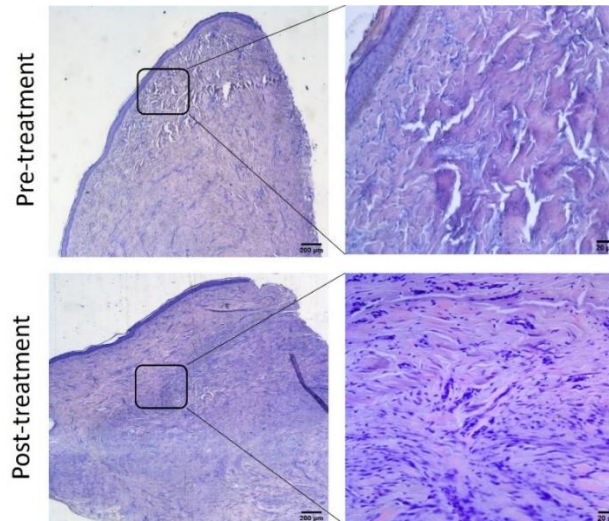


Figure 8. Representative images of a scar treated with saline solution pre and post injection at two magnifications (scale bars 100 µm (left) and 20 µm (right)) to evidence the presence of lymphocytic infiltrates after the treatment.

4. DISCUSSION

The skin is the largest organ of the human body; therefore, it daily subjected to injuries after either trauma, surgery, or skin burns. Annually millions of people develop some sort of skin scar; of these people, more than 11 million require medical treatment around the world, as reported by the World Health Organization (WHO) (10)(25). Aberrant scarring affects the overall well-being of the patients giving them physical and psychological implications in their daily life (26). Aberrant scars, although are asymptomatic, when they grow large and/or are located at the joints may cause functional limitations and discomfort to the patients (27) and their treatment is a burden for the healthcare system (7). Reducing the required time for scar treatment might influence the restoration of the physiological function of the affected area (28).

Despite the number of therapies used for scar treatment, none has shown encouraging results which is why scars remain a medical and cosmetic challenge (10). In this study was evaluated a Low Molecular Weight Hyaluronic Acid to improve skin scar treatment. Initially, ASCs were placed in contact with the evaluated HA to elucidate the influence of concentration in the stimulation of stem cell differentiation through the activation of the CD44 receptor. It has been discovered that the differentiation of ASCs into adipocytes increases wound repair and regeneration capacities of the tissue (29)(30). The HA interacts with the cells by bonding with the cell surface receptor CD44; some studies have demonstrated that upregulation of CD44 expression is characteristic in cancer cells, increasing the possibilities for metastasis (31).

The results show that the evaluated HA stimulates the differentiation of stem cells to different degree by modifying the concentration. It was seen that both lower concentrations and higher take a longer time to promote lipid accumulation, probably because lower concentrations required more time to activate the differentiative pathways of cells. Meanwhile, higher concentrations encapsulate the cell avoiding its cell-cell communication, which affects the differentiation process. Our results demonstrated that concentrations of 2.5 and 5 mg/mL presented the fastest stimulation, as it can be seen with the accumulation of lipid droplets in the cytoplasm of the cells in contact with both treatments, which increased in size during the days of the study. According to the literature, mature adipocytes possess one lipid droplet of a size more significant than the cell nucleus (32). Considering the differentiation results, the selected concentrations for the study of CD44 regulation were 2.5 and 5 mg/mL. It was found that the presence of LMW-HA downregulates the CD44 expression being more remarkable for the concentration of 5 mg/mL. It could be possible that once the cell receives enough stimulation, it does not generate additional antigens, which means that there are no more receptors available for bonding with the used antibody for the FACS analysis resulting in an under-expressed antigen. These results suggest that HA concentration directly influences cellular differentiation mechanisms.

Translating these results into the clinical study, it was noticeable that the adipogenesis stimulation generated by the evaluated HA promotes the restitution of the tissue from a damaged structure into a healthy one. It was seen that using HA in the scar treatment increases the wound healing capacities inducing the formation of microvessels and a smoother appearance. The tissue regeneration in scar treatment may increase the possibility of total recovery of the tissue and therefore improve the quality of life of patients with difficult-to-treat scars. Reducing the required time for scar treatment might influence the restoration of the physiological function of the affected area (28).

5. CONCLUSION

The results suggest that the activation of ASC to differentiate and the degree of activation depends on the physicochemical characteristics of biomaterials, as seen in this study with HA. The results also reveal that adipogenesis stimulation is strongly dependent on the HA concentration, confirming that HA is a crucial player in the tissue regeneration process and that an increase in concentration may reduce the recovery time of damage tissue.

REFERENCES

1. National Geographic. Skin is the human body's largest organ [Internet]. 2017 [cited 2019 Nov 6]. Available from: <https://www.nationalgeographic.com/science/health-and-human-body/human-body/skin/>
2. Dimatteo R, Darling NJ, Segura T. In situ forming injectable hydrogels for drug delivery and wound repair ☆. *Adv Drug Deliv Rev* [Internet]. 2018;127:167–84. Available from: <http://dx.doi.org/10.1016/j.addr.2018.03.007>

3. Graham HK, Eckersley A, Ozols M, Mellody KT, Sherratt MJ. Human Skin : Composition , Structure and Visualisation Methods. :1–18.
4. Chen H, Cheng J, Ran L, Yu K, Lu B, Lan G. An injectable self-healing hydrogel with adhesive and antibacterial properties effectively promotes wound healing. *Carbohydr Polym* [Internet]. 2018;201(June):522–31. Available from: <https://doi.org/10.1016/j.carbpol.2018.08.090>
5. Xu H, Huang S, Wang J, Lan Y, Feng L, Zhu M, et al. Enhanced cutaneous wound healing by functional injectable thermo- sensitive chitosan-based hydrogel encapsulated human umbilical cord- mesenchymal stem cells. *Int J Biol Macromol* [Internet]. 2019;137:433–41. Available from: <https://doi.org/10.1016/j.ijbiomac.2019.06.246>
6. Editorial. Wound healing and scar wars. *Adv Drug Deliv Rev*. 2018;129:1–3.
7. Xue M, Zhao R, Lin H, Jackson C. Delivery systems of current biologicals for the treatment of chronic cutaneous wounds and severe burns. *Adv Drug Deliv Rev* [Internet]. 2018;129:219–41. Available from: <https://doi.org/10.1016/j.addr.2018.03.002>
8. Rahimnejad M, Derakhshanfar S, Zhong W. Biomaterials and tissue engineering for scar management in wound care. *Burn Trauma* [Internet]. 2017;5(1):1–9. Available from: <http://dx.doi.org/10.1186/s41038-017-0069-9>
9. Fernandes MG, da Silva LP, Cerqueira MT, Ibañez R, Murphy CM, Reis RL, et al. Mechanomodulatory biomaterials prospects in scar prevention and treatment. *Acta Biomater*. 2022;150:22–33.
10. Stoica AE, Grumezescu AM, Hermenean AO, Andronescu E, Vasile BS. Scar-free healing: Current concepts and future perspectives. *Nanomaterials*. 2020;10(11):1–18.
11. Dhivya S, Padma VV, Santhini E. Wound dressings – a review. *BioMedicine*. 2015;5(4):24–8.
12. Qu J, Zhao X, Liang Y, Xu Y, Ma PX, Guo B. Degradable conductive injectable hydrogels as novel antibacterial , anti- oxidant wound dressings for wound healing. *Chem Eng J* [Internet]. 2019;362(January):548–60. Available from: <https://doi.org/10.1016/j.cej.2019.01.028>
13. Zhu Y, Kruglikov IL, Akgul Y, Scherer PE. Hyaluronan in adipogenesis, adipose tissue physiology and systemic metabolism. *Matrix Biol* [Internet]. 2019;78–79:284–91. Available from: <https://doi.org/10.1016/j.matbio.2018.02.012>
14. Papakonstantinou E, Roth M, Karakiulakis G. Hyaluronic acid: A key molecule in

- skin aging. *Dermatoendocrinol.* 2012;4(3):253–8.
15. Chun C, Lee DY, Kim JT, Kwon MK, Kim YZ, Kim SS. Effect of molecular weight of hyaluronic acid (HA) on viscoelasticity and particle texturing feel of HA dermal biphasic fillers. *Biomater Res* [Internet]. 2016;20(1). Available from: <http://dx.doi.org/10.1186/s40824-016-0073-3>
 16. Abednejad A, Ghaee A, Morais ES, Sharma M, Neves BM, Freire MG, et al. Polyvinylidene fluoride–Hyaluronic acid wound dressing comprised of ionic liquids for controlled drug delivery and dual therapeutic behavior. *Acta Biomater* [Internet]. 2019 Dec;100(xxxx):142–57. Available from: <https://linkinghub.elsevier.com/retrieve/pii/S1742706119306749>
 17. Govindaraju P, Todd L, Shetye S, Monslow J, Puré E. CD44-dependent inflammation, fibrogenesis, and collagenolysis regulates extracellular matrix remodeling and tensile strength during cutaneous wound healing. *Matrix Biol* [Internet]. 2019 Jan;75–76(1):314–30. Available from: <https://linkinghub.elsevier.com/retrieve/pii/S0945053X18301276>
 18. Bhattacharya DS, Svechkarev D, Soucek JJ, Hill TK, Taylor MA, Natarajan A, et al. Impact of structurally modifying hyaluronic acid on CD44 interaction. *J Mater Chem B* [Internet]. 2017;5(41):8183–92. Available from: <http://xlink.rsc.org/?DOI=C7TB01895A>
 19. Litwiniuk M, Krejner A, Grzela T. Review: Hyaluronic Acid in Inflammation and Tissue Regeneration. *Wounds.* 2016;28(3):78–88.
 20. Oliferenko S, Kaverina I, Small J V., Huber LA. Hyaluronic acid (HA) binding to CD44 activates Rac1 and induces lamellipodia outgrowth. *J Cell Biol.* 2000;148(6):1159–64.
 21. Misra S, Hascall VC, Markwald RR, Ghatak S. Interactions between hyaluronan and its receptors (CD44, RHAMM) regulate the activities of inflammation and cancer. *Front Immunol.* 2015;6(MAY).
 22. Kwon MY, Wang C, Galarraga JH, Puré E, Han L, Burdick JA. Influence of hyaluronic acid modification on CD44 binding towards the design of hydrogel biomaterials. *Biomaterials* [Internet]. 2019 Nov;222(1):119451. Available from: <https://linkinghub.elsevier.com/retrieve/pii/S0142961219305502>
 23. Peroni D, Scambi I, Pasini A, Lisi V, Bifari F, Krampera M, et al. Stem molecular signature of adipose-derived stromal cells. *Exp Cell Res.* 2008;314:603–15.
 24. Busato A, De Francesco F, Biswas R, Mannucci S, Conti G, Fracasso G, et al. Simple and Rapid Non-Enzymatic Procedure Allows the Isolation of Structurally

- Preserved Connective Tissue Micro-Fragments Enriched with SVF. *Cells* [Internet]. 2020 Dec 29;10(1):36. Available from: <https://www.mdpi.com/2073-4409/10/1/36>
25. Monavarian M, Kader S, Moeinzadeh S, Jabbari E. Regenerative Scar-Free Skin Wound Healing. *Tissue Eng - Part B Rev*. 2019;25(4):294–311.
 26. Ziolkowski N, Kitto SC, Jeong D, Zuccaro J, Adams-Webber T, Miroshnychenko A, et al. Psychosocial and quality of life impact of scars in the surgical, traumatic and burn populations: A scoping review protocol. *BMJ Open*. 2019;9(6):1–6.
 27. Seo BF, Lee JY, Jung S. Models of Abnormal Scarring. *Biomed Res Int*. 2013;2013(423147):8.
 28. Shen W, Chen L, Tian F. Research progress of scar repair and its influence on physical and mental health. *Int J Burns Trauma*. 2021;11(6):442–6.
 29. Storti G, Scioli MG, Kim BS, Orlandi A, Cervelli V, De Francesco F. Adipose-Derived Stem Cells in Bone Tissue Engineering: Useful Tools with New Applications. *Stem Cells Int*. 2019;2019.
 30. Polotto S, Bergamini ML, Pedrazzi G, Arcuri MF, Gussago F, Cattelani L. One-step prepectoral breast reconstruction with porcine dermal matrix-covered implant: A protective technique improving the outcome in post-mastectomy radiation therapy setting. *Gland Surg*. 2020;9(2):219–28.
 31. Chen C, Zhao S, Karnad A, Freeman JW. The biology and role of CD44 in cancer progression: Therapeutic implications. *J Hematol Oncol*. 2018;11(1):1–23.
 32. Weidlich D, Honecker J, Boehm C, Ruschke S, Junker D, Van AT, et al. Lipid droplet-size mapping in human adipose tissue using a clinical 3T system. *Magn Reson Med* [Internet]. 2021 Sep;86(3):1256–70. Available from: <https://onlinelibrary.wiley.com/doi/10.1002/mrm.28755>

CHAPTER IV:

A NOVEL TRANSLATIONAL SYSTEM IN STEM CELL THERAPY: CASE STUDY

PROLOGUE

Since its discovery, the use of stem cells in tissue regeneration is increasingly gaining attention. However, the ethical implications of cellular-based therapies reduced their wide applications. In this regard, new approaches are required. This chapter presents a study using a novel system to obtain not only stem cells but a new type of stromal vascular fraction that might provide new possibilities for cellular therapies.

1. BACKGROUND

The autologous fat graft is used mainly in aesthetic medicine, particularly for face rejuvenation and volume restoration, but also for reconstructive purposes such as breast reconstruction, hypertrophic scars and painful hand neuromas, thanks to its simple harvesting through liposuction and its autogenous and biocompatible nature [1]. Nevertheless, fat graft presents some limitations, such as the size of the injectable product, the unpredictable fat resorption rates [2] and subsequent adverse events [3]. Moreover, injecting the fat graft into the dermal layer to treat superficial rhytides, wrinkles, and atrophic scars is still challenging [4]. Therefore, many patients still need to be convinced to use this procedure. Fortunately, modern commercial medical devices can make up for the shortcomings of the original techniques [5]. Moreover, during the last years, surgeons and researchers tested different protocols to manipulate fat and inject it rapidly without inflammatory reactions. In particular, the adipose tissue should adequately integrate within the damaged tissue through sufficient vascularization. This makes the fate of the fat uncertain when used as a volumetric filler. Derivatives of adipose tissue, such as microfat, nanofat, microvascular fragments, stromal vascular fraction, and stem cells, are commonly used in research but also clinically to enhance the vascularization of implants and grafts at defect sites. In plastic surgery, adipose tissue is harvested via liposuction and can be manipulated in three ways (macro-, micro- and nanofat) in the operating room, depending on its ultimate use and the disgregation system [6]. Whereas macro- and microfat are used as a filling material, nanofat is a viscous extract that can induce tissue remodelling because it is rich in growth factors and stem cells [6].

Nanofat is defined as an autologous liquid-like tissue obtained through the mechanical manipulation of lipoaspirates. During the process, the harvested fat is filtered and shuffled between two 10-cc syringes with a 30 passes connector, destroying nearly all adipocytes, resulting in a purified emulsion product [6]. The final product can be directly injected into the target site with high precision, even in difficult areas, allowing it to work superficially with finer sharp needles (27 or 30 gauge) [7,8]. Nanofat is widely used in clinical practice to treat facial compartments, hypertrophic and atrophic scars, wrinkle attenuation, skin rejuvenation and alopecia [9–12]. Recently, Nanofat has been investigated for broader applications, such as wound healing by the paracrine effect of nanofat products [13] [1]. The regenerative effect of Nanofat is attributable to the presence of microfragments of stromal connective tissue composed of adipose-derived stem cells (ASCs), endothelial precursor cells, endothelial cells, macrophages, smooth muscle cells, lymphocytes, pericytes and pre-adipocytes [1,14–16]. The nanofat main secretome consists of proliferative, pro-angiogenic, pro-differentiative and pro-antiapoptotic factors such as Platelet-Derived Growth Factor (PDGF), Vascular Endothelial Growth Factor (VEGF), Insulin-like Growth Factor (IGF), among others [14][17].

Among cellular components of nanofat, ASCs represent the leading actor of tissue regeneration, cooperating with other cellular elements in the whole process of *restitutio ad integrum* [18]. ASCs are adult plastic-adherent mesenchymal stem cells easily isolable from adipose tissue allowing autologous cell transplantation [19,20]. According to the literature, ASCs module the inadequate healing responses which

lead to tissue degeneration, such as chronic inflammation [21], hypermetabolic responses [22] and fibrosis [23]. Moreover, ASCs stimulate extracellular matrix production, new collagen deposition and early revascularisation [24,25]. Initial *in vitro* experiments demonstrated the angiogenic effect of ASC [26], were then attributed to the presence of the secretome [27]. Their biological effect is due to the self-renewal property, immunosuppressive potential and ability to differentiate into different mesodermal cell lineages, such as adipocytes, osteocytes and chondrocytes [28–30]. For these reasons, *in vitro* characterization of nanofat in terms of ASCs content could reflect the regenerative potential of the product, indicating how many cells are capable of duplicating and differentiating in a short time, which can guarantee a replicable result for patients and reduce the recovery time.

Recent studies have focused on a subpopulation of mesenchymal stem cells defined as Multi-lineage differentiating stress enduring cells (MUSE). MUSE cells are defined as non-tumorigenic stress-tolerant and pluripotent cells with high regenerative potential [31–34] and migration capacity into the damaged tissue [35]. MUSE, were isolated from different sources such as skin, bone marrow and hair bulbs, but principally were isolated from adipose tissue, in which researchers found a higher number of MUSE cells [36–38]. MUSE cells are characterized by high integration capacity, and restoration of tissue function, as evidenced in numerous preclinical studies [34][39]. Thanks to their unique features, MUSE cells are a promising candidate for tissue regeneration and stem cell therapy.

This study aimed to characterize at morphological and cellular levels a promising and standardized single-use assembled system named *Hy-Tissue Nanofat* that allows obtaining a final product enriched in pluripotent and proliferative ASCs with highly potential use in clinical practice.

2. MATERIALS AND METHODS

2.1. Adipose Tissue Collection

The adipose tissue was collected from 8 women undergoing liposuction for aesthetic purposes, aged between 41 and 69 years. Informed consent was taken before collecting lipoaspirates following the ethical guidelines established by the review committee for human studies of AOU “Ospedali Riuniti”, Ancona, Italy (Micro-adipose graft_01, 18 May 2017). Klein solution (2% Lidocaine solution: 0.08% w/v; Adrenaline 1mg/mL solution: 0.1% v/v in 0.9% saline) was injected 10 min after the liposuction. A cannula of 11 G, 6 holes, and 20 mL Vac-Lock syringe provided with the *Hy-Tissue Nanofat Plus* system was used to obtain lipoaspirate (about 30 mL of fat from each donor's) from the abdominal area. The fat was transported in an adiabatic container to the laboratory and processed within 20 h from harvest.

2.2. Procedure for NANO FAT-derived microfragment production

Each adipose tissue sample (about 30 mL) was divided into 3 portions. The first portion (about 10 mL) was processed with the *Hy-Tissue Nanofat* system (Fidia Farmaceutici, Abano Terme, Italy). The lipoaspirate was shuffled and emulsified

through two 10 cc coupled syringes via a 30 passes connector. The emulsified lipoaspirate was filtered into the inner bag with a pore size of 120 µm and was collected into a lower syringe.

To characterise the product at a cellular level, it was centrifuged at 3000 rpm for 6 min and filtered through a 70 µm nylon mesh. The product obtained by this method was named “Nanofat-derived SVF (N-ASC)”.

2.3. Enzymatic Digestion of Fat

The second portion of lipoaspirate (about 10 mL) was processed using an enzymatic method, as reported by Busato et al., 2020 [30]. The samples were digested with collagenase type I at the concentration of 1 mg/mL (GIBCO Life Technology, Monza, Italy) dissolved in Hank’s Balanced Salt Solution (HBSS, GIBCO Life Technology, Monza, Italy) with 2% of Bovine Serum Albumin (BSA, GIBCO Life Technology, Monza, Italy) for 45 min at 37°C. Complete culture medium (Dulbecco’s Modified Eagle’s Medium (DMEM), Sigma-Aldrich, Italy), supplemented with 10% of Fetal Bovine Serum (FBS, GIBCO Life Technologies, USA), 1% of 1:1 penicillin/streptomycin (P/S solution, GIBCO Life Technologies, USA) and 0.6% of Amphotericin B (GIBCO Life Technologies, USA), was added to neutralise the enzyme action. After the neutralisation process, the sample was centrifuged at 3000 rpm for 5 min. The cell pellet was incubated with 1 mL of erythrocyte lysis buffer 1X (Macs Miltenyi Biotec, Milan, Italy) for 10 min at room temperature. Again, the cell suspension was centrifuged and resuspended with 1 mL of complete culture medium. Finally, the cells were filtered through a 70 µm nylon mesh. The product obtained by this method was named “collagenase derived ASCs (ED-ASCs)”.

2.4. Enzymatic Digestion of Hy-Tissue Nanofat-SVF

The remaining portion of lipoaspirate (10 mL) was first processed with the *Hy-Tissue Nanofat kit*, followed by the treatment with collagenase type I. The Nanofat-SVF, obtained, as described in the paragraph a), was incubated with collagenase type I at a concentration of 1 mg/mL (GIBCO Life Technology, Monza, Italy) dissolved in Hank’s Balanced Salt Solution (HBSS, GIBCO Life Technology, Monza, Italy) with 2% of Bovine Serum Albumin (BSA, GIBCO Life Technology, Monza, Italy) for 45 min at 37°C. Complete culture medium (Dulbecco’s Modified Eagle’s Medium (DMEM), Sigma-Aldrich, Italy), supplemented with 10% of Fetal Bovine Serum (FBS, GIBCO Life Technologies, USA), 1% of 1:1 penicillin/streptomycin (P/S solution, GIBCO Life Technologies, USA) and 0.6% of Amphotericin B (GIBCO Life Technologies, USA), was added to neutralise the enzyme action. After the neutralisation process, the sample was centrifuged at 3000 rpm for 5 min. The cell pellet was incubated with 1 mL of erythrocyte lysis buffer 1X (Macs Miltenyi Biotec, Milan, Italy) for 10 min at room temperature. Again, the cell suspension was centrifuged and resuspended with 1 mL of complete culture medium. Finally, the cells were filtered through a 70 µm nylon mesh. The product obtained by this method was named “enzymatic digestion of Nanofat-SVF (N-ED-ASCs)”.

Table 1 summarizes the used code names to identify the different processes employed to treat the fat tissue.

Table 1. Code names of the products obtained with the evaluated protocols for fat tissue digestion.

Evaluated protocol	Code name
Nanofat-derived SVF	N-ASC
Collagenase-derived ASC	ED-ASC
Enzymatic digestion of Nanofat SVF	N-ED-ASC

2.5. Morphological analysis

To evaluate the morphology of the *Hy-Tissue Nanofat* SVF whole-mount assay was performed, as reported in Busato et al. 2020 [30]. The emulsion was swiped in a histological glass and stained with Toluidine Blue (Sigma-Aldrich, Milan, Italy). All slides were examined under an Olympus BX-51 microscope (Olympus, Tokyo, Japan) equipped with a digital camera (DKY-F58 CCD JVC, Yokohama, Japan). In addition, for a deeper morphological understanding the *Hy-Tissue Nanofat* SVF was studied in a Scanning Electron Microscopy (SEM). The sample was fixed with glutaraldehyde 2% diluted in 0.1M phosphate buffer (pH 7.4) for 2 hours at 4°C, post-fixed in 1% osmium tetroxide (OsO₄) diluted in 0.2M potassium hexacyanoferrate for 1 hour at 4°C. The samples were dehydrated in a graded concentration of ethanol, followed by a critical point dryer (CPD 030, Balzers, Vaduz, Liechtenstein), mounted to stubs with colloidal silver and sputtered with gold by a MED 010 coater (Balzers), and examined with FEI XL30 scanning electron microscope (FEI Company, Eindhoven, Netherlands).

2.6. Cellular Yield

Collected cells from the evaluated procedures were counted using Trypan Blue exclusion assay using a CytoSMART counter (Automated Image-Based Cell Counter, version 1.5.0.16380, CytoSMART Technologies B.V, Eindhoven, Netherlands). Cell yield was calculated considering the total amount of cells of N-ASC, ED-ASC, and N-ED-ASC divided by the fat volume.

2.7. Proliferation capacity

To evaluate the cell proliferation capacity of the cells derived from the three different isolation procedures (N-ASC, ED-ASC, and N-ED-ASC), 2×10^5 cells of each procedure were plated on a 25 cm² T-flask and incubated in a humidified atmosphere with 5% CO₂ at 37°C. 72 h after the cell extraction, the complete culture medium was changed and, subsequently, every 48 h until 80% confluence. The days required for the cultured cells to reach confluence (cellular passage 1) were used for determining the proliferation capacity. Furthermore, the population doubling

time (PDT) assay was performed to estimate the time request for cell replication. Four days after the seeding, 5×10^4 cells from N-ASC, ED-ASC, and N-ED-ASC were plated in T-25 Flasks (in triplicates) with 4 mL of complete culture media. They were incubated in a humidified atmosphere with 5% CO₂ at 37°C for different time points, 24, 72, and 96 h. At each time point, after a brief wash with PBS, the cells were incubated with 0.25% trypsin (GibcoBRL/Life Technologies) at 37°C for 5 min, centrifugated, and the cell pellet was resuspended in 1 mL of complete culture media. CytoSMART counter (Automated Image-Based Cell Counter, version 1.5.0.16380, CytoSMART Technologies B.V, Eindhoven, Netherlands) was used to detect the number of cells at each time point. PDT was calculated using the following equation: $PDT = [t(h) \cdot \log 2] / \log (N_f / N_i)$ [40], where N_i and N_f are initial and final cell numbers, respectively.

2.8. Clonogenic capacity

N-ASC, ED-ASC, and N-ED-ASC were seeded in a 6-well plate in triplicate. For N-ASC were plated 5×10^3 , while for N-ED-ASC and ED-ASC were used 1×10^3 cells. Cells were cultured for 14 days. Toluidine Blue (Sigma-Aldrich, Milan, Italy) staining was performed to count the colonies. The frequency of CFU-F within N-ASC, ED-ASC, and N-ED-ASC was expressed as a percentage of seeded cells.

2.9. Immunophenotyping

N-ASC, ED-ASC, and N-ED-ASC and the subsequent subculture cells (cellular passage 2) were characterised by flow cytometry. To perform cytofluorimetric analysis, the different cells product was centrifuged at 3000 rpm for 6 min. The cell pellet obtained was resuspended in complete culture medium, incubated with 1 mL of erythrocyte lysis buffer 1X (Macs Miltenyi Biotec, Milan, Italy) for 10 min at room temperature, and filtered through a 70 µm cell-strainer. Subsequently, cells were washed with 1 mL in PBS and incubated (1×10^5 for each tube) with conjugated antibodies on ice for 30 min. After incubation, the pellets were centrifuged (5000 rpm, 7 min) and resuspended in 100 µL of PBS.

The antibodies used were: CD105 APC conjugate (1:20 dilution), CD73 BV421 conjugate (1:20 dilution), CD34 PE conjugate (1:5 dilution), CD45 FITC conjugate (1:20 dilution), CD146 APC conjugate (1:20 dilution), SSEE3 FITC conjugate (1:20 dilution). All antibodies were purchased from BD Biosciences (Becton Dickinson Italy S.P.A., Milano, Italy). Also the isotypes of each antibody were incubated with cells, in order to determine the threshold of fluorescence and to exclude not specific signal. Isotypes were indicated by the datasheet of each primary antibody and incubated with cells at the same concentration of primary antibodies.

Immunophenotyping was performed through a chant II FACS (BD, Becton Dickinson, Milano, Italy).

2.10. Differentiation assay

The differentiation potential was evaluated *in vitro* for the N-ASC compared with ED-ASC and N-ED-ASC. Not-induced cells were used as control (CTR). Differentiation was carried out employing expanded cultured cells from passage 4. For adipogenic differentiation, 5000 cells were seeded on a 12-well plate containing one slide per well to make the cells grow adherent, incubated at 37°C, 5% CO₂, and after 24 h, the complete culture medium was replaced with adipogenic media (Sigma-Aldrich, Milan, Italy). To evaluate the adipogenic differentiation capacity, after 4 and 9 days of incubation, the cells were fixed with Baker's fixative (Bio-Optica, Milan, Italy) for 10 min at 4 °C, washed with tap water for 10 min, and stained with Oil-Red-Oil solution (Bio-Optica, Milan, Italy) for 10 min and Mayer's hematoxylin (Bio-Optica, Milan, Italy) for 5 min. Finally, the glass coverslips were mounted with Mount Quick aqueous (Bio-Optica, Milan, Italy).

For chondrogenic differentiation, 1×10^6 cells resuspended in 5 μ L of complete culture media were seeded in a 12-well plate, and after 2 h, the chondrogenic media was added (StemPro chondrogenic differentiation Kit -GIBCO Life Technology, Monza, Italy). After 4 and 9 days of incubation, changing the media every 3 days, cells were fixed with 4% formaldehyde (Bioptica, Milan, Italy) in PBS 0.05M for 30 min at 4 °C, washed twice with distilled water, and stained with Alcian Blue solution (Merck KGaA, Darmstadt, Germany) for 40 min and with Nuclear Fast Red (Bioptica, Milan, Italy) for 20 min. Finally, after brief dehydration, the glass coverslips were mounted with Entellan (Merck KGaA, Darmstadt, Germany).

For osteogenic differentiation, 5000 cells were seeded on a 12-well plate with complete culture media, and after 24 h, the media was replaced with osteogenic media (StemPro osteogenesis differentiation Kit-GIBCO Life Technology, Monza, Italy). To evaluate the osteogenic differentiation capacity, after 4 and 9 days of incubation, the cells were fixed with 4% formaldehyde (Bioptica, Milan, Italy) in PBS 0.05M for 30 min at 4 °C, washed twice with distilled water, and incubated with Alizarin Red Solution (Merck KGaA, Darmstadt, Germany) for 2/3 min and Mayer's hematoxylin (Bio-Optica, Milan, Italy) for 30 sec. Finally, after brief dehydration, the glass coverslips were mounted with Entellan (Merck KGaA, Darmstadt, Germany).

The stained cells were imaged using a bright-field optical microscope, Olympus BX-51 (Olympus, Tokyo, Japan) and equipped with a digital camera (DKY-F58 CCD JVC, Yokohama, Japan). Slides were gently cleaned with ethanol, then placed on the microscope slides holder, and 5 images for each slide were acquired using a 20X objective for quantifying the lipid droplets and a 10X objective for the calcified and collagenous matrices quantification. The acquired images contained 8 to 12 cells to standardize the quantification.

The semi-quantitative analysis was performed using a custom-designed Image J Software plug-in (U.S. National Institutes of Health), in blind condition, with previously treated images (binary images). In the case of adipogenic differentiation, the number of red spots (lipid droplets) on the cytoplasm of the cell was considered. For chondrogenic and osteogenic differentiation was considered, the area covered by collagen aggregates stained in blue and calcification deposits stained in red, respectively.

2.11. Immunostaining for MUSE detection

An immunostaining assay was used to reveal the presence of MUSE cells in Nanofat derived ASCs at cellular passage 4. N-ASC were seeded on a glass with a diameter of 24 mm in six well-plates in triplicates with complete medium. The wells were incubated at 37 °C and 5% of CO₂. After 24 h, cells were fixed with 4% buffered formalin for 1 h at 4 °C in the dark, washed three times with sterile PBS 1x and incubated with SEEA3 (FITC conjugate, 1:200 dilution) and CD105 (APC conjugate, 1:200 dilution) antibodies in the dark at 4 °C for 30 min. At the end of the incubation with the antibodies, the glasses were washed with PBS, and mounting medium containing DAPI was added. The slices were imaged with an Olympus BX-51 microscope (Olympus, Tokyo, Japan) equipped with a digital camera (DKY-F58 CCD JVC, Yokohama, Japan) at 60× objective. Images were prepared using Las X software.

2.12. Statistical Analysis

The data were reported as mean ± standard deviation (SD). Mann–Whitney tests were performed, and differences between groups were considered statistically significant when p-value < 0.05. All statistical analyses were performed using GraphPad Prism version 8.00 for Windows, GraphPad Software, La Jolla, CA, USA.

3. RESULTS

3.1. Microscopical Analysis of Hy-Tissue Nanofat SVF

Hy tissue Nanofat-SVF was examined at a morphological level to investigate its composition. For this purpose, lipoaspirates were processed following the protocol recommended by the manufacturer (Figure 1.A). The adipose tissue was shuffled 30 times between two connected syringes, filtered through a membrane of 120 µm, and collected with a syringe using the lower valve port of the outer bag, resulting in an autologous whitish emulsion ready to inject.

The microscopical analysis revealed that the Nanofat SVF was mainly composed of intact lipid droplets of different sizes (Figure 1.B). The size distribution of the lipid droplets (Figure 1.C) showed that Nanofat SVF was composed of droplets classified in four main clusters: with a diameter lower than 60 µm (42.42 ± 10.10 µm), between 60-100 µm (76.59 ± 11.77 µm), between 100-200 µm (143.43 ± 33.42 µm) and over 200 µm (245.45 ± 38.07 µm). At the end of procedure, Hy Tissue Nanofat-SVF appears as connective tissue micro-fragments consisting of an extracellular matrix, preserved capillaries with endothelial and perivascular cells (Figure 1.C). The morphologies observed with SEM images (Figure 1.D) allows to evidence the presence of some adipocytes, elastic fibres (dotted arrow in Figure 1.D), connective tissue lamina (asterisk in Figure 1.D) and single collagen fibres (arrow in Figure 1.D). The images shows that the mechanical treatment consents a possible scaffold-like connective tissue formation.

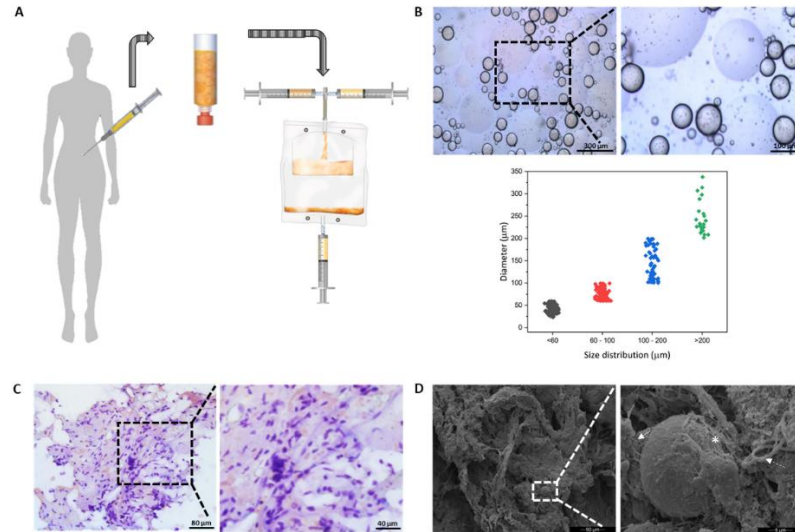


Figure 1. Morphological analysis of Hy-Tissue Nanofat product. (A) Scheme of the Hy-Tissue Nanofat procedure; (B) Light microscopy of Hy-Tissue Nanofat product obtained with the whole-mount method. The square (in Figure 1B, left) indicates the location of the higher magnification (right). (Scale bar: (left) 300 µm, (right) 100µm). The graph represents the size distribution of the lipid droplets. (C). Light microscopy of Hy-Tissue Nanofat product obtained with the whole-mount method after centrifugation. The square (in Figure 1C, left) indicates the location of the higher magnification (Figure 1C, right) (Scale bar: (left) 80 µm, (right) 40 µm). (D) Scanning electron microscopy of Hy-Tissue Nanofat product after centrifugation. The square (in Figure 1D, left) indicates the location of the higher magnification (Figure 1D, right), the elastic fibre, the connective tissue lamina and the single collagen fibre are showed with a dotted arrow, an asterisk and an arrow, respectively. (Scale bar: (left) 50 µm, (right) 5 µm).

To characterise the *Hy-Tissue Nanofat* SVF at a cellular level, ASCs were isolated (N-ASC) and compared with ASCs enzymatically extracted (ED-ASC). Moreover, to verify the total amount and quality of the regenerative units, the *Hy-Tissue Nanofat*-SVF was subjected to enzymatic digestion (N-ED-ASC) (see Material and Methods section). Figure 2 shows the experimental procedure followed to characterise the product in cellular yield, proliferative and clonogenic capability, immunophenotyping and multipotential capacity.

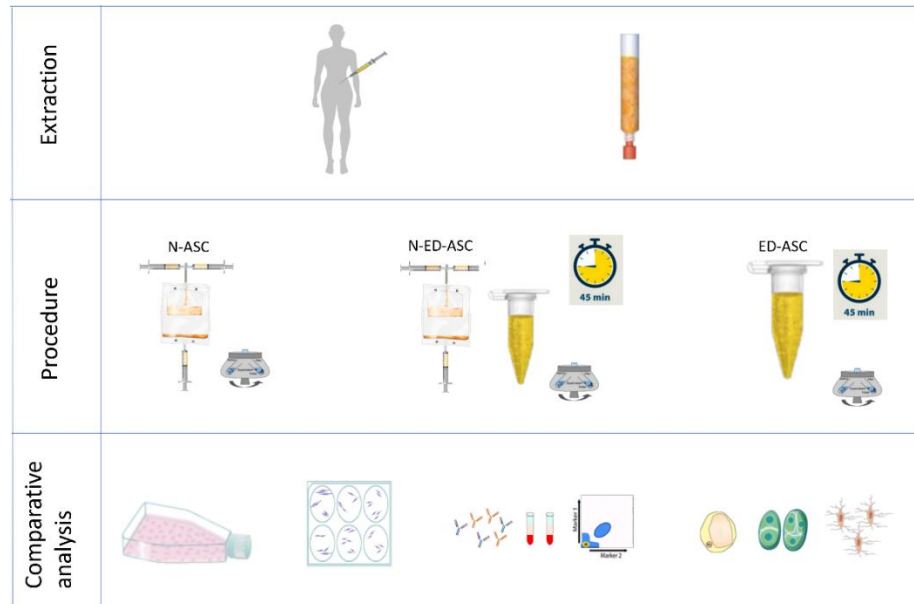


Figure 2. Experimental methodology. The fat sample was divided into three portions to be processed in N-ASC, N-ED-ASC and ED-ASC and evaluated for cell proliferation capacity, CFU-F assay, immunophenotyping and differentiation potential.

3.2. Cell yield, proliferation capacity, and clonogenic potential of N-ASC

The Nanofat derived-SVF obtained by the mechanical disaggregation were analysed in terms of cell yield, product quality, viability, proliferation capacity, and clonogenic potential.

The number of nucleated cells (N-ASC) for ml of fat obtained with the *Hy-Tissue Nanofat* system was $3.74 \times 10^4 \pm 1.31 \times 10^4$ cells/ml FAT (Figure 3.A), while the number of cells extracted after enzymatic digestion of the filtered emulsion (N-ED-ASC) and after the enzymatic digestion of fat (ED-ASC) was $1.20 \times 10^5 \pm 3.90 \times 10^4$ and $4.13 \times 10^5 \pm 1.15 \times 10^4$, respectively. Considering the enzymatic treatment as the gold standard protocol (cell yield 100%), the cellular yield for N-ASC resulted in $9.02 \pm 3.18\%$, which increased to 28.98 ± 9.44 after the enzymatic digestion of the emulsion (N-ED-ASC), as reported in the table in Figure 3.A.

Cells were seeded in T-flasks until confluence to analyse the ASC adhesion and proliferation capacity (Figure 3.B, left). The results show that ED-ASC required less time to reach confluence (4.80 ± 2.28 days) than N-ASC (10.8 ± 2.59 days). This finding reflects the higher frequency of adherent cell content obtained with the enzymatic digestion of the fat. On the contrary, no significant statistical differences were shown between ED-ASC and N-ED-ASC (7.60 ± 3.29 days). Proliferation capacity results were confirmed with a Population Doubling Time assay (PDT) (Figure 3.C, right). PDT reveals that the replication rate of ED-ASC and N-ED-ASC was comparable (52.84 ± 6.40 and 57.06 ± 25.41 h, respectively), while cells obtained from N-ASC required more time to duplicate their number (81.85 ± 18.87 h).

Figure 3.C shows a representative image of N-ASC, N-ED-ASC, and ED-ASC morphology three days after extraction (first change of culture media). *Hy-Tissue Nanofat* treatment did not affect the cell morphology compared to cells obtained from enzymatic digestion, exhibiting a homogeneous fibroblast-like morphology.

Moreover, cellular membranes and nuclei were well-preserved, indicating no sign of cell suffering.

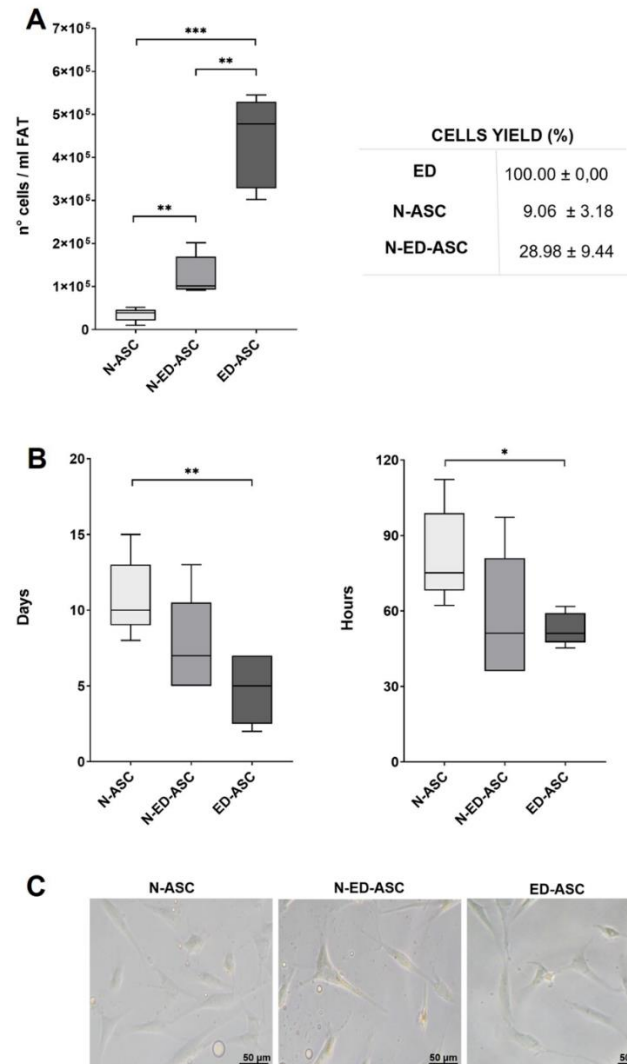


Figure 3. Cellular yield and proliferation capacity obtained with the three evaluated procedures (A) Obtained nucleated cells after the three evaluated treatments. Cells yield (n° of cell/ml FAT) was evaluated considering the enzymatic digestion as 100%; (B, left) Proliferation capacity N-ASC, N-ED-ASC and ED-ASC in T25 flasks. The days required for the adherent cells to reach confluence (passage 1) were counted. (B, right) The PDT of N-ASC, N-ED-ASC and ED-ASC were analysed to evaluate the growth rate of adherent cells; (C) Microscopic images of adherent cells 3 days after the extraction. All the results are shown as mean ± standard deviation represented by the error bars. Box and whisker plots represent the median. Significant statistical differences are indicated (p-value <0.05=*, 0.005<p-value <0.001=** or p-value <0.001=***).

Colony-forming unit-fibroblast (CFU-F) assays were performed to assess the ability of the evaluated methods to grow as colonies. Figure 4.A shows a representative micrograph of CFU-F detected by Toluidine Blue staining after 14 days of seeding. On day 14th, the morphology of CFU-F appeared comparable between the three treatments. CFU-F yield of N-ASC was 61.29 ± 45.10 CFU-F/ml FAT, while the CFU-F yield of N-ED-ASC increased over 11-times (702.29 ± 368.40 CFU/mL FAT, Figure 4.B). Furthermore, the relative proportion of CFU-F in the N-ED-ASC (0.54 ± 0.09 %) increases significantly after the enzyme digestion of the emulsion compared to N-ASC (0.18 ± 0.05 %, Figure 4.C). CFU-F obtained with ED-ASC

resulted in 29- and 3-times more (1830.59 ± 1190.82 CFU-F/mL FAT) compared to the N-ASC and N-ASC-ED, respectively (Figure 4B), with a relative proportion of CFU-F of 2.54 ± 0.69 % (Figure 4.C).

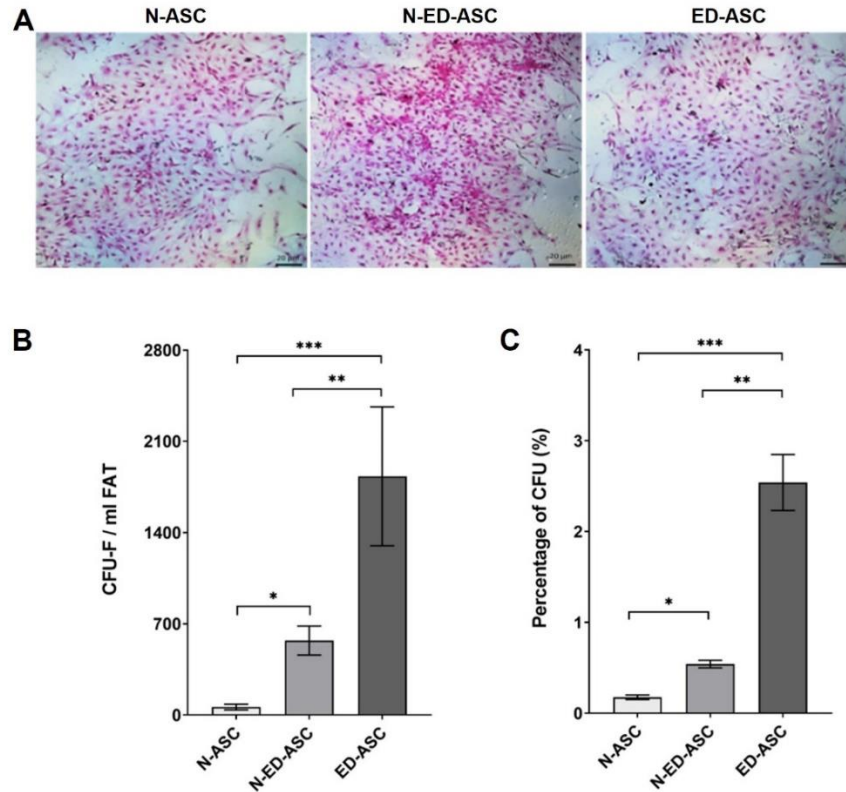


Figure 4. Clonogenic potential of Hy-Tissue Nanofat product. (A) Representative light microscope of CFU-F assay stained with Toluidine Blue (scale bar 20 μ m); (B) CFU-F yields of N-ASC, N-ED-ASC, and ED-ASC. (C) Percentage of CFU-F of N-ASC, N-ED-ASC, and ED-ASC. All the results are shown as mean \pm standard deviation represented by the error bars. Significant statistical differences are indicated (p-value <0.05=*, 0.005<p-value <0.001=* * or p-value <0.001=***).

3.3. Immunophenotyping

To characterise N-ASC immunophenotypically, a cytofluorimetric analysis was performed immediately after the treatments (at cellular passage 0, P0) and after *in vitro* cellular expansion (cellular passage 2, P2). Specific single antigens (such as CD34, CD45, CD105, CD29, CD73) were analysed on the previously selected cells. The proportion of CD34 cells in N-ASC was $3.37 \pm 1.67\%$ (Figure 5.A), not thus far from the percentage of CD34 expression obtained in N-ED-ASC and ED-ASC (7.99 ± 4.6 % and 4.91 ± 2.5 %, respectively). The hematopoietic surface marker CD45 resulted in less expressed (1.27 ± 0.45 %, 1.35 ± 0.71 % and 1.53 ± 0.40 % for N-ASC, N-ED-ASC, and ED-ASC, respectively), as reported in Figure 5.B. Moreover, the frequency of CD105, CD29, and CD73 positive cells (Mesenchymal Stem Cells marker) was evaluated. In N-ASC, the percentage of antibody expression was 15.9 ± 8.86 %, 3.59 ± 2.00 % and 1.79 ± 0.23 % for CD105, CD29 and CD73, respectively (Figure 5.A), comparable with the results obtained for the same antibody in N-ED-ASC and ED-ASC (Figure 5.B). Finally, cultured cells (P2) were also analysed to confirm the phenotype preservation over time (Figure 5.C).

The immunophenotypic analysis after the cellular expansion showed that the surface marker expression profiles of N-ASC, N-ED-ASC and ED-ASC were comparable, revealing a low expression for CD45 and CD34 and a high expression for Mesenchymal Stem Cells associated markers such as CD105, CD73, and CD29 (Figure 5.C).

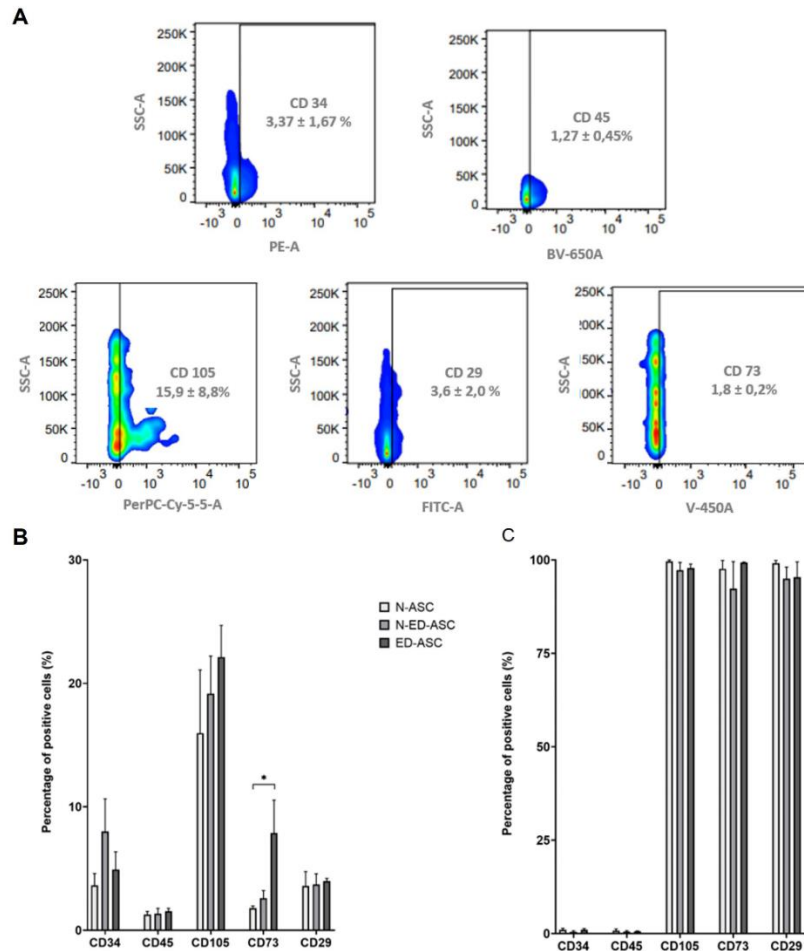


Figure 5. Surface markers expression was detected by flow cytometric analysis of N-ASC. The percentage of positive cells for each marker was calculated after subtracting the non-specific fluorescence obtained with the control (unmarked). (A) Representative set of flow cytometry analysis for CD34, CD45, CD105, CD29, and CD73 markers performed on N-ASC. Percentage of positive cells to CD markers was indicated as an average of the samples; (B) Percentage of positive cells to CD markers (as an average of the samples) in N-ASC compared to N-ED-ASC and ED-ASC; (C) Percentage of positive cells to CD markers after in vitro cell expansion in N-ASC, N-ED-ASC, and ED-ASC. Results are presented as the mean ± standard deviation portrayed with error bars. Significant statistical differences are indicated (p-value <0.05=*).

3.4. Analysis of multipotency

The multilineage differentiation ability of N-ASC was determined by analysing qualitatively and semi-quantitatively the ability of adherent cells to differentiate toward adipocytes, chondrocytes, and osteocytes. The differentiation assay was conducted for 4 and 9 days of evaluation after the induction with a selective medium containing lineage-specific induction factors for the lineages mentioned above. Induced N-ASC were stained with Oil-Red-Oil, Alizarin Red, and Alcian Blue to visualise the adipogenic, osteogenic, and chondrogenic differentiation,

respectively; and the results were compared with ED-ASC and N-ED-ASC. Figure 6.A and Figure 6.B show that N-ASC were clearly differentiated into the three mesodermal lineages on days 4 and 9. Applying the Oil-Red-Oil solution, red spots revealed the generation of lipid droplets on day 4, which increases during adipogenesis differentiation until day 9. In the case of osteogenic differentiation, Alizarin Red staining shows the formation of *in vitro* calcification 4 days after medium induction with an intensification of the calcium deposits on day 9 of the study.

Similarly, the chondrogenic differentiation assay revealed the generation of cartilage-like matrix started from the 4th day upon the specific culture media induction. On day 9, a well-organised cartilage-like matrix rich in collagen III and sulfated proteoglycans was detectable, as shown with Alcian blue staining (Figure 6.A and 6.B). Likewise, the multipotency assay was performed on N-ED-ASC and ED-ASC, showing positive staining compared with non-induced cells (CTR). For N-ED-ASC, the assay reveals that multilineage differentiation started on day 4, while ED-ASC differentiation started 9 days after the specific medium induction, suggesting a slower differentiation capacity than N-ASC for both methodologies. Figure 6.C shows the semi-quantitative analysis of the number of lipid droplets for the adipogenic differentiation, Figure 6.D the calcified area for the osteogenic differentiation and Figure 6.E the cartilage-like matrix area for the chondrogenic differentiation. These results confirmed the previous optical analyses where the number of lipid droplets for N-ASC after 9 days of induction was 469.20 ± 44.35 , which was higher than those found for ED-ASC (110.60 ± 22.81), N-ED-ASC (158.00 ± 34.10) and CTR (7.40 ± 2.29). In the same manner, the calcium deposition area was higher for N-ASC ($3010.4 \pm 699.4 \mu\text{m}^2$) compared to ED-ASC ($493.2 \pm 167.4 \mu\text{m}^2$), N-ED-ASC ($1273.2 \pm 268.7 \mu\text{m}^2$) and CTR ($41.0 \mu\text{m}^2 \pm 23.17 \mu\text{m}^2$) after 9 days of the osteogenic induction. Finally, the semi-quantification of the cartilage-like deposition area reveals a faster formation of a collagen matrix for the N-ASC ($79716 \pm 31360 \mu\text{m}^2$) in comparison with ED-ASC ($1744 \pm 372 \mu\text{m}^2$), N-ED-ASC ($13740 \pm 5944 \mu\text{m}^2$) and CTR ($0 \mu\text{m}^2$) after 9 days of study.

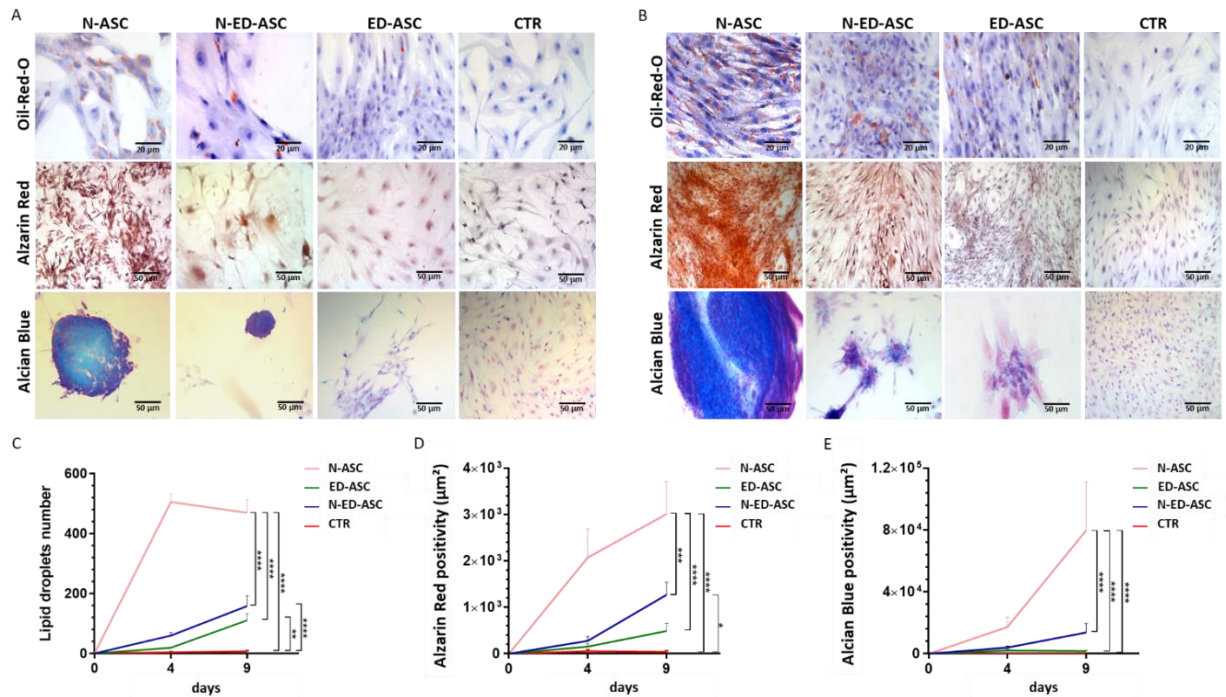


Figure 6. Multilineage differentiation assay. (A) Optical microscopy images of induced N-ASC, N-ED-ASC and ED-ASC and not induced (CTR) with differentiation medium at days 4 (Oil-Red O staining scale bar 10 μm; Alzarin Red staining scale bar 20 μm; Alcian blue staining scale bar 10 μm); (B) Optical microscopy images of induced N-ASC, N-ED-ASC and ED-ASC and not induced (CTR) with differentiation medium at days 9 (Oil-Red O staining scale bar 10 μm; Alzarin Red staining scale bar 20 μm; Alcian blue staining scale bar 10). Red spots indicated by the accumulation of neutral lipid vacuoles stained with Oil-Red-Oil; Alzarin Red staining reveals in red the extracellular matrix calcification; deposition of sulfated proteoglycan-rich matrix was marked in blue with Alcian Blue staining; (C) Graph represents the mean amount of lipid droplets of the induced ASC. After 9 days of the induction, N-ASC shows higher lipid droplets formation than ED-ASC, N-ED-ASC, and CTR. (D) The graph showed the extracellular matrix calcification area measurement (μm²) of the induced ASC. After 9 days of treatment, N-ASC showed the highest calcium deposit formation. (E) The graph represents the area measurement of the generated cartilage-like matrix (μm²). On the 9th day, N-ASC showed the larger cartilage deposit formation. In graphics C, D and E, the pink line represents N-ASC, the green line ED-ASC and the blue line N-ED-ASC. The data is presented as the mean ± standard deviation, significant statistical differences are indicated (p-value<0.05=*, 0.05<p-value<0.001=**, p-value<0.001=*** or p-value<0.0001=****).

To confirm the pluripotency of N-ASC, cells were then analysed at flow cytometry to verify the presence of the Multi-lineage differentiating stress enduring cells (MUSE cells), investigating the SSEA-3 and CD-105 antibodies expression. Figure 7.A shows the percentage expression of the evaluated antibodies. N-ASC expressed $25.5 \pm 6.5\%$ of SSEA-3, while for N-ED-ASC and ED-ASC was $3.12 \pm 2.2\%$ and $0.5 \pm 0.2\%$, respectively. Finally, the immunofluorescence assay (Figure 7.B) confirmed the presence of MUSE cells in N-ASC, revealing positive cells for the expression of CD105 and SEEA3 simultaneously.

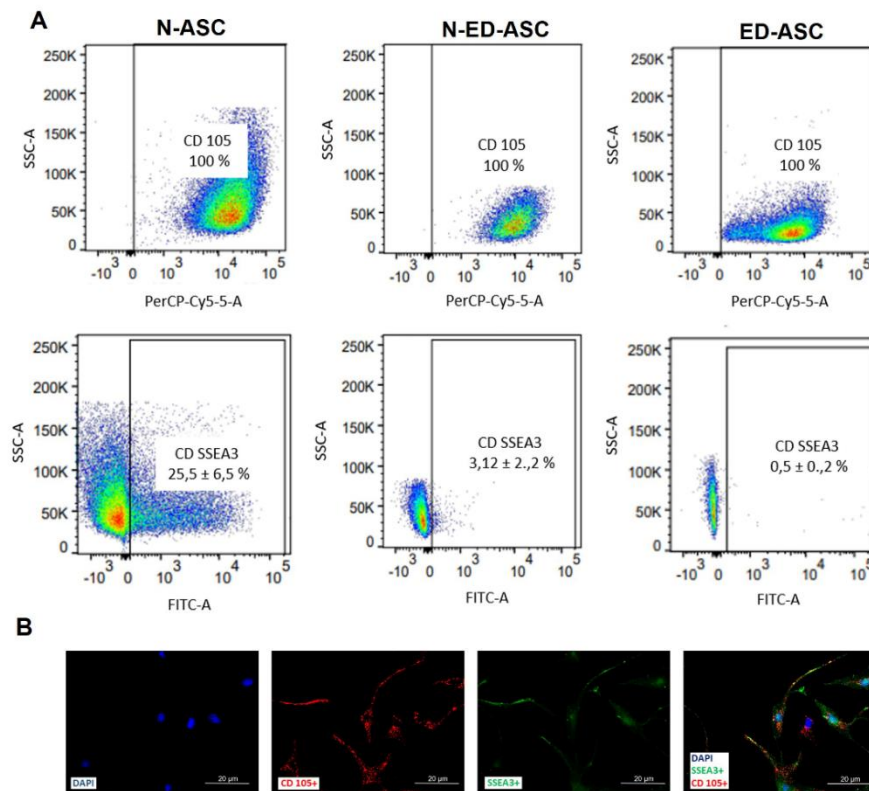


Figure 7. Multilineage differentiating stress enduring cells expression. A) Flow cytometry of N-ASC, N-ED-ASC, and ED-ASC to investigate the presence of MUSE cells. The percentage of positive cells to SEEA-3 and CD105 markers were indicated as an average of three samples, and the results are presented as the mean \pm standard deviation. B) Immunofluorescence microscopy of MUSE cells. MUSE cells in N-ASC were detected as a positive cell for CD105 (left), SEEA3 (middle) and the simultaneous expression of CD105-SEEA3 (right).

4. DISCUSSION

Nanofat is a simple and well-described procedure that allows small volumes of adipose tissue injection. The product obtained is an emulsified fat, rich in viable cells avoiding expansion or enzymatic treatments. The emulsification procedure reduces the size of adipose fragments harvested by liposuction, by a delicate filtration, obtaining an immediately injectable product [41]. Thanks to its fluid consistency, surgeons have promoted nanofat for face treatments rejuvenation, volume restoration, wrinkles, hypertrophic and atrophic scars, and defects correction [9–12].

This micro-fragmentation is able to produce smaller adipose niches than traditional techniques of adipose tissue manipulation with enormous advantages, allowing ASCs to migrate easily from the adipose lobules. Additionally, Nanofat is a “gentle” fragmentation that enables the preservation of the regenerative components in connective niches increasing cellular vitality, migration rate and allows a faster secretion of growth factors. This could be of crucial importance in clinical practice because it provides more beneficial regenerative effects for patients.

Hy-Tissue Nanofat is a new, simple system that reduces the time of adipose tissue processing drastically and guarantees the survival of regenerative units. The device reduces the size of the fat microfragments obtained after emulsification by shuffling the lipoaspirates 30 times between two connected syringes and filtering the emulsified adipose tissue through a membrane of 120 μm . In this study, deep characterisation of the product has been performed, and the abundance of regenerative cells has been described.

Morphological analysis of the emulsified fat shows the presence of lipid droplets of different dimensions, mainly ranging between 60 and 100 μm , making the product easy to inject into the desired location with high precision and suitable for injection in difficult areas with thin skin. The liquid consistency of nanofat, which also contains several endogenous cytokines and growth factors that are beneficial for vascularization initiation, allows it to be easily injected or be loaded onto a scaffold for various applications throughout body [1][42].

The microanatomy of emulsified fat is primarily comparable to that of native adipose tissue, with capillaries and microvessels organized and disseminated between adipocytes, and pericytes wrapped around endothelial cells. Consequently, if the therapeutic value of *Hy-Tissue Nanofat* is related to the extraction of the adipose-connective niche, those complexes (cells, extracellular matrix, and ASCs) might exercise their regenerative performance more indirectly, via growth factor secretion, than as progenitor cells.

In vitro results obtained with the *Hy-Tissue Nanofat* system have been compared with the results obtained through enzymatic digestion (collagenase type I), considered the gold standard technique to purify mesenchymal stem cells [43,44], and with the enzymatic digestion of Nanofat -SVF. Specifically, this last procedure was performed to evaluate the total amount of regenerative units, in terms of mesenchymal stem cells, that contribute to the tissue remodelling, rejuvenation and regeneration, describing the real regenerative potential of the *Hy-Tissue Nanofat* SVF. The results of cellular yield and CFU assay, showed that N-ASCs was characterized by lower cellular yield and capacity to form colonies, if compare with the classic enzymatic digestion, used to collect regenerative units from adipose tissue. The cellular yield resulted in about 9% (N-ASC), which increased to 29% after the enzymatic digestion of the emulsion (N-ED-ASC), suggesting that the system was highly efficient in extracting nucleated cells. Indeed, the number of N-ED-ASC resulted in $1.20 \times 10^5 \pm 3.90 \times 10^4$ cells employing 10 ml of lipoaspirate, not so far from the results obtained in Tonnard et al. 2013 [6] for 100 ml of lipoaspirates. Subsequently, duplication and clonogenic assays have been performed to characterise the regenerative units present in the *Hy-Tissue Nanofat* SVF. The growth rate and the clonogenic capability of N-ASC resulted lower than ED-ASC, which agrees with cellular yield results. Mechanical emulsification represents the minimal manipulation required to consider the injection of Nanofat-SVF an autologous fat implant. On the contrary, enzymatic digestion represents stronger method to isolate regenerative units, higher in number, but characterized by slower differentiation capability.

Previous studies established that CD34^+ cells represent a stem cell population with higher proliferative capacity. Immunophenotypic analysis of N-ASC reveals $3,37 \pm 1,67\%$ of CD34^+ expressing marker, which is in accordance with the literature [23]. Tonnard et al. [6] have reported 4,5 to 6,5% of CD34^+ cells in nanofat SVF.

Moreover, a non-statistically significant difference has been noted between the treatments. When cultured, cells acquired a strong mesenchymal stem cell phenotype, increasing the expression of specific surface markers (CD73, CD105 and CD 29) and confirming phenotype maintenance after 4 passages in culture.

N-ASC have also been tested for the capacity to differentiate in three mesenchymal cell types: adipocytes, osteocytes, and chondrocytes. The differentiation ability was evaluated after 4 and 9 days from specific media induction. N-ASC can efficiently differentiate starting from the 4th day, underling a higher differentiative potential comparable with cells enzymatically extracted. Usually, the uptake of lipid droplets, a marker of adipogenic differentiation, is detectable between 10 and 14 days after media stimulation [6,15,29,30], while the calcification and proteoglycan matrix formation are detectable after 21 days [15,29,30].

In addition, N-ASC were immunophenotypically analysed for SEEA3 expression as a specific marker for a subpopulation of mesenchymal stem cells called MUSE cells [31–35,45]. These cells are composed of pluripotent mesenchymal stem cells, able to migrate in damaged areas, as described in different preclinical and clinical models [46–48]. The results showed that N-ASC expressed $25.5 \pm 6.5\%$ of SEEA3 marker, while ED-ASC was $0.5 \pm 0.2\%$. This difference might be due to mechanical manipulation of fat tissue since MUSE cells are mainly expressed after severe cellular stress conditions [29,34]. These cells differentiate in numerous tissues, not only of mesenchymal origin, in a short time and could contribute to supporting the results obtained with differentiation assay. The use of emulsified fat-enriched MUSE cells in regenerative medicine could represent a novel aspect, increasing the treatment efficacy and the recovery time, even if a deeper analysis to understand the mechanism that undergoes high differentiative potential and MUSE expression is necessary.

Particularly, it is known that tissue enzymatic disaggregation can cause alterations in gene expression [49] and exosome amount [50] and this research displays how much the emulsified adipose tissue seems to be enriched with growth factors which are necessary to promote the reparative actions in damage tissues [51][52]. Taken together, our data reveal a greater regenerative and differentiative impact of the adipo-connective niches that emerge from this “gentle micro-fragmentation”, which provide the basis on which to build an explanation of therapeutic superiority. These results indicate *Hy-Tissue Nanofat* as a rapid, standardised and efficient system able to produce an emulsified fat rich in viable, proliferative and multipotent ASC; suggesting a potential use in regenerative medicine and tissue engineering when translated into clinical practice.

5. CONCLUSION

In this study, we demonstrated that *Hy-Tissue Nanofat Plus* is a rapid, easy to use and standardised device that allows the extraction of live and proliferative multipotent and pluripotent adipose-derived stem cells able to rapidly differentiate into adipocyte, osteocyte, and chondrocytes, making this product of potential interest in regenerative medicine. The regenerative potential of nanofat product is a safer alternative treatment given its intrinsic immunomodulatory, antiapoptotic, angiogenic, proliferative factors without administering whole cells. Nevertheless,

further research is needed to understand the specific role of nanofat secretome in repairing damaged and diseased tissues.

REFERENCES

- 1 Grünherz L, Sanchez-Macedo N, Frueh FS, et al. Nanofat applications: from clinical esthetics to regenerative research. *Curr Opin Biomed Eng* 2019;10:174–180.
- 2 Eto H, Kato H, Suga H, et al. The Fate of Adipocytes after Nonvascularized Fat Grafting. *Plast Reconstr Surg* 2012;129:1081–1092.
- 3 Gir P, Brown SA, Oni G, et al. Fat Grafting. *Plast Reconstr Surg* 2012;130:249–258.
- 4 Kato H, Mineda K, Eto H, et al. Degeneration, Regeneration, and Cicatrization after Fat Grafting: Dynamic Total Tissue Remodeling during the First 3 Months. *Plast Reconstr Surg* 2014;133.
- 5 Coleman SR, Lam S, Cohen SR, et al. Fat Grafting. *Atlas Oral Maxillofac Surg Clin* 2018;26:81–84.
- 6 Tonnard P, Verpaele A, Peeters G, et al. Nanofat Grafting. *Plast Reconstr Surg* 2013;132:1017–1026.
- 7 Lindenblatt N, van Hulle A, Verpaele AM, et al. The Role of Microfat Grafting in Facial Contouring. *Aesthetic Surg J* 2015;35:763–771.
- 8 Mesguich Batel F, Bertrand B, Magalon J, et al. Traitement des ridules de la lèvre supérieure par graisse émulsifiée ou « Nanofat » : étude biologique et clinique à propos de 4 cas. *Ann Chir Plast Esthétique* 2018;63:31–40.
- 9 Gu Z, Li Y, Li H. Use of Condensed Nanofat Combined With Fat Grafts to Treat Atrophic Scars. *JAMA Facial Plast Surg* 2018;20:128–135.
- 10 Uyulmaz S, Sanchez Macedo N, Rezaeian F, et al. Nanofat Grafting for Scar Treatment and Skin Quality Improvement. *Aesthetic Surg J* 2018;38:421–428.
- 11 Bhooshan LS, Devi MG, Aniraj R, et al. Autologous emulsified fat injection for rejuvenation of scars: A prospective observational study. *Indian J Plast Surg* 2018;51:077–083.
- 12 Martin A, Maladry D, Esmaeli A, et al. Fat grafting of hairy areas of head and neck - comparison between lipofilling and nanofat grafting procedures in a cadaveric study. *J Stomatol Oral Maxillofac Surg* 2018;119:274–278.
- 13 Gimble JM, Bunnell BA, Guilak F. Human adipose-derived cells: an update on the transition to clinical translation. *Regen Med* 2012;7:225–235.
- 14 Bora P, Majumdar AS. Adipose tissue-derived stromal vascular fraction in regenerative medicine: a brief review on biology and translation. *Stem Cell Res*

- Ther 2017;8:145.
- 15 Wei H, Gu S-X, Liang Y-D, et al. Nanofat-derived stem cells with platelet-rich fibrin improve facial contour remodeling and skin rejuvenation after autologous structural fat transplantation. *Oncotarget* 2017;8:68542–68556.
 - 16 LO FURNO D, TAMBURINO S, MANNINO G, et al. Nanofat 2.0: Experimental Evidence for a Fat Grafting Rich in Mesenchymal Stem Cells. *Physiol Res* 2017:663–671.
 - 17 Kachgal S, Putnam AJ. Mesenchymal stem cells from adipose and bone marrow promote angiogenesis via distinct cytokine and protease expression mechanisms. *Angiogenesis* 2011;14:47–59.
 - 18 Clevers H, Loh KM, Nusse R. An integral program for tissue renewal and regeneration: Wnt signaling and stem cell control. *Science* (80-) 2014;346.
 - 19 Rigotti G, Marchi A, Sbarbati A. Adipose-Derived Mesenchymal Stem Cells: Past, Present, and Future. *Aesthetic Plast Surg* 2009;33:271–273.
 - 20 Dai R, Wang Z, Samanipour R, et al. Adipose-Derived Stem Cells for Tissue Engineering and Regenerative Medicine Applications. *Stem Cells Int* 2016;2016:1–19.
 - 21 Shang Q, Bai Y, Wang G, et al. Delivery of Adipose-Derived Stem Cells Attenuates Adipose Tissue Inflammation and Insulin Resistance in Obese Mice Through Remodeling Macrophage Phenotypes. *Stem Cells Dev* 2015;24:2052–2064.
 - 22 Prasai A, El Ayadi A, Mifflin RC, et al. Characterization of Adipose-Derived Stem Cells Following Burn Injury. *Stem Cell Rev Reports* 2017;13:781–792.
 - 23 Kotani T, Masutani R, Suzuka T, et al. Anti-inflammatory and anti-fibrotic effects of intravenous adipose-derived stem cell transplantation in a mouse model of bleomycin-induced interstitial pneumonia. *Sci Rep* 2017;7:14608.
 - 24 Kalinina N, Kharlampieva D, Loguinova M, et al. Characterization of secretomes provides evidence for adipose-derived mesenchymal stromal cells subtypes. *Stem Cell Res Ther* 2015;6:221.
 - 25 Charles-de-Sá L, Gontijo-de-Amorim NF, Maeda Takiya C, et al. Antiaging Treatment of the Facial Skin by Fat Graft and Adipose-Derived Stem Cells. *Plast Reconstr Surg* 2015;135:999–1009.
 - 26 De Francesco F, Tirino V, Desiderio V, et al. Human CD34+/CD90+ ASCs Are Capable of Growing as Sphere Clusters, Producing High Levels of VEGF and Forming Capillaries. *PLoS One* 2009;4:e6537.
 - 27 Kober J, Gugerell A, Schmid M, et al. stem. *Ann Plast Surg* 2016;77:156–163.

- 28 Paliwal S, Chaudhuri R, Agrawal A, et al. Regenerative abilities of mesenchymal stem cells through mitochondrial transfer. *J Biomed Sci* 2018;25:31.
- 29 Dai Prè E, Busato A, Mannucci S, et al. In Vitro Characterization of Adipose Stem Cells Non-Enzymatically Extracted from the Thigh and Abdomen. *Int J Mol Sci* 2020;21:3081.
- 30 Busato A, De Francesco F, Biswas R, et al. Simple and Rapid Non-Enzymatic Procedure Allows the Isolation of Structurally Preserved Connective Tissue Micro-Fragments Enriched with SVF. *Cells* 2020;10:36.
- 31 Kushida Y, Wakao S, Dezawa M. Muse Cells Are Endogenous Reparative Stem Cells 2018:43–68.
- 32 Conti G, Zingaretti N, Amuso D, et al. Proteomic and Ultrastructural Analysis of Cellulite-New Findings on an Old Topic. *Int J Mol Sci* 2020;21:2077.
- 33 Conti G, Bertossi D, Dai Prè E, et al. Regenerative potential of the Bichat fat pad determined by the quantification of multilineage differentiating stress enduring cells. *Eur J Histochem* 2018;62.
- 34 Fisch SC, Gimeno ML, Phan JD, et al. Pluripotent nontumorigenic multilineage differentiating stress enduring cells (Muse cells): a seven-year retrospective. *Stem Cell Res Ther* 2017;8:227.
- 35 Simerman AA, Phan JD, Dumesic DA, et al. Muse Cells: Nontumorigenic Pluripotent Stem Cells Present in Adult Tissues—A Paradigm Shift in Tissue Regeneration and Evolution. *Stem Cells Int* 2016;2016:1–8.
- 36 Wakao S, Kitada M, Kuroda Y, et al. Multilineage-differentiating stress-enduring (Muse) cells are a primary source of induced pluripotent stem cells in human fibroblasts. *Proc Natl Acad Sci U S A* 2011;108:9875–9880.
- 37 Ogura F, Wakao S, Kuroda Y, et al. Human Adipose Tissue Possesses a Unique Population of Pluripotent Stem Cells with Nontumorigenic and Low Telomerase Activities: Potential Implications in Regenerative Medicine. *Stem Cells Dev* 2014;23:717–728.
- 38 Simerman AA, Dumesic DA, Chazenbalk GD. Pluripotent muse cells derived from human adipose tissue: a new perspective on regenerative medicine and cell therapy. *Clin Transl Med* 2014;3.
- 39 Liu Q, Zhang R, Li D, et al. Muse Cells, a New Type of Pluripotent Stem Cell Derived from Human Fibroblasts. *Cell Reprogram* 2016;18:67–77.
- 40 Martinello T, Bronzini I, Maccatrozzo L, et al. Cryopreservation Does Not Affect the Stem Characteristics of Multipotent Cells Isolated from Equine Peripheral

- Blood. *Tissue Eng Part C Methods* 2010;16:771–781.
- 41 Kamat P, Frueh FS, McLuckie M, et al. Adipose tissue and the vascularization of biomaterials: Stem cells, microvascular fragments and nanofat—a review. *Cytotherapy* 2020;22:400–411.
- 42 Weinzierl A, Harder Y, Schmauss D, et al. Boosting Tissue Vascularization: Nanofat as a Potential Source of Functional Microvessel Segments. *Front Bioeng Biotechnol* 2022;10.
- 43 Peroni D, Scambi I, Pasini A, et al. Stem molecular signature of adipose-derived stromal cells. *Exp Cell Res* 2008;314:603–615.
- 44 Alstrup T, Eijken M, Bohn AB, et al. Isolation of Adipose Tissue-Derived Stem Cells: Enzymatic Digestion in Combination with Mechanical Distortion to Increase Adipose Tissue-Derived Stem Cell Yield from Human Aspirated Fat. *Curr Protoc Stem Cell Biol* 2019;48:e68.
- 45 Wakao S, Kitada M, Kuroda Y, et al. Multilineage-differentiating stress-enduring (Muse) cells are a primary source of induced pluripotent stem cells in human fibroblasts. *Proc Natl Acad Sci* 2011;108:9875–9880.
- 46 Yamasaki T, Wakao S, Kawaji H, et al. Genetically Engineered Multilineage-Differentiating Stress-Enduring Cells as Cellular Vehicles against Malignant Gliomas. *Mol Ther - Oncolytics* 2017;6:45–56.
- 47 Yabuki H, Wakao S, Kushida Y, et al. Human Multilineage-differentiating Stress-Enduring Cells Exert Pleiotropic Effects to Ameliorate Acute Lung Ischemia–Reperfusion Injury in a Rat Model. *Cell Transplant* 2018;27:979–993.
- 48 Mahmoud EE, Kamei N, Shimizu R, et al. Therapeutic Potential of Multilineage-Differentiating Stress-Enduring Cells for Osteochondral Repair in a Rat Model. *Stem Cells Int* 2017;2017:1–8.
- 49 van den Brink SC, Sage F, Vértesy Á, et al. Single-cell sequencing reveals dissociation-induced gene expression in tissue subpopulations. *Nat Methods* 2017;14:935–936.
- 50 Garcia-Contreras M, Ricordi C, Robbins PD, et al. Exosomes in the pathogenesis, diagnosis and treatment of pancreatic diseases. *CellR4* 2014;2:e807.
- 51 De Francesco F, Gravina P, Busato A, et al. Stem Cells in Autologous Microfragmented Adipose Tissue: Current Perspectives in Osteoarthritis Disease. *Int J Mol Sci* 2021;22:10197.
- 52 Senesi L, De Francesco F, Farinelli L, et al. Mechanical and Enzymatic Procedures to Isolate the Stromal Vascular Fraction From Adipose Tissue: Preliminary Results.

Front Cell Dev Biol 2019;7.

FINAL REMARKS

PROLOGUE:

Abraham Lincon said, “the best way to predict the future is to create it.”

Part of the work of a researcher is to be aware that every small contribution to science can allow it to grow and develop humanity. This thesis intends to contribute to how new strategies can be approached to improve Tissue Engineering and Regenerative Medicine applications. This final chapter presents a general discussion and some future perspectives that elucidate the broader possibilities that can be accomplished when applying the proposed Regenerative Algorithm.

DISCUSSION

Tissue Engineering and Regenerative Medicine (TERM) is a field of research that has been increasingly growing, and its main objective is to promote the healing or replacement of damaged tissue (1). The term “tissue engineering” was only known to the scientific community until 1997, when a BBC documentary showed for the first time the experiment performed by Vacanti when made grow a human ear in the back of a nude mouse (2). Since then, the world has become well-known for the words “Regenerative Medicine and Tissue Engineering.”

TERM is a multidisciplinary field that involves cell engineering, molecular biology, and biomaterial engineering, among others, to develop structures that help to replace/repair injured or damaged tissue (3). The research in TERM for the last decades has been focused on three main approaches: 1) cell implantation, 2) substances delivery and 3) cell implantation using biomaterials (4). However, spite the various research in the field, these studies are centered on one part of the problem; the efforts are focused on “filling” the missing or damaged part limiting the effectiveness and safety of the current treatments (5).

This work introduced a new concept in the TERM field, the Regenerative Algorithm, Figure 1 presents a summary of the Regenerative Algorithm. In the Introductory chapter, a construction analogy was used to explain the importance of understanding the regeneration process in living tissues.

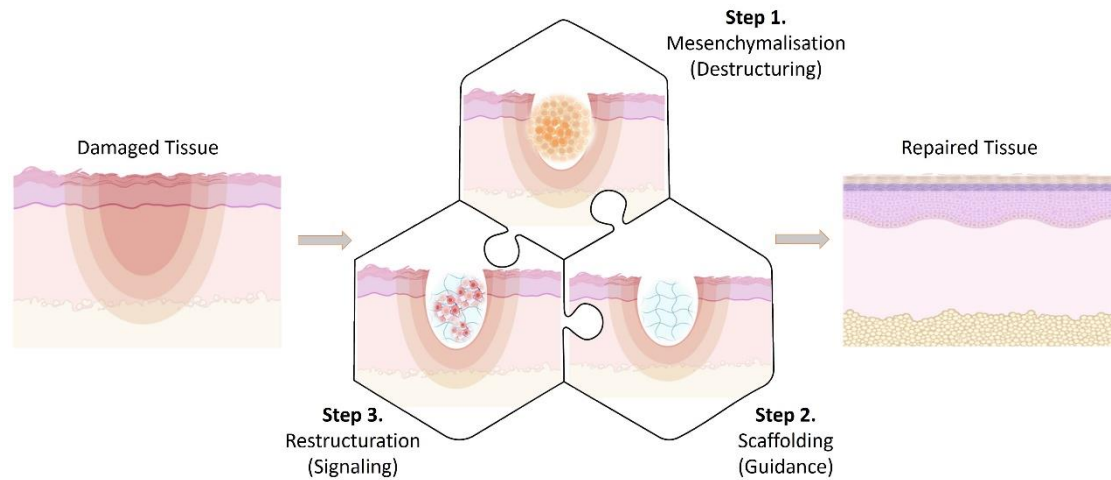


Figure 1. Representative scheme of the proposed Regenerative Algorithm.

The proposed Regenerative Algorithm explains the importance of the initial destructuring of the tissue. To elucidate this concept, it was presented a study case in Chapter 1. It described the use of a novel enzyme for the debridement of wounded tissue. The study presented the *in vitro* analysis of the *Vibrio alginolyticus*-based collagenase, where it was proved its efficacy in the digestion of collagen structure; in the case of the study, this was performed for the liberation of stem cells. However, it allows to predict its future applications in treating injured tissue because destructuring damaged structures stimulates the endogen regenerative capacity. As part of the algorithm, the tissue debridement is vital for the remotion of injured structures that might affect the correct restructuring of the tissue and

the possible induction to the tissue dedifferentiation. It has been discovered in some eukaryotic organisms that to repair damaged tissue, it is critical to recreate tissue formation from its initial structure instead of forming a scar (6). Recent studies have demonstrated that in mammals, it is possible to promote self-regeneration mechanisms by impeding the formation of scars (7). Using the studied collagenase to remove the disorganized collagen structure that tends to appear during scar formation might provide an appropriate environment, to begin the healing process. The second part of the algorithm uses pre-formed structures that emulate the original natural structure. In this regard were introduced Chapters 2 and 3 with studies using biomaterials that support the newly formed tissue. Chapter 2 showed a research on 3D structures conformed on descellularized collagen for the prevention of capsular contracture formation, and Chapter 3 presented a research on hyaluronic acid for the treatment of scars. Both of these studies are examples of using structures biomaterials that provide a framework in which the new tissue can grow. During the classic stages of wound repair, this frame is formed by a fibrin matrix that is later colonized by cells that will form the new tissue (6). However, the greater the damage, the more disorganized is the natural healing processes of the body, because of this, external aid is required. In superficial situations non-invasive treatment is preferred; in this regard, injectable materials are a plus, such as the studied hyaluronic acid, while for more complex damages, 3D configurations are the alternatives. Additionally, the constructs that support the newly formed tissue must provide some degree of stimulation on the peri-wound tissue that induces the self-healing processes (8). Both presented studies showed the guided stimulation of the descellularized membranes and hyaluronic acid *in vitro* and *in vivo*.

The last part of the proposed algorithm is the promotion of the restructuration of damaged tissue using different types of biomolecules. Following this step, it was introduced Chapter 4, where a novel device was validated for the extraction of stromal vascular (SVF) fraction from adipose tissue through mechanical disaggregation. SVF extracted from mechanical methods presents preserved extracellular matrix and all stromal cells providing to the host tissue precursors that activate the natural healing cascade (9)(8). It has been proved that the extracted connective microfragments contribute to pro-angiogenic, pro-differentiative and pro-antiapoptotic factors (10). In the study of chapter 4 was proven that the extracted microfragments with a novel mechanical device is composed of various elements that not only enable cell differentiation but reduce the required time for this process to occur. Moreover, it was found that using this device, it is possible to extract an important subpopulation of cells known as Multi-lineage differentiating stress enduring cells (MUSE). The multipotency of MUSE increases their potential in TERM applications.

FUTURE PERSPECTIVES

Based on the above mentioned, the development of the algorithm has been developed in single steps without progressive feedback among them, because of this the importance on generating complete research where all the steps of the Regenerative Algorithm are employed. However, as it is proposed in the last step of the algorithm, the use of cells is fundamental for the colonization of the structures

formed in the second step, but cells required the necessary nutrients to grow and later differentiate. In the previous section was exposed the first “successful” experiment on the generation of a tissue, the growth of a human ear on the back of a mouse; sadly this ear lack of vascularization, impeding the nutrients transportation to the cells in the center of the structure. This outcome elucidates the importance of using alternative biomolecules that activate the tissue self-reparative pathways. To overcome this impairment, recent studies have shown that using cellular elements such as nanovesicles that can be employed as nanocarriers for different growth factors and can induce vascularization (11). Nevertheless, there are some possible difficulties when applying the Regenerative Algorithm that must be solved. Considering the first step, the remotion of damaged tissue might require extensive time, allowing infections to occur. For this reason, selecting the appropriate method for the destructuring of the tissue is highly important. On the other hand, considering the current research stage, the algorithm is not appropriate for more extensive damages because of the difficulties in creating bigger and steady constructs that can accomplish with the second part of the algorithm. However, the current efforts point out tackling this drawback with new engineered strategies in the field of 3D bioprinting, developing more biocompatible and resistant bioinks that can provide a steady frame and be loaded with different elements that promote and improve the regeneration process (12).

Finally, some ethical problems must be considered when studying the last step of the algorithm given the involvement of cells and biological components. Current controversies of cell-based therapies are the broad differentiative capacities of stem cells that can be seen as a human risk either because they might promote tumor growth or because they can be used in human cloning (13). Additionally, the FDA (Food and Drug Administration) permits only the use of cell and cell-derived product therapies when they undergo minimal manipulations (14). Considering this last statement, the proposed technique in Chapter 4 provides excellent advantage in extracting stem cells and cellular components due to the lowest manipulation of the product without the aforementioned risks.

Notwithstanding the difficulties, the future of Tissue Engineering and Regenerative Medicine is based on a multistep treatment that considers all the natural processes that occur in biological systems during self-healing and attempts to emulate them for more complex damages.

REFERENCES

1. Altyar AE, El-Sayed A, Abdeen A, Piscopo M, Mousa SA, Najda A, et al. Future regenerative medicine developments and their therapeutic applications. *Biomed Pharmacother* [Internet]. 2023;158:114131. Available from: <https://doi.org/10.1016/j.biopha.2022.114131>
2. Cao Y, Vacanti JP, Paige KT, Upton J, Vacanti CA. Transplantation of Chondrocytes Utilizing a Polymer-Cell Construct to Produce Tissue-Engineered Cartilage in the Shape of a Human Ear. *Plast & Reconst Surg* [Internet]. 1997 Aug;100(2):297–302. Available from: <http://journals.lww.com/00006534->

199708000-00001

3. Sefat F, Mozafari M, Atala A. Introduction to tissue engineering scaffolds [Internet]. Handbook of Tissue Engineering Scaffolds: Volume One. Elsevier Ltd; 2019. 3–22 p. Available from: <https://doi.org/10.1016/B978-0-08-102563-5.00001-0>
4. Pina S, Ribeiro VP, Paiva OC, Correlo VM, Oliveira JM, Reis RL. Tissue engineering scaffolds: Future perspectives [Internet]. Handbook of Tissue Engineering Scaffolds: Volume One. Elsevier Ltd; 2019. 165–185 p. Available from: <https://doi.org/10.1016/B978-0-08-102563-5.00009-5>
5. Feng X, Hao J. Identifying New Pathways and Targets for Wound Healing and Therapeutics from Natural Sources. *Curr Drug Deliv*. 2021;18(8):1064–84.
6. Gurtner GC, Werner S, Barrandon Y, Longaker MT. Wound repair and regeneration. *Nature*. 2008;453(7193):314–21.
7. Yannas I V., Tzeranis DS. Mammals fail to regenerate organs when wound contraction drives scar formation. *npj Regen Med* [Internet]. 2021;6(1):1–6. Available from: <http://dx.doi.org/10.1038/s41536-021-00149-9>
8. Raghav PK, Mann Z, Ahlawat S, Mohanty S. Mesenchymal stem cell-based nanoparticles and scaffolds in regenerative medicine. *Eur J Pharmacol* [Internet]. 2022;918(July 2021):174657. Available from: <https://doi.org/10.1016/j.ejphar.2021.174657>
9. Copcu HE, Oztan S. Not Stromal Vascular Fraction (SVF) or Nanofat, but Total Stromal-Cells (TOST): A New Definition. Systemic Review of Mechanical Stromal-Cell Extraction Techniques. *Tissue Eng Regen Med* [Internet]. 2021;18(1):25–36. Available from: <https://doi.org/10.1007/s13770-020-00313-0>
10. Bora P, Majumdar AS. Adipose tissue-derived stromal vascular fraction in regenerative medicine: a brief review on biology and translation. *Stem Cell Res Ther* [Internet]. 2017 Dec 15;8(1):145. Available from: <http://stemcellres.biomedcentral.com/articles/10.1186/s13287-017-0598-y>
11. Tu J, Zeng Y, An R, Sun J, Wen H. Engineered nanovesicles from stromal vascular fraction promote angiogenesis and adipogenesis inside decellularized adipose tissue through encapsulating growth factors. *Sci Rep* [Internet]. 2023;1–13. Available from: <https://doi.org/10.1038/s41598-022-27176-w>
12. Shokouhimehr M, Theus AS, Kamalakar A, Ning L, Cao C, Tomov ML, et al. 3D Bioprinted Bacteriostatic Hyperelastic Bone Scaffold for Damage-Specific Bone Regeneration. *Polymers (Basel)* [Internet]. 2021 Mar 30;13(7):1099. Available

from: <https://www.mdpi.com/2073-4360/13/7/1099>

13. Volarevic V, Markovic BS, Gazdic M, Volarevic A, Jovicic N, Arsenijevic N, et al. Ethical and Safety Issues of Stem Cell-Based Therapy. *Int J Med Sci* [Internet]. 2018;15(1):36–45. Available from: <http://www.medsci.org/v15p0036.htm>
14. Harris AR, Walker MJ, Gilbert F. Ethical and regulatory issues of stem cell-derived 3-dimensional organoid and tissue therapy for personalised regenerative medicine. *BMC Med* [Internet]. 2022;20(1):1–11. Available from: <https://doi.org/10.1186/s12916-022-02710-9>